2010

Autonomous optimal deorbit guidance

Morgan Baldwin
Iowa State University

Autonomous optimal deorbit guidance

by

Morgan Caitlin Baldwin

A dissertation submitted to the graduate faculty

in partial fulfillment of the requirements for the degree of

DOCTOR OF PHILOSOPHY

Major: Aerospace Engineering

Program of Study Committee:
Ping Lu, Major Professor
Dale Chimenti
Wolfgang Kliemann
Thomas Rudolphi
Bong Wie

Iowa State University

Ames, Iowa

2010

TABLE OF CONTENTS

LIST OF TABLES

LIST OF FIGURES

ABSTRACT

The objective of this dissertation is to solve an optimal deorbit guidance problem given initial orbit and vehicle parameters as inputs. Currently, the problem is computationally intensive to solve and approximate methods such as impulsive maneuvers are utilized. The problem is formulated as a fuel-optimal control problem that allows for a variety of terminal conditions at entry interface (EI). Using optimal control methods, the engine on time, engine off time as well as the direction of the thrust vector are solved for a variety of circular and elliptic initial orbits. Single and multiple burn maneuvers for both circular and elliptic orbits are explored. The J_2 gravitational term is added as part of the solution process. The numerical solution is obtained using an analytical multiple shooting method. The results show promising potential of the proposed method and are comparable to NASA's Shuttle results.

CHAPTER 1. Introduction

Changes in the world climate over the past ten or more years have led the United States government to reevaluate the use and capability of their space-based assets. The outcome is the Department of Defense's Operational Responsive Space (ORS). More specifically, Operational Responsive Space:

> "Will provide an affordable capability to promptly, accurately, and decisively position and operate national and military assets in and through space and near space. ORS will be fully integrated and interoperable with current and future architectures and provide space services and effects to war fighters and other users. ORS is a vision for transforming future space and near space operations, integration, and acquisition, all at a lower cost." [1]

Operational Responsive Space gives rise to the need for performing space maneuvers in time critical scenarios and other situations. One such space maneuver is deorbit. Deorbit is the powered flight phase for an on-orbit vehicle during which a decelerating maneuver is performed so that, after the engine cut-off, the vehicle will coast to a desired set of conditions at the entry interface (EI). EI conditions permit the vehicle to have a subsequent safe entry flight to the landing site. Currently, the timing and location of deorbiting maneuvers are carefully planned on the ground. This process works for well planned missions with ample lead time and ground support. However, given the current desire of ORS, the capability of an on-board system to autonomously accomplish the planning and execution of an optimal deorbit maneuver would be an enabling component

for executing on-demand deorbit and entry missions. This work is concerned with the deorbit guidance problem. This entails solving for the direction and magnitude of the thrust vector for each second of flight to achieve the desired terminal, or EI, conditions.

With few exceptions, the problem is usually analyzed as an optimal orbital transfer problem with the approximation of impulsive velocity change. In most cases, the conditions at the EI are considered completely fixed. EI is defined as the point in which deorbit ends and entry begins, at an altitude of 120 km. Figure 1.1 shows an example deorbit maneuver with an impulsive deorbit boost. Generally, solving the deorbit problem has meant determining the location of application of velocity impulse and the velocity impulse vector of minimum magnitude to achieve necessary EI conditions. Space vehicles today are low thrust vehicles, so accurately approximating the required deorbit boost with an impulse is difficult [2].

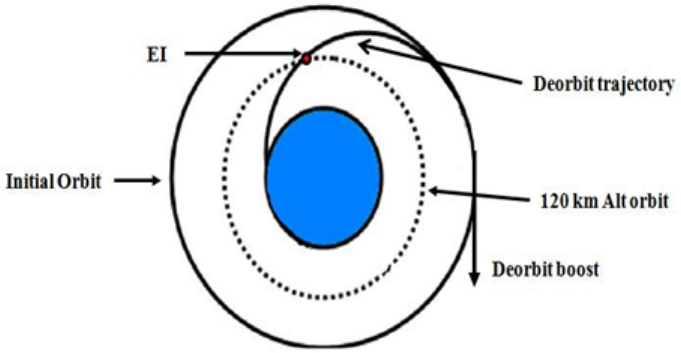

Figure 1.1 Example impulsive deorbit maneuver

NASA's Space Shuttle is a low thrust vehicle that performs a finite time deorbit burn, which depends on the orbit altitude and burn characteristics. Through numerical analysis, the required values of velocity and flight path angle at EI are determined for various values of the apogee altitude [3]. This data forms the desired targeting condition of the deorbit burn. Specifically, in the guidance implementation the Shuttle targets a linear relationship of flight path angle and velocity at EI [4]. The range to the target is controlled by properly timing the burn [3].

An exact solution for the minimum energy deorbit solution for a specified entry path angle and altitude is given in Ref. [5]. The best location of minimum deorbit boost is apoapsis, for shallow entry path angle, and before or after apoapsis for shaper entry path angles for unconstrained EI velocity [5]. The minimum energy and time deorbit exact solution for a given entry path angle, altitude, and velocity is given in Ref. [6]. The required number of space vehicle orbits such that the landing site is lined up with the entry orbit is also determined. This ensures that any required plane change is done during entry flight. In Ref. [7] it is shown that an optimum deorbit altitude exists for a minimum deboost requirement and specified entry path angle.

In Ref. [8], the co-planar single minimum-impulse deorbit problem is considered. The problem of finding optimal deorbit position and impulse from a given initial elliptic orbit is reduced to simultaneously solving two 4-th order polynomials given a specified entry flight path angle and entry altitude. It is shown that for certain ranges of values of semi-major axis and eccentricity, the optimal deorbit point is at a non-apoapsis location of the initial orbit and a significant ΔV savings is achieved. The latter indicates that, depending on the time of initiation of the deorbit maneuver, an optimal coast may be called for before the deorbit burn of the engine. In Ref. [9], a prescribed functional relationship (not necessarily linear) between the entry velocity and flight path angle is allowed. Using Keplerian motion for non-powered flight on orbit and the single impulse assumption, the solution of the problem is reduced to the solutions of two 6-th order

polynomials. The most interesting findings in Ref. [9] include the demonstration that significant savings in ΔV can be achieved by allowing non-fixed entry flight path angle and velocity (but constrained by the given functional relationship for feasibility of entry flight), and for certain ranges of semi-major axis and eccentricity, the optimal deorbit point is at a non-apoapsis location of the initial orbit.

A hodograph method is used in Ref. [10] for solving the minimum-impulse deorbit problem, including the Earth perturbation forces, under fixed transit and landing time constraints, and assuming in-plane impulsive burns. The hodograph method is approximate but can be performed rapidly. In Ref. [2], a strategy for optimal deorbit maneuvers including out-of-plane maneuvers is studied. The higher the altitude, the less likely an impulse is to satisfy EI conditions so an iterative method is used with an impulse as an initial guess, which is then corrected to give more accurate burn, is used. The J_2 perturbation term of the orbit is shown to affect the final flight path angle and needs to be considered for better results. The benefits of two-impulse deorbit maneuvers are also discussed in Ref. [2].

For cases when multiple burns are beneficial, burn timing is crucial. For cases of impulsive transfer, optimal switching in the problem of minimal fuel, time-free, impulsive plane transfer is studied in Ref. [11]. The complete solution to determine the switching sequence (burn, coast, burn, etc.) is obtained by solving an 8-th degree algebraic equation. In [12], the optimal position of vehicle and direction of velocity impulse are determined for the free time coplanar orbit transfer. The switching relations that must be satisfied at the points where the impulse is applied in an optimal trajectory are determined. The necessary conditions for when an additional impulse is required along an optimal trajectory in a time fixed trajectory are given in Ref. [13]. Also, cost reducing measures such as moving impulse location and altering initial and final coasts are presented. In Ref. [14] the primer vector for optimal intercept with time constraint is determined for impulsive maneuver. Then, based on the primer vector,

rules are established to search for the optimal impulsive transfer if the one-impulse is not optimal.

In both Ref. [15] and [16], the impulsive deorbit problem is solved together with the entry flight problem. An approximate analytical solution for atmospheric trajectory is used in Ref. [15]. The results of the orbital phase, transfer phase, and atmospheric phase are then combined to iteratively search for an end-to-end trajectory with an optimal impulsive, in-plane deorbit burn. A complete numerical solution is used in Ref. [16] to study the deorbit mission of the X-38. The performance index investigated in Ref. [16] is the entry flight portion, such as maximum crossrange and downrange, using a direct optimization method. The X-38 deorbit targeting aims at an EI window determined by the crossrange and downrange with Earth's gravitational perturbations used. In treating the deorbit and entry trajectory design problem together, the correct EI condition will be obtained as a part of the solution. The EI condition will ensure the flyability of the ensuing entry trajectory for the vehicle. A negative aspect of this method is that the solution process is numerically intensive, and is not suitable for on-board applications.

This dissertation describes the development of an autonomous optimal deorbit guidance algorithm. Given initial vehicle conditions of position, velocity, and initial orbit parameters, the optimal deorbit guidance solution that meets the required terminal conditions is determined for both initial circular and elliptic orbits. This includes determining the engine on-time and off-time for the given number of finite time burns. The number of burns is determined based on the initial orbit parameters of the vehicle. The direction and magnitude of the thrust vector necessary to meet the required EI conditions is determined for each second of flight. Also, it will be shown that the optimal deorbit point from an elliptic orbit is not apoapsis. The numerical results are in the same range as NASA's Space Shuttle data. The effect of J_2 on the EI conditions of the vehicle are explored. More specifically, the effect of the addition of the J_2 term to the guidance solution and the closed loop simulation is determined. This work is

arranged as follows: Chapter 2 gives a numerical overview and discussion of issues that affect derobit. Chapter 3 gives a description of the problem formulation with specified targeting conditions and a description of the algorithm. Numerical results and analysis is presented in Chapter 4, 5, and 6 for both circular and elliptic orbits, assuming Keplerian motion. Chapter 7 gives an overview of the effect the J2 term has on the deorbit problem. Concluding remarks and a discussion of future work are given in Chapter 8.

CHAPTER 2. Issues that Affect Deorbit

There are several issues that affect the execution of a deorbit maneuver. These include the timing of the burn, number of burns, and earth's gravitational force. The majority of previous work has been done assuming impulsive burns and Keplerian motion. For a first round approximation or mission planning, these assumptions are acceptable but for use in an onboard system in real time, these assumptions cannot be used to accurately solve the guidance problem. The engines on space vehicles today are not capable of producing enough thrust instantaneously to enable an idealistic deorbit maneuver. The flight time of the deorbit maneuver can involve long periods of coasting in which the oblateness of the earth has a profound influence and must be taken into account. The amount of fuel used must be minimized and for some cases of orbit altitude, this is done using a multiple burn maneuver rather than a single burn maneuver. Out of plane maneuvers require a great deal of fuel, so the timing of the burn must ensure that any out of plane maneuver occurs in the atmospheric portion of reentry. The following sections explore each of these issues in greater detail. Specifically, Section 1 reviews impulsive burns, Section 2 defines the different advantages in multiple burn maneuvers, Section 3 explores the effect of the J_2 gravitational term, Section 4 discusses the timing of the deorbit burn, and Section 5 gives an indepth review of previous work presented in Ref. [8].

2.1 Impulsive Burns

The deorbit impulse required to meet a given set of EI conditions has been examined thoroughly in previous work. In Ref. [6], the required impulse to achieve specified entry velocity V_e, flight path angle γ_e, and altitude h_E is determined as follows: The angular momentum of the descent orbit is

$$H_D = (R_e + h_e)V_e \cos\gamma_e \tag{2.1}$$

where R_e is the radius of the earth. The descent orbit's semi-major axis is

$$a_D = \frac{\mu r_e}{2\mu - r_e V_e^2} \tag{2.2}$$

with μ as the earth's gravitational constant and $r_e = R_e + h_e$. After the impulsive retrofire has been applied at original orbit altitude, h_0, the velocity of the descent orbit is

$$V_D = \sqrt{\mu(\frac{2}{R_e + h_0} - \frac{1}{a_D})} \tag{2.3}$$

and the flight path angle is

$$\gamma_D = \cos^{-1}(\frac{H_D}{(R_e + h_0)V_D}). \tag{2.4}$$

As shown in Figure 2.1, the impulse velocity is

$$\Delta V = (V_0^2 + V_D^2 - 2V_0 V_D \cos\Delta\gamma)^{\frac{1}{2}} \tag{2.5}$$

where V_0 is the velocity of the vehicle on the original orbit and $\Delta\gamma = \gamma_D - \gamma_0$ where γ_0 is the flight path angle of the vehicle on the original orbit. Figure 2.1 shows the impulse required to leave the initial orbit and enter the descending orbit. The initial position of the vehicle is denoted by R_0. The direction of the impulse is called the thrust vector direction parameter and is determined by

$$\delta = \sin^{-1}(\frac{V_D \sin\Delta\gamma}{\Delta V}). \tag{2.6}$$

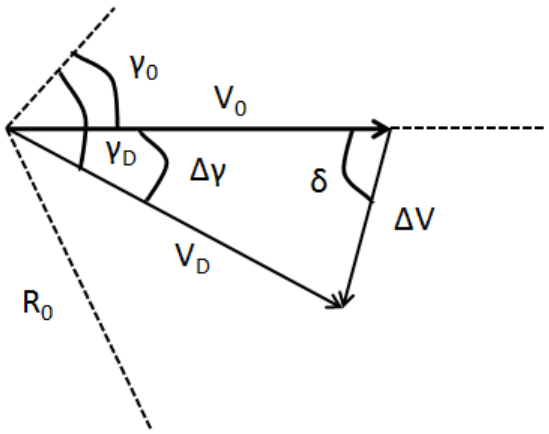

Figure 2.1 Deorbit impulse from initial orbit with velocity V_0

To find the time of the deorbit maneuver, the range covered must be determined. First note that the eccentricty of the descending orbit is

$$e_D = \sqrt{1 - \frac{p_D}{a_D}} \tag{2.7}$$

and is related to the angular momentum through p_D by

$$p_D = \frac{H_D^2}{\mu}. \tag{2.8}$$

The true anomaly, Θ_D, of the vehicle on the descent orbit at the point of impulse application comes from

$$\cos\Theta_D = \frac{p_D - (R_e + h_0)}{e_D(R_e + h_0)} \tag{2.9}$$

and

$$\sin\Theta_D = \frac{p_D \tan\gamma_D}{e_D(R_e + h_0)} \tag{2.10}$$

yielding

$$\Theta_D = \tan^{-1}(\frac{\sin\Theta_D}{\cos\Theta_D}). \tag{2.11}$$

Similarly, the true anomaly, Θ_E, at entry is

$$\cos\Theta_E = \frac{p_D - (R_e + h_e)}{e_D(R_e + h_e)} \tag{2.12}$$

and

$$\sin\Theta_E = \frac{p_D \tan\gamma_E}{e_D(R_e + h_e)} \tag{2.13}$$

yielding

$$\Theta_E = \tan^{-1}(\frac{\sin\Theta_E}{\cos\Theta_E}). \tag{2.14}$$

The angular range from deorbit to entry is

$$\rho = \Theta_E - \Theta_D. \tag{2.15}$$

The eccentric anomalies at deorbit and entry are as follows

$$\sin E_{D,E} = \frac{\sqrt{1 - e_D^2}\sin\Theta_{D,E}}{1 + e_D\cos\Theta_{D,E}} \tag{2.16}$$

and

$$\cos E_{D,E} = \frac{e_D + \cos\Theta_{D,E}}{1 + e_D\cos\Theta_{D,E}} \tag{2.17}$$

yielding

$$E_{D,E} = \tan^{-1}(\frac{\sin E_{D,E}}{\cos E_{D,E}}). \tag{2.18}$$

The time from deorbit to entry is

$$\Delta T_E = \frac{M_E - M_D}{\sqrt{\mu}}(a_D)^{\frac{3}{2}} \tag{2.19}$$

where M_D and M_E are the mean anomalies at deorbit and entry

$$M_D = E_D - e_D\sin E_D \tag{2.20}$$

$$M_E = E_E - e_D\sin E_E. \tag{2.21}$$

The ΔV determined above places the vehicle on a deorbit trajectory that will meet the required EI conditions of velocity, altitude, and flight path angle after a flight time of

Table 2.1 Results of survey of [6]

Initial Altitude (km)	ΔV (km/s)	δ (deg)	ΔT_E (sec)
6578	0.1655	-89.41	510
6588	0.1650	-87.36	3261
6598	0.1639	-85.28	3322
6608	0.1621	-83.15	3383
6618	0.1597	-80.93	3445
6628	0.1566	-78.58	3508
6638	0.1527	-76.07	3573

ΔT_E. A sample survey of this work with initial circular orbits ranging in altitude from 200 km to 260 km and EI conditions of: $V_e = 7.87$ km/s, $h_e = 120$ km, and $\gamma_E = -1$ degrees is conducted. These values are in the range of values the Shuttle would target. The results of the survey are shown in Table 2.1. The time of flight is found using the parameters of the descending orbit and the range the vehicle travels on the orbit. The time of flight to EI increases as altitude increases but the impulse decreases.

For on-orbit maneuvers such as deorbit, the Space Shuttle relies on its Orbital Maneuvering System (OMS), which consists of two engines, both capable of producing a thrust of about 6000 lb. At the typical deorbit weight of the Shuttle, the thrust-to-weight ratio by the OMS is only about 0.05 g. Using the rocket equation,

$$\Delta v = v_* \ln \frac{m_0}{m} \tag{2.22}$$

with $v_* = g_0 \cdot I_{sp}$, where g_0 is gravity at Earth's radius and I_{sp} is specific impulse of the engine, it is determined that the Shuttle is capable of producing a $\Delta V$of at most 5.48×10^{-4} km/sec [21]. Hence, to solve the guidance problem, an impulsive burn is not useful and a finite time burn must be used. A typical burn for the Shuttle returning from the International Space Station lasts anywhere from 160 to 200 seconds. For such a case, while impulsive burn approximation may be reasonable for preliminary analysis, more detailed analysis will have to include the effects of finite burn time. The farther away from apogee the vehicle is during deorbit the more effective a finite time thrust

is than an impulsive one. Also, if the altitude of the orbit is very shallow then a finite time burn is necessary to ensure the proper flight path angle is achieved at EI [2].

2.2 Single versus Multiple Burns

A rendezvous maneuver is done with multiple burns, bringing about the question of whether a multiple burn deorbit is more efficient than a single burn. The two burn maneuver is as follows: retrograde maneuver as near to the apogee of the initial orbit as possible and a second retrograde maneuver at the apogee of the second orbit as shown in Figure 2.2. This involves a total orbit period of 1.5 for the deorbit maneuver. As stated in Ref. [2], one advantage of multiple burns is that the duration of the burns is shorter, so less fuel is used. There is also a higher likelihood that multiple burns will yield less error of the total maneuver and recovery of lost opportunities at EI, such as required flight path angle. It is shown in Ref. [2] that multiple burn maneuvers lead to lower thrust durations, reduced fuel consumption, and greater maneuver time.

There are several disadvantages of using multiple burns. If fast deorbit and entry is required, the multiple burn maneuver would not be optimal because of the length of time it requires to execute the maneuver. Also, the second orbit of the maneuver is an elliptic orbit, which permits no breakdown during the next orbit period. More than two burns have been studied but no appreciable improvements are made over the two burn maneuver.

2.3 J_2 Perturbation

Ref. [2] showed that for deorbiting maneuvers, the J_2 perturbation on a coasting orbit must be taken into consideration for computation purposes. Mainly, J_2 has a profound effect on the flight path angle at EI. The flight path angle at EI is specified based on vehicle requirements. For Shuttle type vehicles, a flight path angle of approximately -1

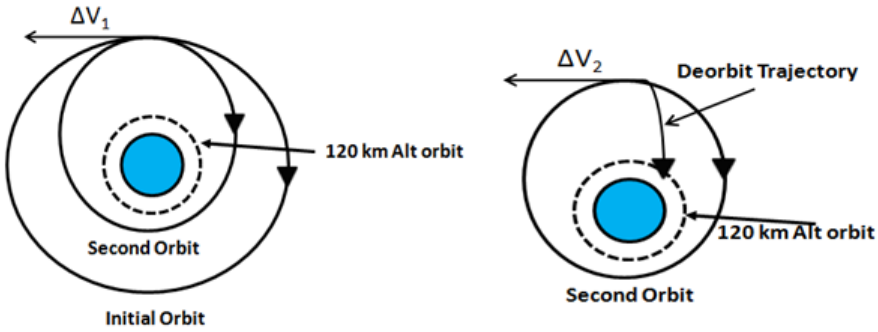

Figure 2.2 Sample two burn maneuver

Table 2.2 Effects of J_2–terms in the gravity on entry flight path angle

initial altitude (km)	2,409	2,210	2,061	1,862	1,664	1,465	1,267	1,069	871	673	475	277
fpa w/o J_2 (deg)	-1.057	-1.058	-1.052	-1.048	-1.044	-1.038	-1.036	-1.029	-1.024	-1.018	-1.011	-1.005
fpa with J_2 (deg)	-1.422	-1.413	-1.402	-1.389	-1.371	-1.353	-1.327	-1.300	-1.271	-1.234	-1.185	-1.101
percent error	34	33	33	32	31	30	28	26	24	21	17	9

degrees is desired, whereas for capsule type vehicles, a flight path angle of approximately -6 degrees is desired. A numerical analysis comparing Keplerian motion and J_2 and higher order perturbed motion shows that for orbits ranging in altitude of 2500 km to 250 km, a significant difference in final flight path angle occurs given the same initial angle. Table 2.2 shows the final results of both Keplerian and J_2-terms perturbed orbits with the same initial flight path angle of -1 degree.

From Table 2.2 it is clear that from the same initial deorbit condition, depending on whether the J_2 term is used in the numerical solutions, the EI flight path angle can

differ as much as over 30% for higher initial orbits and about 10% percent for lower orbits. Since the flight path angle is the most sensitive parameter at EI, it is imperative that the guidance system take into account the higher order effects of the gravitational field for accurate deorbit targeting, especially for deorbit missions from higher orbits. The difference in magnitude between J_2 and the next higher order term is 10^3. For this reason, only J_2 is used in modeling earth's gravitational perturbation.

2.4 Timing of the Burn

Timing deorbit such that landing at a predetermined site is accomplished and minimum fuel is burned is key to the problem. Generally, this part of the problem is solved by modifying when the burn occurs and the length of the coast arc from the end of the burn to EI. As the earth rotates, the landing site traces a circle in the Earth Centered Inertial (ECI) coordinate frame and when the orbit plane has an inclination greater than the latitude of the landing site, the orbit plane and landing site circle plane intersect as seen in Figure 2.3. Two possible intersection points are determined on this intersection line that coincide with an EI altitude of 120 km. Out of plane maneuvers have been shown to be too expensive to complete during deorbit maneuvers. If a change in inclination is needed, it is completed in the atmospheric portion of reentry. To ensure any plane change occurs in the entry portion of return flight, one of these two intersection points is targeted for EI. This may require the vehicle to orbit multiple times before burning to ensure that the landing site will line up with one of the two intersection points when the vehicle reaches EI.

Ref. [6] determines the number of orbits required by the vehicle so the targeted landing site is impacted. The number of orbits is

$$n = \frac{\Omega_0 - GHA_0 + 2\pi m + \Delta\lambda - \omega_e t_D}{\omega_e P_0 - \dot{\Omega}} \tag{2.23}$$

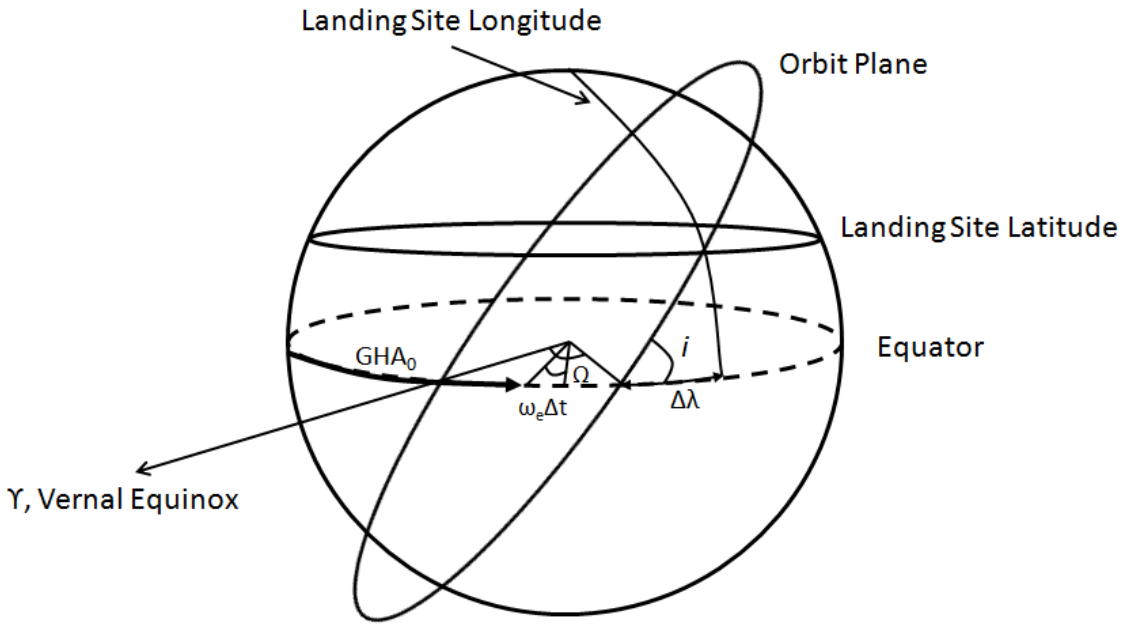

Figure 2.3 Intersection of orbit plane with landing site

where Ω_0 is the right ascension of the node at time zero, GHA_0 is the Greenwich Hour Angle of the vernal equinox at time zero, ω_e is the earth's rotation rate, m is the number of days since time zero, and t_D is the time from deorbit to impact. P_0 is the nodal period of revolution over an oblate earth found by

$$P_0 = \frac{2\pi}{\sqrt{\mu}} a^{3/2} (1 - \frac{3}{2} \frac{J_2 R_e^2}{a^2} (\frac{7\cos^2 i - 1}{4})) \tag{2.24}$$

where J_2 is the J_2 gravitational coefficient, R_e is the radius of the earth, and a is the semi-major axis of the orbit The approach from a southern direction gives

$$\Delta\lambda = \sin^{-1}(\frac{\tan lat_{LS}}{\tan i}) \tag{2.25}$$

where i is the orbit inclination and lat_{LS} is latitude of the landing site. The approach from the northern direction gives

$$\Delta\lambda = \pi - \sin^{-1}(\frac{\tan lat_{LS}}{\tan i}). \tag{2.26}$$

The nodal regression per revolution is determined by

$$\dot{\Omega} = -3\pi J_2 (\frac{R_e}{p})^2 \cos i \tag{2.27}$$

where p is the semi-latus rectum.

If the vehicle allows for an in-plane range tolerance, σ, that can be absorbed during entry then

$$n = n' - \rho \pm \sigma \tag{2.28}$$

where ρ is angular range of deorbit maneuver and n' is

$$n' = N + \frac{1}{2\pi}\Delta\lambda \tag{2.29}$$

for southern or northern approaches and N is the integer number of revolutions. The in-plane range tolerance varies from vehicle to vehicle and can span anywhere from hundreds to thousands of kilometers. This is not a mathematically precise method but can give an idea of the length of time for an initial coast before burn is activated.

After the initial coast time is estimated, when to burn must be determined. For orbit changes, a colinear impulse is to be applied at perigee for maximum change in semi-major axis [22]. The goal of the deorbit problem is not a maximum change in semi-major axis but rather a change in orbit perigee. On a circular orbit, where neither perigee or apogee is defined and the speed is constant, when to burn is determined by finding the time such that the smallest burn time is required to meet EI conditions. For an elliptic orbit this leads to an intuitive assumption that a colinear burn at apogee would yield the best minimum impulse requirement. This result does not consider a constrained velocity at EI. A sample apogee colinear burn is shown in Figure 2.4. However, Refs. [8] and [9] show that considerable fuel savings may be achieved doing a nonapogee maneuver given specific values of semi-major axis and eccentricity. Their approach involves simultaneously solving a system of polynomials. The next section gives an in depth review of the work completed in Refs. [8] and [9].

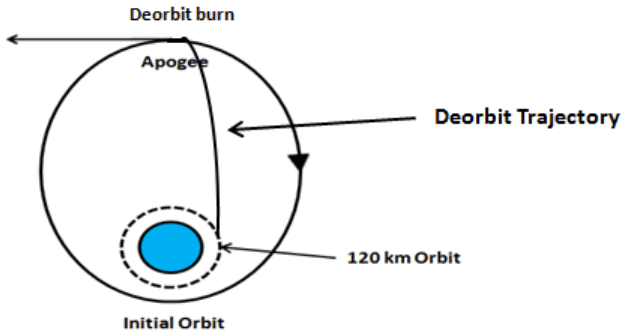

Figure 2.4 Colinear burn at apogee of elliptic orbit

2.5 Optimal Impulsive Deorbit Burn from Elliptic Orbit

As stated earlier, the timing of the deorbit burn is crucial to achieving an optimal solution for deorbit. In Ref. [8], an approach for finding the optimal deorbit position and impulse is given for an initial elliptic geocentric orbit with specified entry flight path angle and altitude criterion. This work is further generalized in Ref. [9], using a similar approach but allowing for a functional relationship between reentry speed and flight path angle. All work in these two references is done assuming Keplerian orbital motion and in plane deorbit.

The following approach is presented in Ref. [8] to determine the minimum impulse required for deorbit. The velocity impulse required to deorbit is

$$\Delta \mathbf{V} = \dot{\mathbf{r}}_{E1} - \dot{\mathbf{r}}_1 \tag{2.30}$$

where $\dot{\mathbf{r}}_1$ and$\dot{\mathbf{r}}_{E1}$ are the velocity vectors before and after the deorbit impulse. The

velocity vectors may be rewritten as

$$\dot{\mathbf{r}}_{E1} = V_{E1} \sin \gamma_{E1} \mathbf{U}_0 + V_{E1} \cos \gamma_{E1} \mathbf{V}_0 \tag{2.31}$$

$$\dot{\mathbf{r}}_1 = V_1 \sin \gamma_1 \mathbf{U}_0 + V_1 \cos \gamma_1 \mathbf{V}_0. \tag{2.32}$$

The speeds before and after deorbit are V_1 and V_{E1} with respective flight path angles γ_1 and γ_{E1}. $\mathbf{U}_0$ is a unit vector in the direction of position vector $\mathbf{r}_1$ and $\mathbf{V}_0$ is a unit vector advanced in plane 90 degrees from $\mathbf{U}_0$ in the direction of motion. Because the ΔV is impulsive, position vectors $\mathbf{r}_1$ and $\mathbf{r}_{E1}$ are identical. Define $\xi = V_1 \cos \gamma_1$ and $\eta = V_1 \sin \gamma_1$. The square of the velocity impulse may then be written as

$$\Delta V^2 = V_{E1}^2 + V_1^2 - 2\xi V_{E1} \cos \gamma_{E1} - 2\eta V_{E1} \sin \gamma_{E1}. \tag{2.33}$$

Utilizing the laws of conservation of angular momentum and energy, γ_{E1} and V_{E1} are related to reentry conditions, denoted by subscript $E1$, by

$$V_{E1}^2 = \alpha + V_{E2}^2 \tag{2.34}$$

$$V_{E1} \cos \gamma_{E1} = \lambda V_{E2} \tag{2.35}$$

where V_{E2} is the reentry velocity, $\alpha = 2\mu(1/r_{E1} - 1/r_{E2})$ and $\lambda = r_{E2}/r_{E1} \cos \gamma_{E2}$. Defining a new independent variable $\zeta = V_{E1} \sin \gamma_{E1}$, V_{E1} and V_{E2} may be rewritten as

$$V_{E1}^2 = \frac{\zeta^2 - \lambda^2 \alpha}{1 - \lambda^2} \tag{2.36}$$

$$V_{E2}^2 = \frac{\zeta^2 - \alpha}{1 - \lambda^2} \tag{2.37}$$

and

$$V_{E1} \cos \gamma_{E1} = \lambda \sqrt{\frac{\zeta^2 - \alpha}{1 - \lambda^2}}. \tag{2.38}$$

Impulse velocity may then be written as

$$\Delta V^2 = \frac{\zeta^2 - \lambda^2 \alpha}{1 - \lambda^2} - 2\xi\lambda \sqrt{\frac{\zeta^2 - \alpha}{1 - \lambda^2}} - 2\eta\zeta + V_1^2. \tag{2.39}$$

Taking the partial derivative of the above equation with respect to ζ and setting it equal to zero yields the following 4-th order polynomial

$$\zeta^4+\zeta^3(-2\eta(1-\lambda^2))+\zeta^2(-\alpha+\eta^2(1-\lambda^2)^2-\xi^2\lambda^2(1-\lambda^2))+\zeta(2\alpha\eta(1-\lambda^2))+(-\alpha\eta^2(1-\lambda^2)^2)=0. \tag{2.40}$$

The only roots of Eq. (2.40) to be considered are those that are real valued and for which $\zeta\eta \geq 0$. The condition $\zeta\eta \geq 0$ requires the orbit transfer begin on a preapogee position on reentry trajectory if deorbit maneuver takes place at a preapogee position on the initial orbit and begin on a postapogee position on reentry trajectory if deorbit maneuver takes place at a postapogee position on the initial orbit. The minimum impulse is the root that meets the stated requirements and yields the smallest value for Eq. (2.39).

To find the optimal deorbit position, the partial derivative of Eq. (2.39) with respect ν_1 is taken. First substitute the following into Eq. (2.39)

$$\xi = \frac{h}{r_1} \tag{2.41}$$

$$\eta = \sqrt{\frac{\mu}{p}} e \sin\nu_1 \tag{2.42}$$

$$V_1^2 = \mu(\frac{2}{r_1} - \frac{1}{a}) \tag{2.43}$$

$$r_1 = \frac{p}{1+e\cos\nu_1} \tag{2.44}$$

resulting in an equation with independent variables V_{E2} and ν_1. Taking the partial derivative with respect to ν_1 and setting it equal to zero gives

$$\frac{\partial \Delta V^2}{\partial \nu_1} = -4\frac{e}{p}\sin\nu_1(\mu - \lambda h V_{E2}) - 2\eta\frac{\partial\zeta}{\partial\nu_1} - 2\zeta\sqrt{\frac{\mu}{p}}e\cos\nu_1 = 0. \tag{2.45}$$

After substituting for V_{E2}

$$V_{E2}^2 = \frac{\zeta^2-\alpha}{1-\lambda^2} \tag{2.46}$$

into (2.45) a 4-th order polynomial results:

$$\zeta^4 \quad ((\frac{\eta r_1\lambda^2\sin\nu_1}{1-\lambda^2} + h\cos\nu_1)^2 - \frac{4\lambda^2h^2\sin^2\nu_1}{1-\lambda^2}) + \zeta^3(4\mu\sin\nu_1(\frac{\eta r_1\lambda^2\sin\nu_1}{1-\lambda^2} + h\cos\nu_1))$$

$$+ \quad \zeta^2(4\mu^2\sin^2\nu_1 - 2(\frac{\eta r_1\lambda^2\sin\nu_1}{1-\lambda^2} + h\cos\nu_1)(\eta\mu\sin\nu_1 + \frac{\eta\alpha r_1\lambda^2\sin\nu_1}{1-\lambda^2}) + \frac{4\alpha\lambda^2h^2\sin^2\nu_1}{1-\lambda^2})$$

$$+ \quad \zeta(-4\mu\eta\sin^2\nu_1(\mu + \frac{\alpha r_1\lambda^2}{1-\lambda^2})) + (\eta^2\sin^2\nu_1(\mu\frac{\alpha r_1\lambda^2}{1-\lambda^2})^2) = 0. \tag{2.47}$$

Solving Eqns. (2.40) and (2.47) simultaneously for ν_1 and V_{E2} yields the minimum impulse and optimal position for deorbit. The minimum impulse and position is symmetric about apogee on the elliptical orbit.

The follow-on work to Ref. [8] is presented in Ref. [9] and takes into consideration a functional relationship between reentry speed V_{E2} and reentry flight path angle γ_{E2} of the form

$$\cos\gamma_{E2} = \Gamma(V_{E2}). \tag{2.48}$$

As with the previous work, the following involves impulsive, in-plane motion. According to the laws of conservation of angular momentum and energy and using the relationship between flight path angle and velocity at reentry, the impulsive velocity vector is

$$\Delta\mathbf{V} = (\zeta - \eta)\mathbf{U}_0 + (\frac{r_2}{r_1}V_{E2}\Gamma(V_{E2}) - \xi)\mathbf{V}_0 \tag{2.49}$$

where $\mathbf{U}_0$ and $\mathbf{V}_0$ are the same as defined above, r_1 and r_2 are the deorbit and reentry radii, ξ and η are the same as previously defined, and

$$\zeta^2 = \alpha + V_{E2}^2(1 - \frac{r_2^2}{r_1^2}\Gamma(V_{E2})^2) \tag{2.50}$$

with $\alpha = 2\mu(\frac{1}{r_1} - \frac{1}{r_2})$. The impulsive velocity is the absolute value of $\Delta\mathbf{V}$, or

$$\Delta V^2 = \alpha + V_{E2}^2 + V_1^2 - \frac{2\xi r_2 V_{E2}\Gamma(V_{E2})}{r_1} - 2\eta\zeta \tag{2.51}$$

where ζ is the value of Eq. (2.50) that minimizes ΔV^2. Using Keplerian motion equations, ΔV^2 may be put in terms of ν_1. Taking the partial derivative of ΔV with respect to ν_1 and V_{E2} gives the following pair of 6-th order polynomials:

$$\Sigma_{n=0}^{6}A_n(V_{E2})\cos^n\nu_1 = 0 \tag{2.52}$$

$$\Sigma_{n=0}^{6} B_n(V_{E2}) \cos^n \nu_1 = 0 \tag{2.53}$$

where

$$\begin{aligned}
A_0 &= \beta_7\beta_1^2 - \beta_4^2 \\
A_1 &= 2\beta_7\beta_1\beta_2 + \beta_8\beta_1^2 - 2\beta_4\beta_5 \\
A_2 &= \beta_7\beta_2^2 + 2\beta_7\beta_1\beta_3 + 2\beta_8\beta_1\beta_2 + \beta_9\beta_1^2 + \beta_4^2 - \beta_5^2 - 2\beta_4\beta_6 \\
A_3 &= 2\beta_7\beta_2\beta_3 + \beta_8\beta_2^2 + 2\beta_8\beta_1\beta_3 + 2\beta_9\beta_1\beta_2 - 2\beta_5\beta_6 + 2\beta_4\beta_5 \\
A_4 &= \beta_7\beta_3^2 + 2\beta_8\beta_2\beta_3 + \beta_9\beta_2^2 + 2\beta_9\beta_1\beta_3 + \beta_5^2 - \beta_6^2 + 2\beta_4\beta_6 \\
A_5 &= \beta_8\beta_3^2 + 2\beta_9\beta_2\beta_3 + 2\beta_5\beta_6 \\
A_6 &= \beta_9\beta_3^2 + \beta_6^2
\end{aligned}$$

$$\begin{aligned}
B_0 &= \beta_7\beta_{10}^2 - \beta_8^2 \\
B_1 &= 2\beta_7\beta_{10}\beta_{11} + \beta_8\beta_{10}^2 - 4\beta_8(\beta_9 - \beta_7) \\
B_2 &= \beta_7(\beta_{11}^2 - \beta_{10}^2) + 2\beta_8\beta_{10}\beta_{11} + \beta_9\beta_{10}^2 - 4(\beta_9 - \beta_7)^2 + 6\beta_8^2 \\
B_3 &= -2\beta_7\beta_{10}\beta_{11} + \beta_8(\beta_{11}^2 - \beta_{10}^2) + 2\beta_9\beta_{10}\beta_{11} + 20\beta_8\beta_9 - 12\beta_7\beta_8 \\
B_4 &= -\beta_7\beta_{11}^2 - 2\beta_8\beta_{10}\beta_{11} + \beta_9(\beta_{11}^2 - \beta_{10}^2) - 9\beta_8^2 + 16\beta_9(\beta_9 - \beta_7) \\
B_5 &= -\beta_8\beta_{11}^2 - 2\beta_9\beta_{10}\beta_{11} - 24\beta_8\beta_9 \\
B_6 &= -\beta_9\beta_{11}^2 - 16\beta_9^2
\end{aligned}$$

in which

$$\begin{aligned}
\beta_1 &= V_{E2} - \frac{hr_2\psi}{p^2} \\
\beta_2 &= -\frac{2hr_2\psi e}{p^2} \\
\beta_3 &= -\frac{hr_2\psi e^2}{p^2} \\
\beta_4 &= \sqrt{\frac{\mu}{p}} e(V_{E2} - \frac{r_2^2\Gamma V_{E2}\psi}{p^2}) \\
\beta_5 &= -2\sqrt{\frac{\mu}{p}} \frac{e^2 r_2^2 \Gamma V_{E2}\psi}{p^2}
\end{aligned}$$

$$
\begin{aligned}
\beta_6 &= -\sqrt{\frac{\mu}{p}}\frac{e^3 r_2^2 \Gamma V_{E2}\psi}{p^2} \\
\beta_7 &= \frac{2\mu}{p} - \frac{2\mu}{r_2} + V_{E2}^2(1 - \frac{r_2^2\Gamma^2}{p^2}) \\
\beta_8 &= \frac{2\mu e}{p} - \frac{2V_{E2}^2 r_2^2 \Gamma^2 e}{p^2} \\
\beta_9 &= -\frac{V_{E2}^2 r_2^2 \Gamma^2 e^2}{p^2} \\
\beta_{10} &= \frac{4}{h}(\mu - \frac{r_2 h V_{E2}\Gamma}{p}) \\
\beta_{11} &= -\frac{4 r_2 V_{E2}\Gamma e}{p}
\end{aligned}
$$

with $\psi = \Gamma + \frac{d\Gamma}{dV_{E2}} V_{E2}$ and $h = \sqrt{\mu p}$. Solving both 6-th order polynomials simultaneously yields the optimal deorbit position.

Using the polynomials presented in Ref. [8], a numerical survey using Eq. (2.40) determined that, for certain values of periapsis altitude and entry flight path angle, non-apoapsis deorbit yields a significant savings in ΔV. The periapsis altitude is ranged from 150 to 1050 km, eccentricity is ranged from .001 to .015, and entry flight path angle spans from -1 to -8 degrees. For shallow entry flight path angles, less than 4 degrees, an apoapsis deorbit yielded minimum required ΔV for the different periapsis altitudes and eccentricities. For high periapsis altitude orbits greater than 400 km, the minimum ΔV deorbit was at the apoapsis.

Figure 2.5 shows that for cases of low orbit periapsis altitude and eccentricity, at entry flight path angles from -5.5 to -7.5 degrees, a non-apoapsis deorbit position is optimal. The variation of non-apoapsis deorbit with relation to entry flight path angle at a constant altitude is shown in Figure 2.6. The steeper the entry flight path angle at low altitude, the more likely a non-apoapsis deorbit is optimal.

The savings in ΔV of the non-apoapsis deorbit is presented in Figure 2.7. An appreciably savings is yielded in the low periapsis altitude cases of 150 and 250 km for entry flight path angle values from -5.5 to -7.5 degrees. Given a constant entry flight

path angle of -6.5 degrees, Figure 2.8 shows how the deorbit velocity varies with orbit periapsis altitude along specified eccentricities. At low periapsis altitude, low eccentricity orbits and steep entry flight path angles, a non-apoapsis deorbit position yields a significant savings in ΔV from an apoapsis deorbit. A plot relating the EI conditions of flight path angle and velocity at constant perigee altitude of 150 km for different values of eccentricity is shown in Figure 2.9.

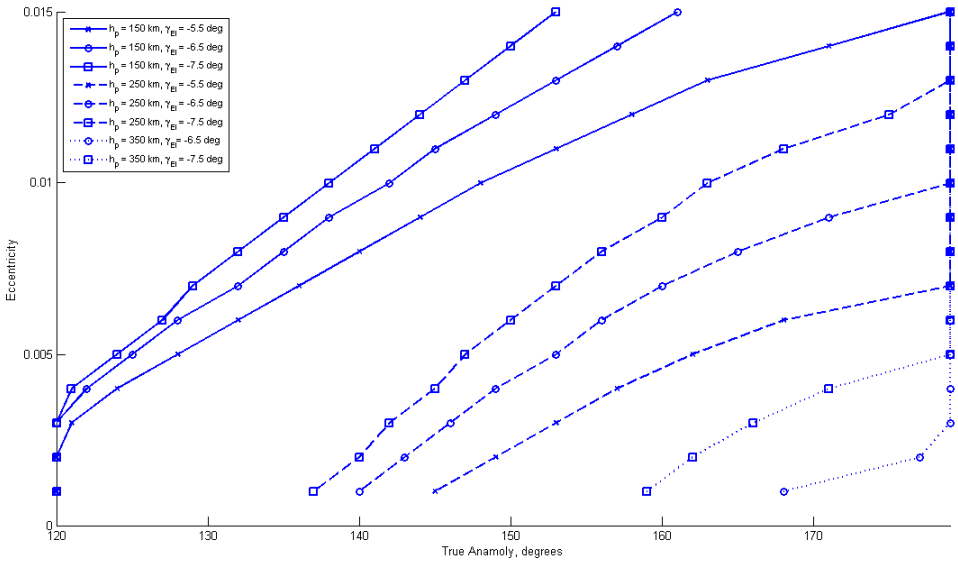

Figure 2.5 True anomaly of deorbit position for specified values of periapsis altitude and entry flight path angle

A similar numerical survey of the work in Ref. [9] is attempted. The results presented in Ref. [9], which showed a significant savings in ΔV required for deorbit for the case involving a functional relationship between V_{E2} and γ_{E2}, are relevant for semi-major axis values between 6500 km and 6454 km for an eccentricity of .01. This orbit has a periapsis altitude less than the nominal EI altitude of approximately 122 km. The 6-th order polynomials for varying values of ν_1 decrease rapidly across the ν_1 axis, practically a vertical line. This verifies that the problem is ill-posed.

As is shown above, an appreciable savings in fuel can be achieved by locating the

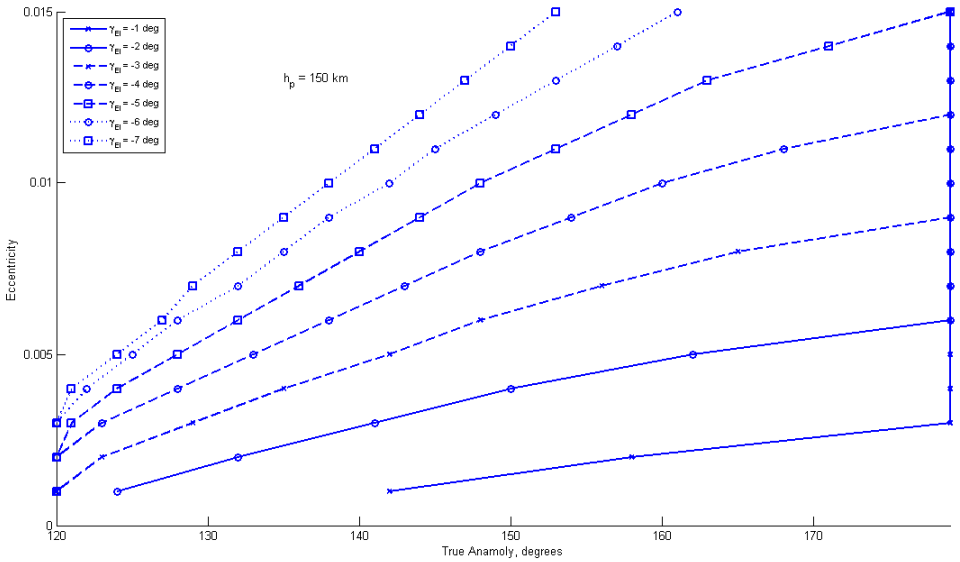

Figure 2.6 True anomaly of deorbit position for periapsis altitude of 150 km with different entry flight path angle values

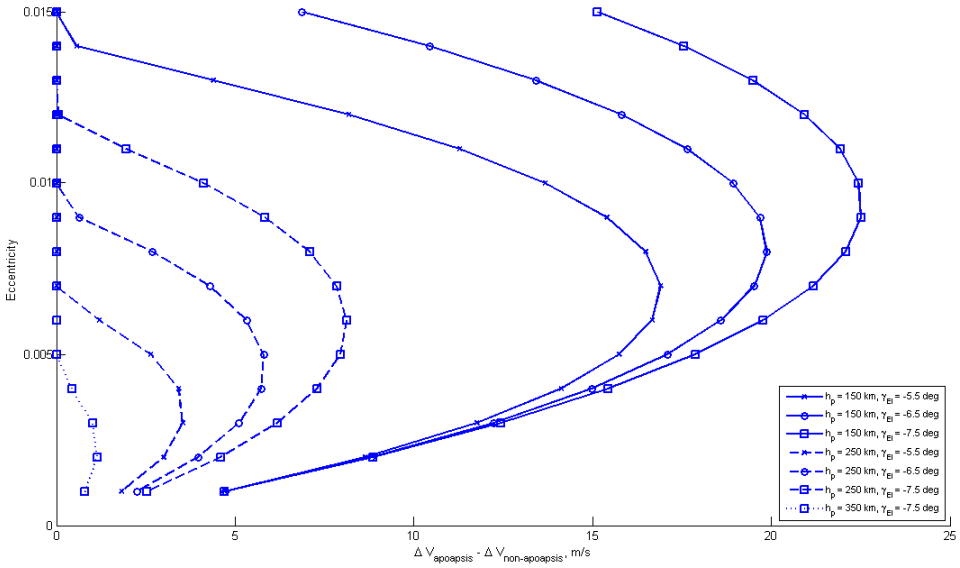

Figure 2.7 Impulse difference between deorbit at apogee and deorbit at optimal off apogee deorbit position for specified values of periapsis altitude and entry flight path angle

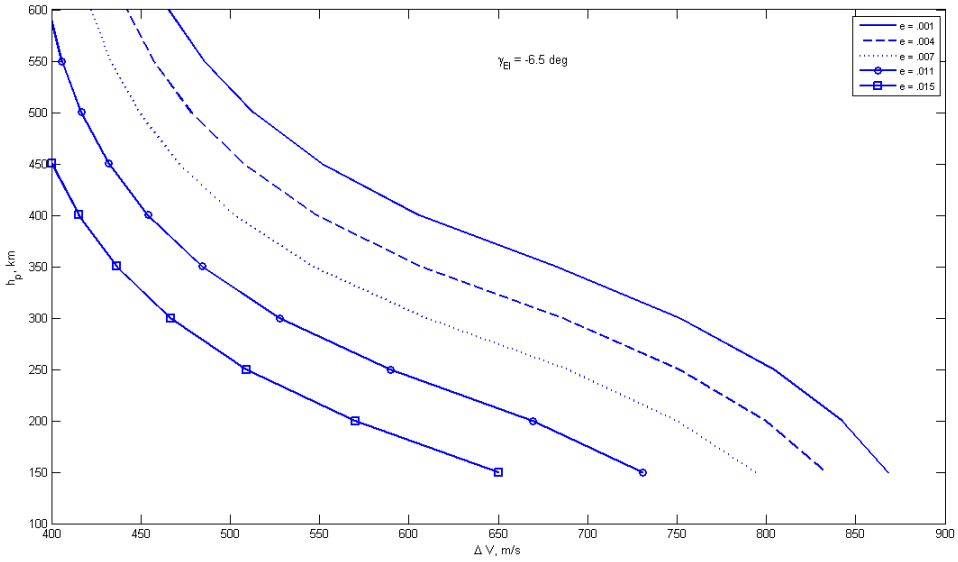

Figure 2.8 Deorbit velocity at optimum deorbit position for FPA = -6.5 degrees at different eccentricities

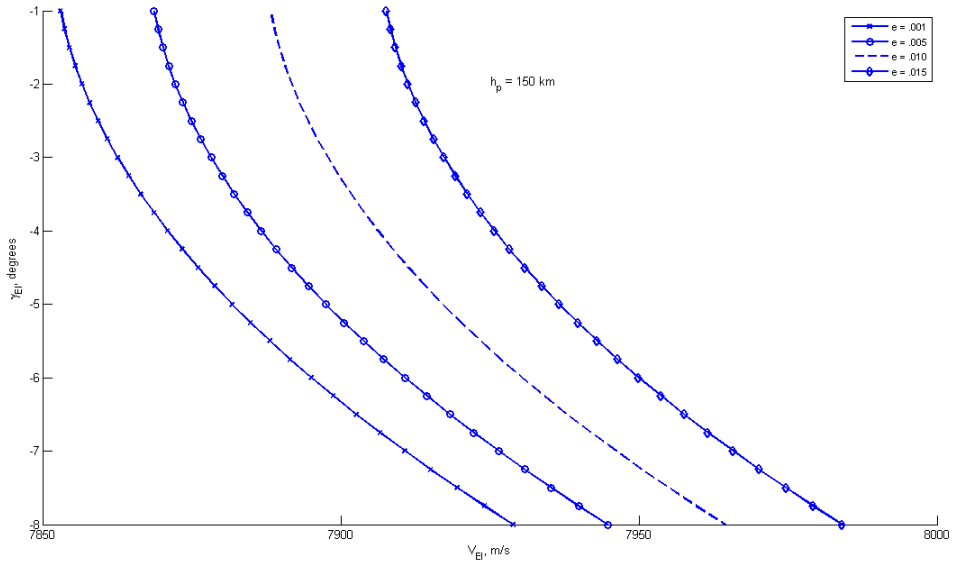

Figure 2.9 Deorbit velocity at optimum deorbit position for FPA = -6.5 degrees at different eccentricities

position of the impulse appropriately, showing that the timing of the burn is an imperative part of the solution. The above methods are not necessarily appropriate for this finite time burn problem but provide insight into the necessity of finding a method for determining the timing of the burn given any orbit.

CHAPTER 3. Finite-Thrust Deorbit Guidance Problem and Algorithm

The majority of previous work has assumed impulsive maneuvers. As is evident by NASA's Space Shuttle, this is not a realistic solution for the deorbit problem. The deorbit burn for such low thrust vehicles will last for minutes. The following sections describe the finite burn time optimal control problem to determine the thrust vector direction and magnitude, as well as the algorithm formulation. Section 1 gives the overview of the coordinate system used from the problem formulation. Section 2 gives the optimal control problem formulation for the finite time burn deorbit guidance problem. The different sets of targeting conditions for the problem are given in Section 3. The algorithm formulation is discussed in Section 4. In Section 5, the model of the Space Shuttle as well as its targeting functions are given.

3.1 Coordinate Frame

The deorbit guidance problem is solved using the Earth Centered Inertial (ECI) Coordinate System. The ECI coordinate frame has its origin at the center of the Earth and is designated with IJK. The I axis lies in the equatorial plane and is in the direction of the vernal equinox, the J axis is 90 degrees east of the I axis in the equatorial plane, and the K axis completes the right-handed system and extends north through the North Pole [19]. The ECI frame is shown in Figure 3.1.

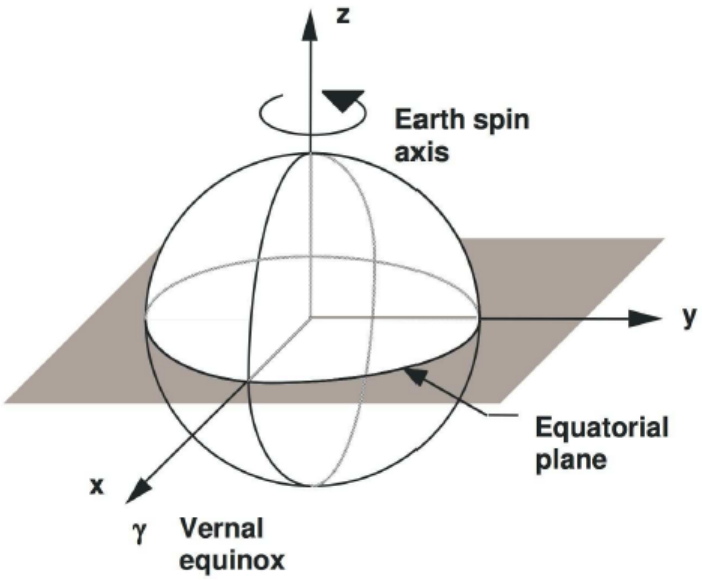

Figure 3.1 ECI coordinate system

3.2 Finite Thrust Problem Formulation

The following description of the burn-coast problem formulation is from Ref. [23]. A complete summary of the optimal control problem formulation is presented in Appendix A. The three-dimensional point-mass equations of motion in vacuum are

$$\dot{\mathbf{r}} = \mathbf{V} \tag{3.1}$$

$$\dot{\mathbf{V}} = \mathbf{g}(\mathbf{r}) + \frac{T\mathbf{1}_T}{m(t)} \tag{3.2}$$

$$\dot{m} = -\frac{T}{g_0 I_{sp}} \tag{3.3}$$

where $\mathbf{r} \in \mathbf{R}^3$ is the position vector, $\mathbf{V} \in \mathbf{R}^3$ is the inertial velocity vector in an inertial frame, and $\mathbf{g}$ is the gravitational acceleration as a function of $\mathbf{r}$. The magnitude of $\mathbf{g}$ at a reference radius, R_0, is g_0. The engine thrust magnitude is T in the direction of $\mathbf{1}_T$. The specific impulse of the engine is I_{sp} and is used to determine the mass rate $\dot{m}$. The

gravitational acceleration is approximated by

$$\mathbf{g} = -\frac{\mu}{\bar{r}^2}\frac{\mathbf{r}}{\bar{r}} = -\bar{\omega}^2\mathbf{r} \tag{3.4}$$

where μ is Earth's gravitational parameter, $\bar{r}$ is a reference radius and ω is the Schuler frequency at the reference radius, $\bar{\omega} = \sqrt{\mu/\bar{r}^3}$. The equations of motion are normalized using R_0 for distance, $\sqrt{R_0 g_0}$ for velocity, and $\sqrt{R_0/g_0}$ for time. The nondimensional equations of motion are

$$\mathbf{r}' = \mathbf{V} \tag{3.5}$$

$$\mathbf{V}' = -\omega^2\mathbf{r} + A_T\mathbf{1}_T \tag{3.6}$$

$$m' = -\frac{T}{c} \tag{3.7}$$

where the differentiation is with respect to nondimensional time, $\omega = \sqrt{R_0/\bar{r}^3}$ is nondimensional Schuler frequency, $A_T = T/(mg_0)$ is instantaneous thrust acceleration, and $c = I_{sp}/\sqrt{R_0/g_0^3}$ is a constant for each powered stage.

The EI conditions are represented as k final state conditions

$$\phi(\mathbf{r}_f, \mathbf{V}_f) = 0. \tag{3.8}$$

The performance index that is minimized by the optimal thrust direction vector $\mathbf{1}_T$ is

$$J = -\int_{\tau_0}^{\tau_f} m' d\tau = \int_{\tau_0}^{\tau_f} \frac{T}{c} d\tau, \tag{3.9}$$

a minimization of propellant-consumption for a given initial mass. The Hamiltonian is

$$\begin{aligned} H &= \mathbf{p}_r^T\mathbf{V} - \omega^2\mathbf{p}_V^T\mathbf{r} + \mathbf{p}_V^T\mathbf{1}_T A_T - p_m\frac{T}{c} - \frac{T}{c} \\ &= \mathbf{p}_r^T\mathbf{V} - \omega^2\mathbf{p}_V^T\mathbf{r} + T(\frac{\mathbf{p}_V^T\mathbf{1}_T}{mg_0} - \frac{p_m}{c} - \frac{1}{c}) := H_0 + TS. \end{aligned} \tag{3.10}$$

The costate vector is comprised of $\mathbf{p}_r$ and $\mathbf{p}_V$ and satisfies the differential equations

$$\begin{pmatrix} \mathbf{p}_r' \\ \mathbf{p}_V' \end{pmatrix} = -\begin{pmatrix} \partial H/\partial\mathbf{r} \\ \partial H/\partial\mathbf{V} \end{pmatrix} = \begin{pmatrix} \omega^2\mathbf{p}_V \\ -\mathbf{p}_r \end{pmatrix}. \tag{3.11}$$

The optimal thrust vector is in the direction $\mathbf{1}_T = \mathbf{p}_V / \parallel \mathbf{p}_V \parallel$ and $\mathbf{p}_V$ is called the primer vector. See Appendix B for complete description of the primer vector. When to coast, $T = 0$, and when to burn full thrust is determined by the switching function S.

$$T = \begin{cases} T_{max} & \text{if } S > 0 \\ 0 & \text{if } S < 0 \end{cases} \tag{3.12}$$

From the optimal control theory for the free final-time deorbit problem, $H \equiv 0$ since H is not an explicit function of time. If the optimal deorbit burn ends at τ_2, then $S(\tau_2) = 0$ necessarily. This is equivalent to

$$H_0(\tau_2) = 0. \tag{3.13}$$

3.2.1 Analytical Solution from Burn Arcs

The analytical solution to the costate equation and nondimensional equations of motion is shown. Let the starting time be represented by τ_0 and $\mathbf{p}_{V_0}$ and $\mathbf{p}_{r_0}$ are the to-be-determined initial conditions of the costate vector. Let

$$\lambda(\tau) = \begin{pmatrix} \mathbf{p}_V(\tau) \\ -\mathbf{p}_r(\tau)/\omega \end{pmatrix}, \quad \lambda_0 = \begin{pmatrix} \mathbf{p}_{V_0} \\ -\mathbf{p}_{r_0}/\omega \end{pmatrix} \tag{3.14}$$

and for $\tau \geq \tau_0$, the costate equation has the closed-form solution

$$\lambda(\tau) = \begin{bmatrix} \cos[\omega(\tau-\tau_0)]I_3 & \sin[\omega(\tau-\tau_0)]I_3 \\ -\sin[\omega(\tau-\tau_0)]I_3 & \cos[\omega(\tau-\tau_0)]I_3 \end{bmatrix} \lambda_{\mathbf{0}} := \Phi(\tau-\tau_0)\lambda_{\mathbf{0}} \tag{3.15}$$

where I_3 is the 3×3 identity matrix. Let

$$I_c(\tau,\tau_0) = \int_{\tau_0}^{\tau} \mathbf{1}_{p_V}(\zeta)\cos(\omega\zeta)A_T(\zeta)d\zeta = \int_{\tau_0}^{\tau} \mathbf{i}_c(\zeta)d\zeta \in R^3 \tag{3.16}$$

$$I_s(\tau,\tau_0) = \int_{\tau_0}^{\tau} \mathbf{1}_{p_V}(\zeta)\sin(\omega\zeta)A_T(\zeta)d\zeta = \int_{\tau_0}^{\tau} \mathbf{i}_s(\zeta)d\zeta \in R^3 \tag{3.17}$$

where $\mathbf{1}_{p_V}$ is the unit vector of $\mathbf{p}_V$. Define

$$\mathbf{x}(\tau) = \begin{pmatrix} \mathbf{r}(\tau) \\ \frac{-\mathbf{v}(\tau)}{\omega} \end{pmatrix}, \quad \mathbf{x}_0 = \begin{pmatrix} \mathbf{r}_0 \\ \frac{-\mathbf{v}_0}{\omega} \end{pmatrix}, \quad \mathbf{I}(\tau,\tau_0) = \begin{bmatrix} \mathbf{I}_c(\tau,\tau_0) \\ \mathbf{I}_s(\tau,\tau_0) \end{bmatrix}. \tag{3.18}$$

The state equations have the solution

$$\mathbf{x}(\tau) = \Phi(\tau - \tau_0)\mathbf{x}_0 + \Gamma(\tau)\mathbf{I}(\tau, \tau_0) \tag{3.19}$$

where

$$\Gamma(\tau) = \frac{1}{\omega}\begin{bmatrix} \sin(\omega\tau)I_3 & -\cos(\omega\tau)I_3 \\ \cos(\omega\tau)I_3 & \sin(\omega\tau)I_3 \end{bmatrix}\lambda_{\mathbf{0}}. \tag{3.20}$$

The thrust integrals $\mathbf{I}_c$ and $\mathbf{I}_s$ are evaluated using a quadrature formula, which is shown to be accurate enough for powered flight arcs up to several hundred seconds. Milne's rule is used with the following formulation:

$$\begin{aligned} I_j(\tau, \tau_0) &\approx \frac{\tau - \tau_0}{90}[7\mathbf{i}_j(\tau_0) + 32\mathbf{i}_j(\tau_0 + \delta) \\ &+ 12\mathbf{i}_j(\tau_0 + 2\delta) + 32\mathbf{i}_j(\tau_0 + 3\delta) + 7\mathbf{i}_j(\tau_0 + 4\delta)] \end{aligned} \tag{3.21}$$

for $j = \mathbf{c}, \mathbf{s}$.

3.2.2 Solution for Coast Arcs

An inverse-square gravity model is used for the solution of Keplerian motion during the first coast arcs. The accuracy of the solution is not affected by the linear gravity approximation. Goodyear's method, presented in Ref. [24], is used to solve the Kepler initial value problem and yields the result of the future state and it's gradients as functions of current state. The solution of the costate is propagated using Eq. (3.15).

When the J_2 gravitational term is added as part of the gravity model, the final coast from the end of the final burn to entry interface is modeled using an inverse-square gravity model with the addition of the J_2 gravitational effects [25]. This is modeled as

$$\ddot{x} = -\mu\frac{x}{r^3}[1 - J_2\frac{3}{2}(\frac{r_0}{r})^2(5\frac{Z^2}{r^2} - 1)] \tag{3.22}$$

$$\ddot{y} = -\mu\frac{y}{r^3}[1 - J_2\frac{3}{2}(\frac{r_0}{r})^2(5\frac{Z^2}{r^2} - 1)] \tag{3.23}$$

$$\ddot{z} = -\mu\frac{z}{r^3}[1 - J_2\frac{3}{2}(\frac{r_0}{r})^2(5\frac{Z^2}{r^2} - 3)] \tag{3.24}$$

The solution is determined via numerical integration and the gradients are found using a finite difference method. Without the J_2 gravitational term, Goodyear's method finds the solution using the analytical solution. The addition of the J_2 gravitational term means the solution must be solved for using numerical integration. The numerical integration scheme used is a 4-th order Runge-Kutta method. This is a key difference between whether or not the J_2 gravitational term is included. Numerical integration is computationally intensive and therefore adds a great deal of time to the solution process.

3.3 EI Targeting Conditions

The targeting conditions are a very important part of the deorbit guidance problem because they ensure a safe reentry flight. The following sections describe different sets of EI targeting conditions and their formulation.

Let $\mathbf{V}_f$ and $\mathbf{r}_f$ be the position and velocity vector at EI following the deorbit trajectory. Define $\mathbf{1}_{HAC}$ to be the unit vector from the origin of the coordinate system to the location of the landing site. $\mathbf{1}_{HAC}$ is a function of time, moving in the ECI coordinate frame as the Earth rotates. See Fig. 3.2 for the geometry.

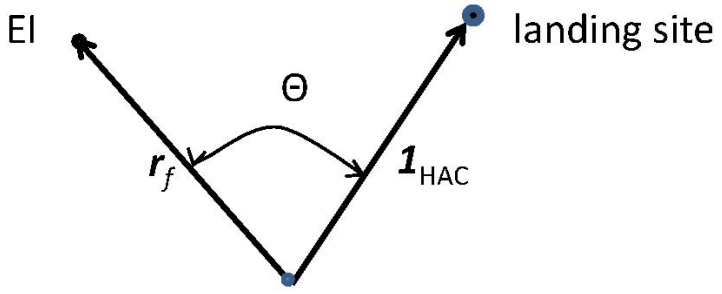

Figure 3.2 EI range-to-go landing site

To begin with, define a vector

$$\mathbf{R}_h = \mathbf{r}_f \times \mathbf{1}_{HAC}. \tag{3.25}$$

$\mathbf{R}_h$ is perpendicular to $\mathbf{r}_f$ and $\mathbf{1}_{HAC}$ and in the same plane as $\mathbf{r}_f$ and $\mathbf{1}_{HAC}$.

3.3.1 EI Targeting Conditions with Specified Functions for EI velocity and flight path angle (Set 1)

The terminal conditions to be met at the EI are defined as follows:

$$s_1 = \frac{1}{2}\mathbf{r}_f^T\mathbf{r}_f - \frac{1}{2}r_{EI}^2 = 0 \tag{3.26}$$

$$s_2 = \mathbf{V}_f^T\mathbf{R}_h = 0 \tag{3.27}$$

$$s_3 = \mathbf{V}_f^T\mathbf{r}_f - V_f r_{EI}\sin\gamma^*(\Theta_f) = 0 \tag{3.28}$$

$$s_4 = \frac{1}{2}\mathbf{V}_f^T\mathbf{V}_f - \frac{1}{2}V^{*2}(\Theta_f) = 0. \tag{3.29}$$

The first constraint simply sets the EI altitude to be equal to the given value r_{EI}, which gives an altitude of 120 km. The second constraint requires the velocity vector at EI to be in the same plane of $\mathbf{r}_f$ and $\mathbf{1}_{HAC}$. This ensures that the velocity vector of the vehicle at EI is pointed towards the landing site. For most deorbit scenarios, this constraint is met without any problems. For some scenarios such as when the vehicle's orbit has an inclination smaller than the landing site latitude, an out-of-plane maneuver would be necessary. Out-of-plane maneuvers are very costly in terms of fuel consumption but are necessary for some scenarios. For those cases, Eq. (3.27) ensures that the crossrange distance to the landing site is kept small and within the range of the lifting capability of the vehicle. Constraints Eqs. (3.28) and (3.29) require that the EI flight path angle and velocity be equal to certain values determined by the range angle Θ_f at EI, defined by (see Fig. 3.2 for the geometry)

$$\cos\Theta_f = \mathbf{1}_{r_f}^T\mathbf{1}_{HAC} \tag{3.30}$$

where $\mathbf{1}_{r_f} = \mathbf{r}_f / r_f$. The functions $\gamma^*(\Theta_f)$ and $V^*(\Theta_f)$ are two given functions (but otherwise can have any functional form) of Θ_f. For a specific vehicle, these two functions will define how the EI conditions on γ and V are expected to vary as the range from EI to the landing site changes as a result of different deorbit maneuvers. The known practice for the Space Shuttle can be easily included in this formulation as a special case. For instance, V and γ are specified as

$$V^*(\Theta_f) = a_1 \Theta_f + a_2 \tag{3.31}$$

$$\gamma^*(\Theta_f) = b_1 \Theta_f + b_2 \tag{3.32}$$

where a_1, a_2, b_1 and b_2 are constants. Then Eqs. (3.28) and (3.29) imply that

$$V_f = V^* = a_1 \Theta_f + a_2 \tag{3.33}$$

$$\gamma_f = \gamma^* = b_1 \Theta_f + b_2. \tag{3.34}$$

Eliminating Θ_f between the two equations gives

$$a_1 \gamma_f - b_1 V_f - b_2 + a_2 b_2 := c_1 \gamma_f + c_2 V_f + c_3 = 0 \tag{3.35}$$

This is a linear relationship between γ_f and V_f, just as is done for the Shuttle [4]. Our current formulation in Eqs. (3.28) and (3.29), however, allows much more flexibility to accommodate different evaluations of desired EI conditions and offers a mechanism to relate the EI velocity to range condition, which will be crucial for the minimum-fuel problem of deorbiting to be well posed.

Let us first consider the targeting conditions Eqs. (3.26)–(3.29). The transversality conditions on the co-state vectors corresponding to the terminal constraints Eqs. (3.26)–(3.29) are

$$\begin{aligned} \mathbf{p}_{r_f} &= \nu_1 \frac{\partial s_1}{\partial \mathbf{r}_f} + \nu_2 \frac{\partial s_2}{\partial \mathbf{r}_f} + \nu_3 \frac{\partial s_3}{\partial \mathbf{r}_f} + \nu_4 \frac{\partial s_4}{\partial \mathbf{r}_f} = \nu_1 \mathbf{r}_f + \nu_2 \mathbf{R}_V \\ &+ \nu_3 \left(\mathbf{V}_f - V_f r_{EI} \gamma^{*\prime} \cos\gamma^* \frac{\partial \Theta_f}{\partial \mathbf{r}_f} \right) - \nu_4 V^* V^{*\prime} \frac{\partial \Theta_f}{\partial \mathbf{r}_f} \end{aligned} \tag{3.36}$$

$$\begin{aligned}\mathbf{p}_{V_f} &= \nu_1\frac{\partial s_1}{\partial \mathbf{V}_f} + \nu_2\frac{\partial s_2}{\partial \mathbf{V}_f} + \nu_3\frac{\partial s_3}{\partial \mathbf{V}_f} + \nu_4\frac{\partial s_4}{\partial \mathbf{V}_f} \\ &= \nu_2\mathbf{R}_h + \nu_3\left(\mathbf{r}_f - \mathbf{1}_{V_f} r_{EI}\sin\gamma^*\right) + \nu_4\mathbf{V}_f\end{aligned} \tag{3.37}$$

where $\mathbf{1}_{V_f} = \mathbf{V}_f/V_f$, and

$$\mathbf{R}_V = \mathbf{1}_{HAC} \times \mathbf{V}_f \tag{3.38}$$

$$\gamma^{*\prime} = \frac{\partial\gamma^*(\Theta_f)}{\partial\Theta_f} \tag{3.39}$$

$$V^{*\prime} = \frac{\partial V^*(\Theta_f)}{\partial\Theta_f}. \tag{3.40}$$

Recall that $\cos\Theta_f = \mathbf{1}_{HAC}\cdot\mathbf{r}_f/r_f$, and taking the gradient of Θ_f with respect to $\mathbf{r}_f$ gives

$$\frac{\partial\Theta_f}{\partial\mathbf{r}_f} = -\frac{1}{\sin\Theta_f}\cdot\frac{1}{r_f}(\mathbf{1}_{HAC} - \cos\Theta_f\mathbf{1}_{r_f}). \tag{3.41}$$

This equation indicates that $\partial\Theta_f/\partial\mathbf{r}_f$ is a vector in the plane of $\mathbf{1}_{HAC}$ and $\mathbf{1}_{r_f}$.

The above transversality conditions contain additional unknown multipliers ν_1–ν_4. Not only do they increase the number of unknowns needed to be solved, but their magnitudes may differ significantly from those of the state and costate variables. The latter makes the numerical solution much more difficult. In the following, the multipliers are eliminated from the equations and two more independent terminal conditions are derived that do not involve the multipliers. Consider first the dot product

$$\begin{aligned}\mathbf{R}_h^T\mathbf{p}_{r_f} &= \nu_1\mathbf{R}_h^T\mathbf{r}_f + \nu_2\mathbf{R}_h^T\mathbf{R}_V + \nu_3\left(\mathbf{R}_h^T\mathbf{V}_f - V_f r_{EI}\gamma^{*\prime}\cos\gamma^*\mathbf{R}_h^T\frac{\partial\Theta_f}{\partial\mathbf{r}_f}\right) \\ &- \nu_4 V^* V^{*\prime}\mathbf{R}_h^T\frac{\partial\Theta_f}{\partial\mathbf{r}_f}.\end{aligned} \tag{3.42}$$

From Eq. (3.27) we have $\mathbf{R}_h^T\mathbf{V}_f = 0$ and by the definition of $\mathbf{R}_h$ we know $\mathbf{R}_h^T\mathbf{r}_f = 0$, and $\mathbf{R}_h^T\partial\Theta_f/\partial\mathbf{r}_f = 0$ because of Eq. (3.41) (and $\mathbf{R}_h \perp \mathbf{1}_{HAC}$ as well). These observations lead to

$$\mathbf{R}_h^T\mathbf{p}_{r_f} = \nu_2\mathbf{R}_h^T\mathbf{R}_V. \tag{3.43}$$

Considering the following dot product and using similar reasoning results in

$$\mathbf{R}_h^T\mathbf{p}_{V_f} = \nu_2\mathbf{R}_h^T\mathbf{R}_h + \nu_3(\mathbf{R}_h^T\mathbf{r}_f - \mathbf{R}_h^T\mathbf{1}_{V_f}r_{EI}\sin\gamma^*) + \nu_4\mathbf{R}_h^T\mathbf{V}_f = \nu_2\mathbf{R}_h^T\mathbf{R}_h. \tag{3.44}$$

Eliminating ν_2 between Eqs. (3.43) and (3.44) yields the 5-th terminal constraint free of the multipliers:

$$s_5 = (\mathbf{R}_h^T \mathbf{R}_h)\mathbf{R}_h^T \mathbf{p}_{r_f} - (\mathbf{R}_h^T \mathbf{p}_{V_f})(\mathbf{R}_h^T \mathbf{R}_V) = 0. \tag{3.45}$$

Next, define

$$\mathbf{R}_{hr} = \mathbf{R}_h \times \mathbf{r}_f \tag{3.46}$$

$$\mathbf{R}_{hV} = \mathbf{R}_h \times \mathbf{V}_f. \tag{3.47}$$

The first vector above is in the plane of $\mathbf{1}_{HAC}$ and $\mathbf{1}_{r_f}$ and perpendicular to $\mathbf{r}_f$. By constraint Eq. (3.27), $\mathbf{V}_f$ is in the plane of $\mathbf{1}_{HAC}$ and $\mathbf{r}_f$ and by the definition of $\mathbf{R}_V$ in Eq. (3.38) we have $\mathbf{R}_{hr}^T \mathbf{R}_V = 0$. The second vector $\mathbf{R}_{hV}$ is also in the plane of $\mathbf{1}_{HAC}$ and $\mathbf{r}_f$ when constraint Eq. (3.27) is met and it is perpendicular to $\mathbf{V}_f$. Taking the dot product $\mathbf{R}_{hr}$ with $\mathbf{p}_{r_f}$ in Eq. (3.37) produces

$$\mathbf{R}_{hr}^T \mathbf{p}_{r_f} = \nu_3 \left(\mathbf{R}_{hr}^T \mathbf{V}_f - V_f r_{EI} \gamma^{*\prime} \cos\gamma^* \mathbf{R}_{hr}^T \frac{\partial \Theta_f}{\partial \mathbf{r}_f} \right) - \nu_4 V^* V^{*\prime} \mathbf{R}_{hr}^T \frac{\partial \Theta_f}{\partial \mathbf{r}_f} \tag{3.48}$$

where, because $\mathbf{R}_{hr}^T \mathbf{r}_f = 0$,

$$\mathbf{R}_{hr}^T \frac{\partial \Theta_f}{\partial \mathbf{r}_f} = -\frac{1}{\sin\Theta_f} \frac{1}{r_f} (\mathbf{R}_{hr}^T \mathbf{1}_{HAC}) = -\frac{1}{\sin\Theta_f} \frac{1}{r_{EI}} \mathbf{R}_{hr}^T \mathbf{1}_{HAC}. \tag{3.49}$$

Therefore,

$$\mathbf{R}_{hr}^T \mathbf{p}_{r_f} = \nu_3 \left(\mathbf{R}_{hr}^T \mathbf{V}_f + \frac{V_f \gamma^{*\prime} \cos\gamma^*}{\sin\Theta_f} \mathbf{R}_{hr}^T \mathbf{1}_{HAC} \right) + \nu_4 \frac{V^* V^{*\prime}}{r_{EI} \sin\Theta_f} \mathbf{R}_{hr}^T \mathbf{1}_{HAC}. \tag{3.50}$$

Similarly, the dot product of $\mathbf{p}_{V_f}$ by $\mathbf{R}_{hV}$ yields

$$\mathbf{R}_{hV}^T \mathbf{p}_{V_f} = \nu_3 (\mathbf{R}_{hV}^T \mathbf{r}_f). \tag{3.51}$$

Finally, taking the dot product of $\mathbf{p}_{V_f}$ with $\mathbf{V}_f$ and using constraints Eq. (3.27) and Eq. (3.28) arrives at

$$\mathbf{V}_f^T \mathbf{p}_{V_f} = \nu_4 V_f^2. \tag{3.52}$$

Using Eqs. (3.51) and (3.52) to solve for ν_3 and ν_4, respectively, and substituting them back to Eq. (3.50), the end result is the 6-th terminal constraint independent of the multipliers

$$\begin{aligned} s_6 &= \mathbf{R}_{hr}^T \mathbf{p}_{r_f} - \frac{\mathbf{R}_{hV}^T \mathbf{p}_{V_f}}{\mathbf{R}_{hV}^T \mathbf{r}_f} \left(\mathbf{R}_{hr}^T \mathbf{V}_f + \frac{V_f \gamma^{*\prime} \cos\gamma^*}{\sin\Theta_f} \mathbf{R}_{hr}^T \mathbf{1}_{HAC} \right) \\ &- \frac{V^{*\prime} (\mathbf{V}_f^T \mathbf{p}_{V_f})(\mathbf{R}_{hr}^T \mathbf{1}_{HAC})}{V_f r_{EI} \sin\Theta_f} = 0. \end{aligned} \tag{3.53}$$

The 7-th terminal constraint for this free final-time problem is based on the transversality condition of $H(\tau_f) = 0$. The last arc in the deorbit maneuver is a coast arc where $T = 0$, $H = H_0$ during this coast arc, and H_0 is the part of the Hamiltonian independent of the thrust, as defined in Eq. (3.10). Therefore, the 7th terminal constraint is

$$s_7 = H_0(\tau_f) = \mathbf{p}_{r_f}^T \mathbf{V}_f + \mathbf{p}_{V_f}^T \mathbf{g}(\mathbf{r}_f) = 0. \tag{3.54}$$

3.3.2 EI Targeting Conditions with Specified Range-To-Go (Set 2)

It may be beneficial to explicitly define the range-to-go from the EI to the landing site [2]. Let Θ^* be such a specified range angle. Another set of possible targeting conditions are as follows

$$s_1 = \frac{1}{2} \mathbf{r}_f^T \mathbf{r}_f - \frac{1}{2} r_{EI}^2 = 0 \tag{3.55}$$

$$s_2 = \mathbf{V}_f^T \mathbf{R}_h = 0 \tag{3.56}$$

$$s_3 = \mathbf{1}_{HAC}^T \mathbf{r}_f - r_{EI} \cos\Theta^* = 0 \tag{3.57}$$

$$s_4 = f(V_f,\ \gamma_f) = 0 \tag{3.58}$$

where $f(V_f,\ \gamma_f)$ is a function of V_f and γ_f, the EI velocity and flight path angle. Eq. (3.58) is vehicle dependent. For the Shuttle, $f = V_f + k_1 \gamma_f + k_2$ with two constants k_1 and k_2. Conceivably, the relationship between V_f and γ_f can be nonlinear and this formulation allows for any such function. Constraint Eq. (3.57) specifies that the EI

range to landing site must be equal to Θ^*. In this case the transversality conditions are

$$\mathbf{p}_{r_f} = \nu_1 \mathbf{r}_f + \nu_2 \mathbf{R}_V + \nu_3 \mathbf{1}_{HAC} + \nu_4 f_\gamma \frac{\partial \gamma_f}{\partial \mathbf{r}_f} \tag{3.59}$$

$$\mathbf{p}_{V_f} = \nu_2 \mathbf{R}_h + \nu_4 \left(f_V \mathbf{1}_{V_f} + f_\gamma \frac{\partial \gamma_f}{\partial \mathbf{V}_f} \right) \tag{3.60}$$

where $f_\gamma = \partial f / \partial \gamma_f$ and $f_V = \partial f / \partial V_f$. From the relationship $\mathbf{r}_f^T \mathbf{V}_f = r_f V_f \sin \gamma_f$, we can show that

$$\frac{\partial \gamma_f}{\partial \mathbf{r}_f} = \frac{1}{r_f V_f \cos \gamma_f} \left[\mathbf{V}_f - (\mathbf{1}_{r_f}^T \mathbf{V}_f) \mathbf{1}_{r_f} \right] \tag{3.61}$$

$$\frac{\partial \gamma_f}{\partial \mathbf{V}_f} = \frac{1}{r_f V_f \cos \gamma_f} \left[\mathbf{r}_f - (\mathbf{1}_{V_f}^T \mathbf{r}_f) \mathbf{1}_{V_f} \right] \tag{3.62}$$

i.e., both $\partial \gamma_f / \partial \mathbf{r}_f$ and $\partial \gamma_f / \partial \mathbf{r}_f$ are in the plane of $\mathbf{r}_f$ and $\mathbf{V}_f$. Using the same reasoning it can be argued that s_5 in Eq. (3.45) remains valid in this case, but not s_6 in Eq. (3.54). Instead, taking the dot product of $\mathbf{p}_{V_f}$ in Eq. (3.60) with $\mathbf{r}_f$ and $\mathbf{V}_f$, respectively, gives

$$\begin{aligned} \mathbf{r}_f^T \mathbf{p}_{V_f} &= \nu_4 \left\{ f_V (\mathbf{1}_{V_f}^T \mathbf{r}_f) + \frac{f_\gamma}{r_f V_f \cos \gamma_f} \left[r_f^2 - (\mathbf{1}_{V_f}^T \mathbf{r}_f)^2 \right] \right\} \\ &= \nu_4 \left\{ f_V (\mathbf{1}_{V_f}^T \mathbf{r}_f) + \frac{f_\gamma}{r_{EI} V_f \cos \gamma_f} \left[r_{EI}^2 - (\mathbf{1}_{V_f}^T \mathbf{r}_f)^2 \right] \right\} \end{aligned} \tag{3.63}$$

$$\mathbf{V}_f^T \mathbf{p}_{V_f} = \nu_4 f_V V_f. \tag{3.64}$$

Eliminating ν_4 between them gives a different s_6

$$\begin{aligned} s_6 &= f_V r_{EI} V_f^2 \cos \gamma_f \left(\mathbf{r}_f^T \mathbf{p}_{V_f} \right) \\ &- \left(\mathbf{V}_f^T \mathbf{p}_{V_f} \right) \left\{ r_{EI} V_f \cos \gamma_f f_V \left(\mathbf{1}_{V_f}^T \mathbf{r}_f \right) + f_\gamma \left[r_{EI}^2 - \left(\mathbf{1}_{V_f}^T \mathbf{r}_f \right)^2 \right] \right\} = 0. \end{aligned} \tag{3.65}$$

The expression for s_7 in Eq. (3.54) remains valid since the problem is still a free final-time problem.

3.3.3 EI Targeting Conditions without Crossrange Distance Constraint

The crossrange distance constraint, Eqs. (3.27) and (3.56), is very hard to satisfy. By timing the deorbit flight to limit the crossrange distance, this constraint can be deleted.

By waiting for the $\mathbf{1}_{HAC}$ of the rotating Earth to be within a certain tolerance of the orbit plane at the end of deorbit flight, the crossrange distance is minimized.

3.3.3.1 EI Targeting Conditions with Specified Functions for EI velocity and flight path angle (Set 3)

Let the first three constraints be the same constraints from the first set of targeting conditions with the exception of Eq. (3.27):

$$s_1 = \frac{1}{2}\mathbf{r}_f^T\mathbf{r}_f - \frac{1}{2}r_{EI}^2 = 0 \tag{3.66}$$

$$s_2 = \mathbf{V}_f^T\mathbf{r}_f - V_f r_{EI}\sin\gamma^*(\Theta_f) = 0 \tag{3.67}$$

$$s_3 = \frac{1}{2}\mathbf{V}_f^T\mathbf{V}_f - \frac{1}{2}V^{*2}(\Theta_f) = 0 \tag{3.68}$$

The transversality equations are

$$\mathbf{p}_{r_f} = \nu_1\mathbf{r}_f + \nu_2\left(\mathbf{V}_f - V_f r_{EI}\gamma^{*\prime}\cos\gamma^*\frac{\partial\Theta_f}{\partial\mathbf{r}_f}\right) - \nu_3 V^* V^{*\prime}\frac{\partial\Theta_f}{\partial\mathbf{r}_f} \tag{3.69}$$

$$\mathbf{p}_{V_f} = \nu_2\left(\mathbf{r}_f - \mathbf{1}_{V_f} r_{EI}\sin\gamma^*\right) + \nu_3\mathbf{V}_f. \tag{3.70}$$

Define

$$\mathbf{R}_{hr} = \mathbf{R}_h \times \mathbf{r}_f \tag{3.71}$$

which is a vector in the plane of $\mathbf{r}_f$ and $\mathbf{1}_{HAC}$ and perpendicular to $\mathbf{r}_f$ and

$$\mathbf{R}_{\Theta_{HAC}} = \mathbf{R}_{\Theta_f} \times \mathbf{1}_{HAC} \times \mathbf{R}_{\Theta_f} \tag{3.72}$$

where

$$\mathbf{R}_{\Theta_f} = \mathbf{1}_{HAC} - \cos\Theta_f \mathbf{1}_{r_f}. \tag{3.73}$$

$\mathbf{R}_{\Theta_{HAC}}$ is in the plane of $\mathbf{r}_f$ and $\mathbf{1}_{HAC}$ and perpendicular to $\mathbf{R}_{\Theta_f}$. Taking the dot product of $\mathbf{R}_h$ with Eq. (3.70) yields

$$\mathbf{R}_h^T\mathbf{p}_{r_f} = \mathbf{R}_h^T\mathbf{V}_f\nu_2 \tag{3.74}$$

since $\mathbf{R}_h^T \mathbf{r}_f = 0$ and $\mathbf{R}_h^T \mathbf{R}_{\Theta_f} = 0$. The dot product of $\mathbf{V}_f$ with Eq. (3.70) gives

$$\mathbf{V}_f^T \mathbf{p}_{V_f} = V_f^2 \nu_3 \tag{3.75}$$

since $\left(\mathbf{r}_f - \mathbf{1}_{V_f} r_{EI} \sin\gamma^*\right) = 0$ by Eq. (3.67). Eq. (3.74) is solved for ν_2 and Eq. (3.75) is solved for ν_3. Taking the dot product of $\mathbf{R}_h$ with Eq. (3.70) and $\mathbf{R}_{hr}$ with Eq. (3.70) and substituting in for ν_2 and ν_3 gives a 4-th and 5-th terminal condition

$$s_4 = V_f \mathbf{R}_h^T \mathbf{p}_{V_f} - r_{EI} \sin\gamma^*(\Theta_f)(\mathbf{R}_h^T \mathbf{p}_{r_f}) - (\mathbf{R}_h^T \mathbf{1}_{V_f})(\mathbf{V}_f^T \mathbf{p}_{V_f}) = 0 \tag{3.76}$$

$$\begin{aligned} s_5 = {} & (\mathbf{R}_{h_r}^T \mathbf{p}_{r_f})(\mathbf{R}_h^T \mathbf{V}_f) \sin\Theta_f - (\mathbf{R}_h^T \mathbf{p}_{r_f})(\mathbf{R}_{h_r}^T \mathbf{V}_f \sin\Theta_f + \mathbf{R}_{h_f}^T \mathbf{1}_{HAC} V_f \cos\gamma^*(\Theta_f)\gamma^{*\prime}) \\ & -(\mathbf{R}_h^T \mathbf{V}_f)(\mathbf{R}_{h_r}^T \mathbf{1}_{HAC}) \frac{V^{*\prime} V^*}{r_f} \frac{\mathbf{V}_f^T \mathbf{p}_{V_f}}{V_f^2} = 0. \end{aligned} \tag{3.77}$$

Define

$$\mathbf{R}_{\Theta_V} = \mathbf{R}_{\Theta_f} \times \mathbf{V}_f$$

which is perpendicular to $\mathbf{R}_{\Theta_f}$ and $\mathbf{V}_f$. Taking the dot product of $\mathbf{R}_{\Theta_V}$ with Eq. (3.70) gives

$$\mathbf{R}_{\Theta_V}^T \mathbf{p}_{r_f} = \mathbf{R}_{\Theta_V}^T \mathbf{r}_f \nu_1 \tag{3.78}$$

since $\mathbf{R}_{\Theta_V}^T \mathbf{R}_{\Theta_f} = 0$ and $\mathbf{R}_{\Theta_V}^T \mathbf{V}_f = 0$. The dot product of $\mathbf{R}_{\Theta_{HAC}}$ and Eq. (3.70) is

$$\mathbf{R}_{\Theta_{HAC}}^T \mathbf{p}_{r_f} = \mathbf{R}_{\Theta_{HAC}}^T \mathbf{r}_f \nu_1 + \mathbf{R}_{\Theta_{HAC}}^T \mathbf{V}_f \nu_2. \tag{3.79}$$

Solving Eq. (3.78) for ν_1 and ν_2 found above and substituting them into Eq. (3.79) gives the 6-th terminal condition

$$\begin{aligned} s_6 = {} & (\mathbf{R}_{\Theta HAC}^T \mathbf{p}_{r_f})(\mathbf{R}_{\Theta V}^T r_f)(\mathbf{R}_h^T \mathbf{V}_f) - (\mathbf{R}_{\Theta HAC}^T \mathbf{r}_f)(\mathbf{R}_{\Theta V}^T \mathbf{p}_{r_f})(\mathbf{R}_h^T \mathbf{V}_f) \\ & -(\mathbf{R}_{\Theta HAC}^T \mathbf{V}_f)(\mathbf{R}_{\Theta V}^T r_f)(\mathbf{R}_h^T \mathbf{p}_{r_f}) = 0 \end{aligned} \tag{3.80}$$

The seventh terminal constraint is the same as 3.54.

3.3.3.2 EI Targeting Constraints with Range-To-Go Specified (Set 4)

Let the first three constraints be the same constraints from the first set of targeting conditions with the exception of Eq. (3.56):

$$s_1 = \frac{1}{2}\mathbf{r}_f^T\mathbf{r}_f - \frac{1}{2}r_{EI}^2 = 0 \tag{3.81}$$

$$s_2 = \mathbf{1}_{HAC}^T\mathbf{r}_f - r_{EI}\cos\Theta^* = 0 \tag{3.82}$$

$$s_3 = f(V_f,\ \gamma_f) = 0 \tag{3.83}$$

The transversality equations are

$$\mathbf{p}_{r_f} = \nu_1\mathbf{r}_f + \nu_2\mathbf{1}_{HAC} + \nu_3 f_\gamma\frac{\partial\gamma_f}{\partial\mathbf{r}_f} \tag{3.84}$$

$$\mathbf{p}_{V_f} = \nu_3\left(f_V\mathbf{1}_{V_f} + f_\gamma\frac{\partial\gamma_f}{\partial\mathbf{V}_f}\right) \tag{3.85}$$

To determine three of the remaining terminal constraints, the following dot product is taken

$$\mathbf{R}_h^T\mathbf{p}_{r_f} = f_\gamma\mathbf{R}_h^T\frac{\partial\gamma_f}{\partial\mathbf{r}_f}\nu_3. \tag{3.86}$$

ν_3 is solved for using Eq. (3.86). Taking the dot products of Eq. (3.85) with $\mathbf{R}_f$, $\mathbf{V}_f$ and $\mathbf{R}_h$ and substituting in for ν_3 gives the following three terminal conditions:

$$s_4 = (\mathbf{r}_f^T\mathbf{p}_{V_f})(f_\gamma\mathbf{R}_h^T\gamma_{r_f}) - (f_\gamma\mathbf{r}_f^T\gamma_{V_f} + f_V\mathbf{r}_f^T\mathbf{1}_{V_f})(\mathbf{R}_h^T\mathbf{p}_{r_f}) \tag{3.87}$$

$$s_5 = (\mathbf{V}_f^T\mathbf{p}_{V_f})(f_\gamma\mathbf{R}_h^T\gamma_{r_f}) - (f_\gamma\mathbf{V}_f^T\gamma_{V_f} + f_V\mathbf{V}_f^T\mathbf{1}_{V_f})(\mathbf{R}_h^T\mathbf{p}_{r_f}) \tag{3.88}$$

$$s_6 = (\mathbf{R}_h^T\mathbf{p}_{V_f})(f_\gamma\mathbf{R}_h^T\gamma_{r_f}) - (f_\gamma\mathbf{R}_h^T\gamma_{V_f} + f_V\mathbf{R}_h^T\mathbf{1}_{V_f})(\mathbf{R}_h^T\mathbf{p}_{r_f}) \tag{3.89}$$

The 7-th terminal constraint is the same as Eq. (3.54).

3.3.3.3 EI Targeting Constraints with Velocity and Flight Path Angle Specified (Set 5)

Let the first three constraints be

$$s_1 = \frac{1}{2}\mathbf{r}_f^T\mathbf{r}_f - \frac{1}{2}r_{EI}^2 = 0 \tag{3.90}$$

$$s_2 = \frac{1}{2}\mathbf{V}_f^T\mathbf{V}_f - \frac{1}{2}V_{EI}^2 = 0 \tag{3.91}$$

$$s_3 = \mathbf{V}_f^T\mathbf{r}_f - V_{EI}r_{EI}\sin\gamma_{EI} = 0 \tag{3.92}$$

where V_{EI} and γ_{EI}. The transversality equations are

$$\mathbf{p}_{r_f} = \nu_1\mathbf{r}_f + \nu_3\mathbf{V}_f \tag{3.93}$$

$$\mathbf{p}_{V_f} = \nu_2\mathbf{V}_f + \nu_3\mathbf{r}_f. \tag{3.94}$$

Following the same method to eliminate the multipliers, the next three terminal constraints are

$$\begin{aligned} s_4 &= (\mathbf{R}_h^T\mathbf{V}_f)(\mathbf{r}_f^T\mathbf{p}_{r_f})(\mathbf{V}_f^T\mathbf{r}_f) - (\mathbf{V}_f^T\mathbf{p}_{r_f})(\mathbf{R}_h^T\mathbf{V}_f)(\mathbf{r}_f^T\mathbf{r}_f) + V_f^2(\mathbf{R}_h^T\mathbf{p}_{r_f})(\mathbf{r}_f^T\mathbf{r}_f) \\ &- (\mathbf{R}_h^T\mathbf{p}_{r_f})(\mathbf{r}_f^T\mathbf{V}_f)^2 = 0 \end{aligned} \tag{3.95}$$

$$s_5 = (\mathbf{r}_f^T\mathbf{p}_{V_f})(\mathbf{R}_h^T\mathbf{V}_f) - (\mathbf{R}_h^T\mathbf{p}_{V_f})(\mathbf{r}_f^T\mathbf{V}_f) - (\mathbf{R}_h^T\mathbf{p}_{r_f})(\mathbf{r}_f^T\mathbf{r}_f) = 0 \tag{3.96}$$

$$s_6 = (\mathbf{V}_f^T\mathbf{p}_{V_f})(\mathbf{R}_h^T\mathbf{V}_f) - (\mathbf{R}_h^T\mathbf{p}_{V_f})(\mathbf{V}_f^T\mathbf{V}_f) - (\mathbf{R}_h^T\mathbf{p}_{r_f})(\mathbf{V}_f^T\mathbf{r}_f) = 0 \tag{3.97}$$

The seventh terminal constraint is the same as Eq. (3.54).

3.4 Algorithm Formulation

The algorithm is a closed loop guidance scheme. The numerical solution is obtained by an analytical multiple shooting method described in Ref. [26]. For in depth description of the analytical multiple shooting method see Appendix C. Every second of flight, the guidance problem is solved for the thrust vector, which is used as an input for the vehicle. An initial outer loop is added to the closed loop guidance simulation. This outer loop determines which $\mathbf{1}_{HAC}$ should be targeted as well as a required manual coast time to reach the desired crossrange distance tolerance.

The timing of the burn is essential in the minimum fuel deorbit guidance problem. Out of plane maneuvers are very expensive with regard to fuel and are avoided when

possible. For orbits with inclination values greater than the latitude of the Landing Site on Earth, the Landing Site is in the orbit plane twice in a 24 hour period. The burn (or burns) of the deorbit flight is timed so that when the vehicle reaches EI, the Landing Site is within a specified crossrange distance tolerance of the orbit place.

To ensure a feasible crossrange distance for vehicle during entry flight, $\mathbf{1}_{HAC}$ should be within a certain tolerance of the orbital plane when the vehicle reaches EI. Let $t = 0$ be the time the guidance system starts looking for a solution and $\mathbf{1}_{HAC0}$ is the value of $\mathbf{1}_{HAC}$ at $t = 0$. See Fig. 3.3 for graphical description.

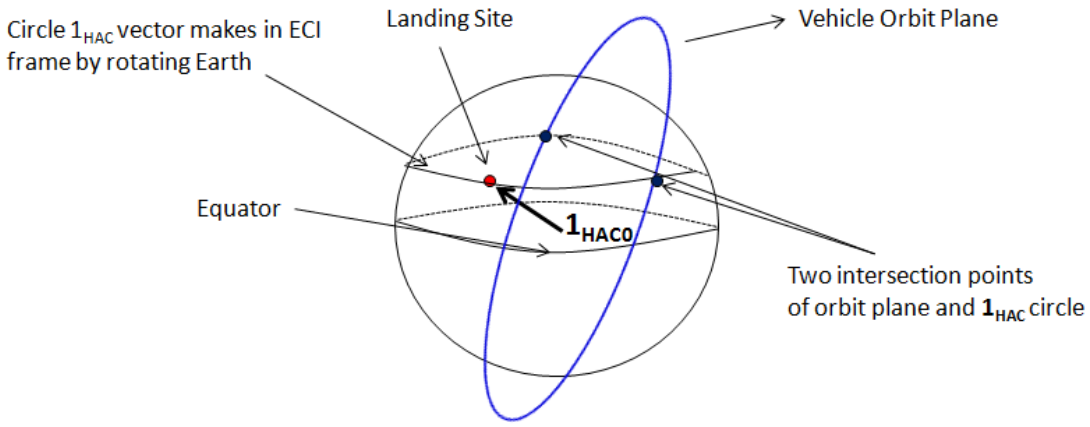

Figure 3.3 $\mathbf{1}_{HAC}$

Define the vector from the origin of the coordinate system to the two intersection points of the landing site and orbit plane as $\mathbf{1}_{HAC1}$ and $\mathbf{1}_{HAC2}$. One of these two $\mathbf{1}_{HAC}$ values is chosen to be targeted for the terminal conditions of the problem. The time for the Landing Site to travel from $\mathbf{1}_{HAC0}$ to $\mathbf{1}_{HAC1}$ and $\mathbf{1}_{HAC2}$ is defined as t_1 and t_2. The time of flight from the vehicles initial position on orbit to $\mathbf{1}_{HAC1}$ and $\mathbf{1}_{HAC2}$ is estimated using Kepler's time-of-flight solution. These times are labeled as t_{v1} and t_{v2} respectively.

The $\mathbf{1}_{HAC}$ to be targeted is chosen in the following fashion:

if $t_1 < t_2$ **then**
  if $t_{v1} < t_1$ **then**
    $\mathbf{1}_{HAC} = \mathbf{1}_{HAC1}$
  else
    $\mathbf{1}_{HAC} = \mathbf{1}_{HAC2}$
  end if
else
  if $t_{v2} < t_2$ **then**
    $\mathbf{1}_{HAC} = \mathbf{1}_{HAC2}$
  else
    $\mathbf{1}_{HAC} = \mathbf{1}_{HAC1}$
  end if
end if

After the $\mathbf{1}_{HAC}$ to be targeted is chosen, a manual coast of the vehicle is determined. The Earth rotates at a rate of 7.2921159×10^{-5} radians per second. For the Landing Site to be within range of the targeted $\mathbf{1}_{HAC}$, a initial manual coast of several orbital periods of the vehicle may be necessary. This manual coast is defined as t_C and is found by dividing t_1 or t_2 (depending on which $\mathbf{1}_{HAC}$ is chosen) by the period of the orbit. This factor is then rounded down to the nearest whole number and decreased by one. Choosing the initial manual coast this way gives ample opportunity for the vehicle to coast and find the point to burn so the vehicle is within the required range of the targeted $\mathbf{1}_{HAC}$ at EI. Once the initial manual coast is determined the problem is then solved using one of the following coast-burn formulations:

1. Burn-Coast (BC)

2. Coast-Burn-Coast (CBC)

3. Burn-Coast-Burn (BCB)

4. Burn-Coast-Burn-Coast (BCBC)

The coast-burn formulation used to solve the problem is based on the characteristics of the vehicle's initial orbit and the vehicle's engine capabilities. For Shuttle-type vehicles with very low thrust-to-weight ratios, multiple burns are needed for higher altitude and higher eccentricity orbits. There is no known analytical method by which to decide the number of burns given the orbit details. The number of burns needed to reach entry optimally is determined via numerical simulation.

After the burn-coast formulation and the initial manual coast is determined for the specified $\mathbf{1}_{HAC}$, the vehicle continues to coast manually until a solution can be found that meets the specified burn time bounds. If no solution is found while the vehicle is coasting and the manual coast becomes greater than the time it takes for $\mathbf{1}_{HAC}$ to reach its targeted position, the vehicle then targets the other desired $\mathbf{1}_{HAC}$ position. If no solution is found, the burn time bound is increased and the process repeats itself till a solution is found that targets one of the desired $\mathbf{1}_{HAC}$ values and the burn time is within the desired burn time bounds. The burn time bounds are a very loose constraint but necessary to keep the burn time within a desired set.

The initial guess used for the vacuum guidance solution is constructed as follows. Given the position and velocity of the vehicle after the manual coast has occurred, if the first arc is a coast arc, propagate position and velocity in time to the first burn arc. At the beginning of the first burn arc, set the costate vector to be

$$\mathbf{p}_V = -\frac{\mathbf{V}}{|\mathbf{V}|} \tag{3.98}$$

$$\mathbf{p}_r = \frac{-r}{|\mathbf{r}|} + \mathbf{p}_V. \tag{3.99}$$

This sets the initial guess of the $\mathbf{p}_V$ vector to be in the opposite direction of the velocity vector, representing a braking maneuver. By the problem setup, $\mathbf{p}_r = -\omega^2 \mathbf{p}_V$, $\mathbf{p}_r$ is approximated using the velocity equation of motion where the thrust vector is taken to be in the direction of the primer vector. This costate is then propagated along the different arcs using the solution given above. For the CBC solution, the costate at the beginning of the burn is propagated backwards to find the initial guess of the costate at the beginning of the initial coast. In [27] an automated initial guess system for burn times, coast times, state, and costate is given. This system is a different initial guess method than the one explained above and will be investigated in the future.

Once an initial solution is found that meets the crossrange distance tolerance and targets an appropriate $\mathbf{1}_{HAC}$ at EI, the closed loop guidance simulation is called. The initial guess of the simulation is the solution found in the outerloop. Since the closed loop simulation is updated each second, the final crossrange distance tolerance at EI may be larger than the crossrange distance that the initial solution determined.

3.5 NASA's Space Shuttle Model and Targeting Functions

NASA's Space Shuttle is the model used in the following numerical work. The Shuttle relies on its Orbital Maneuvering System (OMS) to perform on-orbit maneuvers. The OMS system is capable of producing 53378.6 Newtons of thrust at a mass-rate of 17.02 kg/sec. The engine I_{sp} is 313 seconds. The on-orbit initial mass is 95254.38 kg. The functional relationships for the Shuttle used in the terminal conditions are constructed and shown in the following section. The landing site is Kennedy Space Center with a latitude of 28.615 deg and a longitude of -80.694 deg for all test cases.

To construct representative EI targeting functions $\gamma^*(\Theta)$ and $V^*(\Theta)$ used in Eqs. (3.28), (3.29), (3.67), and (3.68), we examine the historical mission data for the Space Shuttle. Figure 3.4 plots the EI flight path angle versus the range-to-go to the landing

site from a number of past Shuttle missions. It is seen that the data is reasonably fitted by a straight line

$$\gamma^* = 2.65\Theta - 4.5152. \quad (\gamma^* \text{ in deg, } \Theta \text{ in rad}) \tag{3.100}$$

Data corresponding to various values of EI inertial velocity and flight path angle near the middle of the entry corridor can be read off of Figure 3 in Ref. [3]. Approximating these data pairs with a linear equation and then replacing flight path angle with the above equation, we obtain the second linear relationship between the inertial velocity and range at EI

$$V^* = 226.8\Theta + 25551, \quad (V^* \text{ in ft/s, } \Theta \text{ in rad}) \tag{3.101}$$

Note that the above two functions only represent local relationships around typical operating conditions. To use these two functions in the guidance algorithm, care must be exercised. During the search, the value of Θ could vary in a wide range, rendering the values of γ^* and V^* unrealistic. To avoid this problem, these targeting functions are modified to be

$$\gamma^* = \begin{cases} -1.6 \ \text{(deg)}, & \text{if } \Theta < 1.1 \ \text{(rad)} \\ 2.65\Theta - 4.5152 \ \text{(deg)}, & \text{if } 1.1 \leq \Theta \leq 1.4 \ \text{(rad)} \\ -0.805 \ \text{(deg)}, & \text{if } \Theta > 1.4 \ \text{(rad)} \end{cases} \tag{3.102}$$

$$V^* = \begin{cases} 25800.48 \ \text{(ft/s)}, & \text{if } \Theta < 1.1 \ \text{(rad)} \\ 226.8\Theta + 25551 \ \text{(ft/s)}, & \text{if } 1.1 \leq \Theta \leq 1.4 \ \text{(rad)} \\ 25868.52 \ \text{(ft/s)}, & \text{if } \Theta > 1.4 \ \text{(rad)} \end{cases} \tag{3.103}$$

The functional relationship between the EI velocity and flight path angle in Eqs. (3.58) and (3.88) is obtained by eliminating Θ from Eqs. (3.102) and (3.103)

$$f(V_f, \ \gamma_f) = V_f - 85.5849\gamma_f - 2555.27 = 0, \quad (V_f \text{ in ft/s, } \gamma_f \text{ in deg}) \tag{3.104}$$

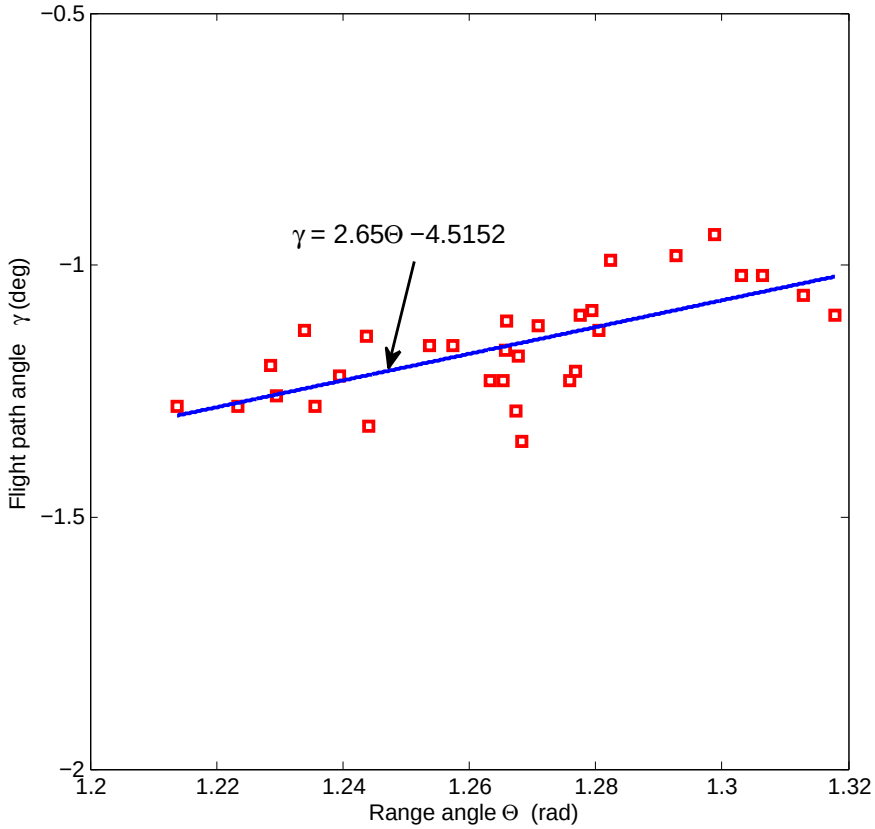

Figure 3.4 Flight path angles and ranges at EI from Space Shuttle missions

CHAPTER 4. Deorbit Guidance for Initial Circular Orbits

Near circular orbits are the most common orbit for the Space Shuttle. Speed is constant on a circular orbit so deorbit timing is based on the timing of the $\mathbf{1}_{HAC}$. In this chapter, the deorbit maneuver from circular orbits of several altitudes is studied. Starting with low altitude of 200 km and ascending to high altitude orbits of 1100 km, the optimal deorbit guidance problem is solved. The impulse maneuver results are given in Section 1. Section 2 presents low altitude finite time burn results. The effects of the crossrange constraint on the problem is explored in Section 3. Section 4 shows the benefits of the multiple burn maneuver for higher altitude orbits and a summary of findings is presented in Section 5. The cases tested are listed in Table 4.1, where i is the inclination of the initial orbit, Ω is the longitude of the ascending node, X, Y, and Z are the components of the position in the ECI frame, and $\dot{X}$, $\dot{Y}$, and $\dot{Z}$ are the components of the velocity in the ECI frame. All results assume Keplerian motion for the coast arcs.

4.1 Impulsive Deorbit Maneuver

Solving the impulsive deorbit maneuver for an initial circular orbit with EI conditions of flight path angle, velocity, and altitude involves solving for the impulse but not the location. The required impulse will be the same for each location of the initial orbit. If there are other terminal conditions besides flight path angle, velocity, and altitude, the location of the impulse will need to be determined. The approach from Ref. [6] described in Section 2.1 is used to solve the impulse problem for cases 1 - 20. The specified EI

Table 4.1 Test Cases for Circular Orbits

Case	Altitude (km)	i (deg)	Ω (deg)	X (km)	Y (km)	Z (km)	$\dot{X}$ (km/s)	$\dot{Y}$ (km/s)	$\dot{Z}$(km/s)
1	200	50	240	1526.692	-4679.246	4363.936	5.537	4.587	2.981
2	210	50	240	1529.013	-4686.359	4370.571	5.533	4.583	2.979
3	220	50	240	1531.334	-4693.473	4377.205	5.528	4.58	2.977
4	230	50	240	1533.655	-4700.586	4383.839	5.524	4.576	2.974
5	240	50	240	1535.976	-4707.7	4390.473	5.52	4.573	2.972
6	250	50	240	1538.297	-4714.813	4397.107	5.516	4.569	2.97
7	260	50	240	1540.618	-4721.927	4403.741	5.512	4.566	2.968
8	270	50	240	1542.939	-4729.04	4410.375	5.508	4.563	2.965
9	280	50	240	1545.259	-4736.154	4417.01	5.504	4.559	2.963
10	290	50	240	1547.58	-4743.267	4423.644	5.499	4.556	2.961
11	300	50	240	1549.901	-4750.381	4430.278	5.495	4.552	2.959
12	310	50	240	1552.222	-4757.494	4436.912	5.491	4.549	2.956
13	320	50	240	1554.543	-4764.608	4443.546	5.487	4.546	2.954
14	330	50	240	1556.864	-4771.721	4450.18	5.483	4.542	2.952
15	340	50	240	1559.185	-4778.835	4456.814	5.479	4.539	2.95
16	350	50	240	1561.506	-4785.948	4463.449	5.475	4.535	2.948
17	360	50	240	1563.827	-4793.062	4470.083	5.471	4.532	2.945
18	370	50	240	1566.148	-4800.175	4476.717	5.467	4.529	2.943
19	380	50	240	1568.468	-4807.289	4483.351	5.463	4.525	2.941
20	390	50	240	1570.789	-4814.402	4489.985	5.459	4.522	2.939
21	400	50	240	1573.11	-4821.516	4496.619	5.455	4.519	2.937
22	500	50	240	1596.319	-4892.65	4562.961	5.415	4.486	2.915
23	600	50	240	1619.528	-4963.785	4629.302	5.376	4.453	2.894
24	700	50	240	1642.738	-5034.92	4695.643	5.338	4.422	2.874
25	800	50	240	1665.947	-5106.055	4761.985	5.3	4.391	2.854
26	900	50	240	1689.156	-5177.19	4828.326	5.264	4.361	2.834
27	1000	50	240	1712.365	-5248.324	4894.668	5.228	4.331	2.815
28	1100	50	240	1735.574	-5319.459	4961.009	5.193	4.302	2.796

Table 4.2 Results from general maneuver procedure shown in [6] with flight path angle equal to −1 degrees and velocity equal to 7879.5 m/s.

Initial Altitude (km)	ΔV (km/s)	δ (deg)	ΔT_E (sec)
200	0.1655	-89.41	510
210	0.1650	-87.36	3261
220	0.1639	-85.28	3322
230	0.1621	-83.15	3383
240	0.1597	-80.93	3445
250	0.1566	-78.58	3508
260	0.1527	-76.07	3573
270	0.1481	-73.31	3641
280	0.1427	-70.22	3712
290	0.1363	-66.65	3787
300	0.1288	-62.39	3868
310	0.1201	-57.02	3958
320	0.1099	-49.70	4062
330	0.0976	-38.19	4195
340	0.0824	-2.357	4493
350	0.0881	0	4511
360	0.0940	0	4511
370	0.0998	0	4511
380	0.1057	0	4511
390	0.1115	0	4511

conditions of flight path angle, velocity, and altitude are −1 degrees, 7879.5 m/s, and 120 km. The results are shown in Table 4.2.

As shown in Table 4.2, after an initial orbit altitude of 340 km, the thrust parameter δ is zero and the time of flight is not changing. By inspecting the solution process in Ref. [6], specifically the momentum, semi-major axis, semi-latus rectum, eccentricity, and apogee altitude equations,

$$H_D = (R_e + h_e)V_e \cos\gamma_e \tag{4.1}$$

$$a_D = \frac{\mu r_e}{2\mu - r_e V_e^2} \tag{4.2}$$

$$e_D = \sqrt{1 - \frac{p_D}{a_D}} \tag{4.3}$$

$$p_D = \frac{H_D^2}{\mu} \tag{4.4}$$

$$r_a = a_D(1 - e_D) \tag{4.5}$$

it is shown that the transfer orbit resulting from the impulsive solution is determined

by the EI conditions. For every set of specified EI conditions, there is an altitude such that for any altitude greater, there is no impulsive solution. Specifically, no impulsive solution exists that places the vehicle on a Keplerian orbit to the required EI conditions. For the case with flight path angle of -1 degrees and velocity of 7879.5 m/s, the transfer orbit apogee altitude is 340 km. Therefore, any initial circular orbit with altitude greater than 340 km will not have an impulsive solution. Figure 4.1 shows the impulsive results for initial circular orbit altitudes starting at 200 km and increasing to 340 km. The impulse decreases as altitude increases from 200 km to 340 km.

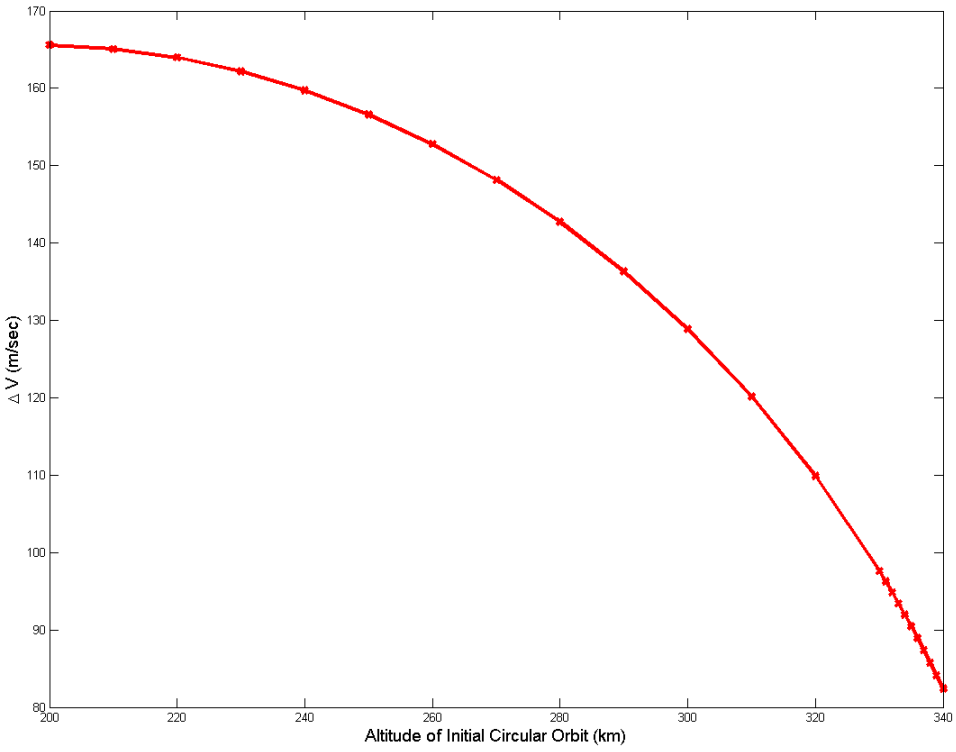

Figure 4.1 Impulse solution for circular orbits with altitude 200 to 340 km (cases 1 - 15). EI conditions are fixed with flight path angle of -1, velocity of 7879.5 m/s, and altitude of 120 km.

The transfer orbit apogee altitude for the extreme cases of flight path angle and velocity for the variable formulation in terminal conditions Set 3 is shown in Table 4.3.

Table 4.3 Apogee altitude of transfer orbit for given cases of EI flight path angle and velocity.

EI γ (deg)	EI Velocity (m/s)	r_a of Transfer Orbit (km)
-.805	7884.66	338
-1	7879.5	340
-1.6	7863.87	364

Table 4.3 shows that the transfer orbit apogee is dependent on the EI conditions. For the entry conditions targeted by a Shuttle type vehicle, no impulsive solution exists, for altitudes higher than 364 km.

4.2 Coast-Burn-Coast Solution for Low Altitude Orbits

Using the variable formulations of flight path angle and velocity at EI for the Shuttle, Eqs. (3.102) and (3.103), in terminal constraints set 3 (Eqs. (3.66)–(3.68), (3.76), (3.77), (3.80), and (3.54)) and a desired CBC solution, results are shown in Table 4.4. The 1-st column is the case number corresponding to Table 4.1. The 2-nd column is the manual coast needed to target the desired $\mathbf{1}_{HAC}$ positions. A manual coast in the range of 20000 to 30000 seconds means the closest $\mathbf{1}_{HAC}$ was targeted while a manual coast time greater than 80000 seconds means the second desired $\mathbf{1}_{HAC}$ was targeted. The 3-rd, 4-th, and 5-th columns are the times of the three arcs for the optimal coast-burn-coast solution. Using the rocket equation, Eq. (2.22), with engine I_{sp} of 313 seconds, the ΔV is calculated given the initial mass and final mass after the burn time. This is shown in column 6. The final crossrange distance at EI is given in column 7 and the flight path angle at EI is given in column 8. The crossrange distance tolerance is set to 1000 km or .1568 radians. The distance in radians is found by dividing the crossrange distance in kilometers by the radius of the Earth.

For cases 1 through 15, the burn time decreases as the altitude increases. For the low altitude deorbit, longer burn time is required to place the vehicle on the correct transfer

Table 4.4 Results for circular cases 1 - 20 with coast-burn-coast formulation, set 3 (Eqs. (3.66)–(3.68), (3.76), (3.77), (3.80), and (3.54)) terminal constraints and constrained crossrange

Case	M CT (s)	CT 1(s)	BT (s)	CT 2 (s)	ΔV (m/s)	CR at EI	FPA at EI (deg)
1	21652.89	1230.13	261.00	3270.55	146.7684	0.1840	-0.8050
2	21851.34	1067.91	261.00	3204.44	146.8950	0.1859	-0.8050
3	21864.82	1058.00	260.45	3138.63	146.3713	0.1899	-0.8050
4	23013.34	0.00	258.00	3072.55	145.2724	0.1885	-0.8050
5	23196.90	0.00	255.00	3006.25	143.3690	0.1812	-0.8050
6	26390.50	1838.33	250.00	795.99	140.8005	0.0000	-0.8050
7	26264.13	1968.50	268.00	736.39	150.6843	0.0032	-1.0367
8	79972.28	1965.91	238.00	946.94	133.5259	0.1478	-0.8050
9	80037.75	2162.00	235.13	1025.81	131.7557	0.1262	-0.8050
10	80268.34	2202.72	219.00	1116.88	122.8347	0.1041	-0.8050
11	80459.07	1671.63	207.00	1212.73	115.9044	0.1205	-0.8050
12	22432.83	1550.13	192.00	2472.39	107.7281	0.1691	-0.8050
13	23056.68	1324.74	175.00	2362.08	97.8398	0.1518	-0.8050
14	22435.57	2103.42	153.00	2214.77	85.7313	0.1525	-0.8050
15	84193.23	0.00	146.00	1827.62	81.2099	0.0470	-0.9973
16	26478.46	1473.99	168.00	1619.76	93.9454	0.0287	-1.2912
17	26577.45	1449.71	189.00	1519.83	105.6377	0.0284	-1.5131
18	26606.49	1136.89	245.00	1463.16	137.8438	0.0102	-1.6000
19	26650.55	1184.72	349.00	1408.17	197.7588	0.0192	-1.6000
20	26854.66	827.31	431.00	1368.52	246.2557	0.0121	-1.6000

orbit, which will ensure that the vehicle has the required flight path angle and velocity at EI. The crossrange distance at EI varies between the cases. The largest crossrange distance at EI is 1211 km and the smallest is less than a kilometer.

For cases 1 - 5, the vehicle is placed on a transfer orbit that has an apogee altitude higher than the initial orbit altitude. As stated in Section 4.1, the EI conditions specify the transfer orbit characteristics. For the specified flight path angle of cases 1 - 5, the apogee altitude of the transfer orbit is 340 km. The vehicle enters the transfer orbit at an preapogee position and must travel through apogee to reach EI with the specified conditions. Figure 4.2 shows the change in altitude of the vehicle during the deorbit maneuver. The vehicle has an increase in altitude, which corresponds to a thrust angle that is greater than 180 degrees and decreasing linearly. The thrust angle of the vehicle for cases 1 - 10 is shown in Figure 4.3. Appendix D gives a thorough description of thrust angle and the method used to deduce whether the angle is greater or less than

180 degrees. A thrust angle greater than 180 degrees is necessary to place the vehicle on a transfer orbit in a preapogee position. Figure 4.4 shows the in-plane trajectory of the vehicle for case 1. Coast 1 in Figure 4.4 is the optimal coast time determined by the solution after the manual coast is complete. The transfer orbit, after burn is complete, is an elliptic orbit with apogee altitude greater than the initial orbit altitude for the CBC solution. There is no increase in altitude on the transfer orbit for cases 6 to 11, which corresponds to a linear decreasing thrust angle less than 180 degrees. The vehicle enters the transfer orbit on a post apogee position and the vehicle altitude decreases as it travels to EI.

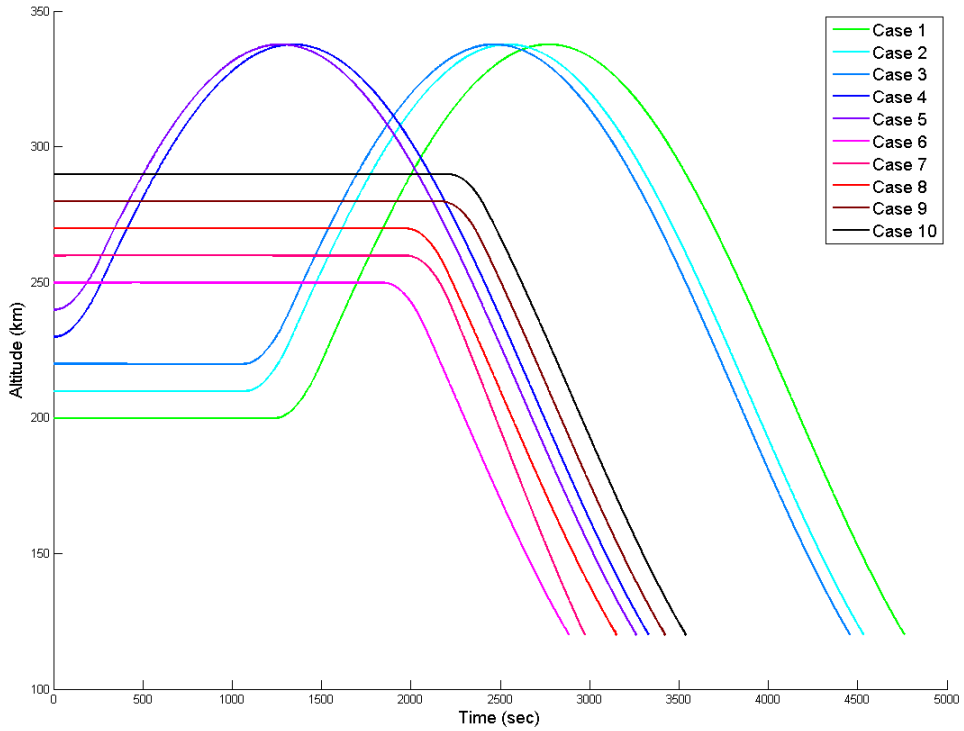

Figure 4.2 Vehicle altitude during flight for coast-burn-coast solution of circular cases 1 through 10

Cases 12, 13, and 14 have the same trend as cases 1 through 5 with the increase in altitude of the transfer orbit to 340 km as shown in Figure 4.5. The thrust angles of

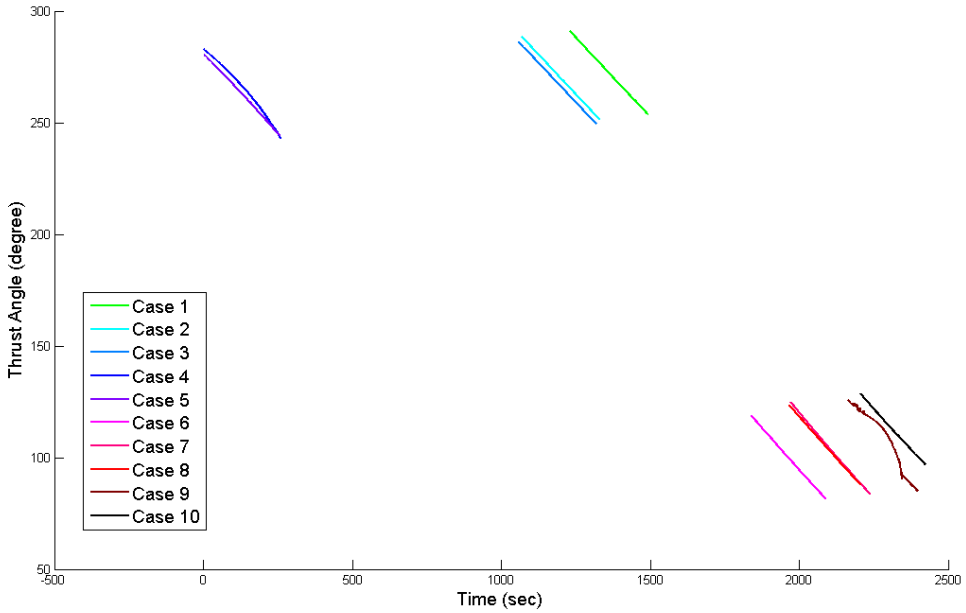

Figure 4.3 Thrust angle during burn for coast-burn-coast solution of circular cases 1 through 10

cases 12, 13, and 14 also follow the same pattern of thrust angle greater than 180 degrees that decreases linearly. The thrust angle for cases 11 - 17 is shown in Figure 4.6. Cases 16 and 17 resemble a braking maneuver with piecewise linear thrust angle very close to 180 degrees. The flight path angle targeted at EI in case 16 and 17 allows for transfer orbit apogee altitude that intersects the initial circular orbit plane.

For initial orbit altitudes corresponding to 370 km and higher, a rapid increase in burn time exists. This is because there is no Keplerian elliptic orbit that the vehicle could travel on that would intersect EI with the required EI conditions. Therefore, a longer burn time is required to place the vehicle on an orbit that would meet the required EI conditions. Figure 4.7 shows the thrust angle for cases 18 - 20. The thrust angle increases from greater than 100 degrees to greater than 200 degrees during the burn. At the beginning of the burn, a decrease in velocity occurs and this is shown by the beginning portion of the thrust angle. An increase in velocity occurs at the end on the

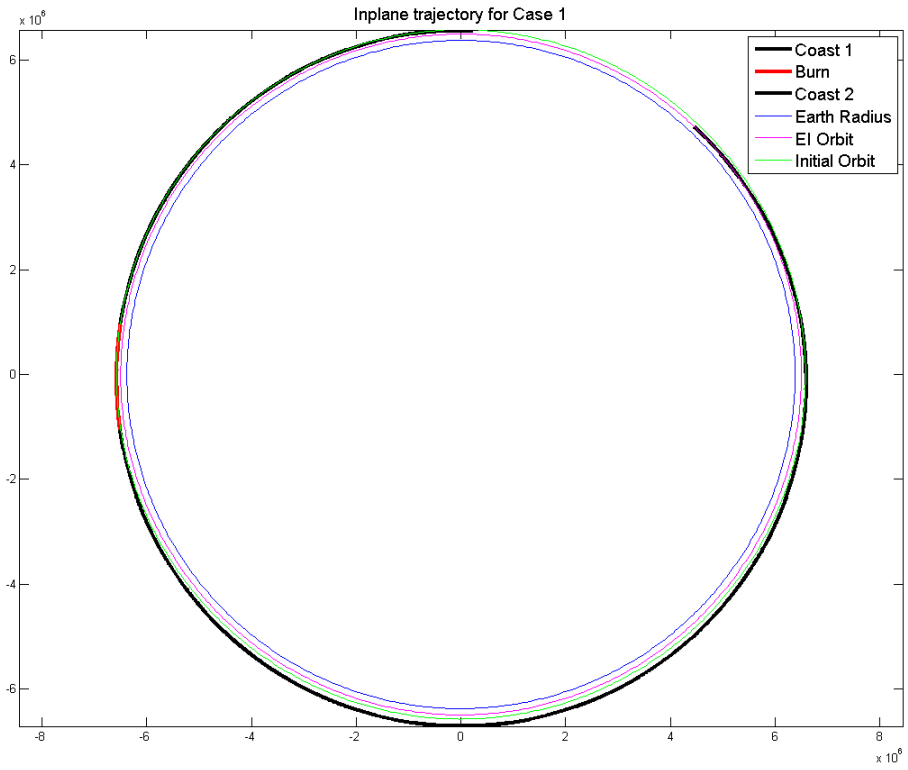

Figure 4.4 Inplane trajectory of Case 1

burn and this is shown by the thrust angle.

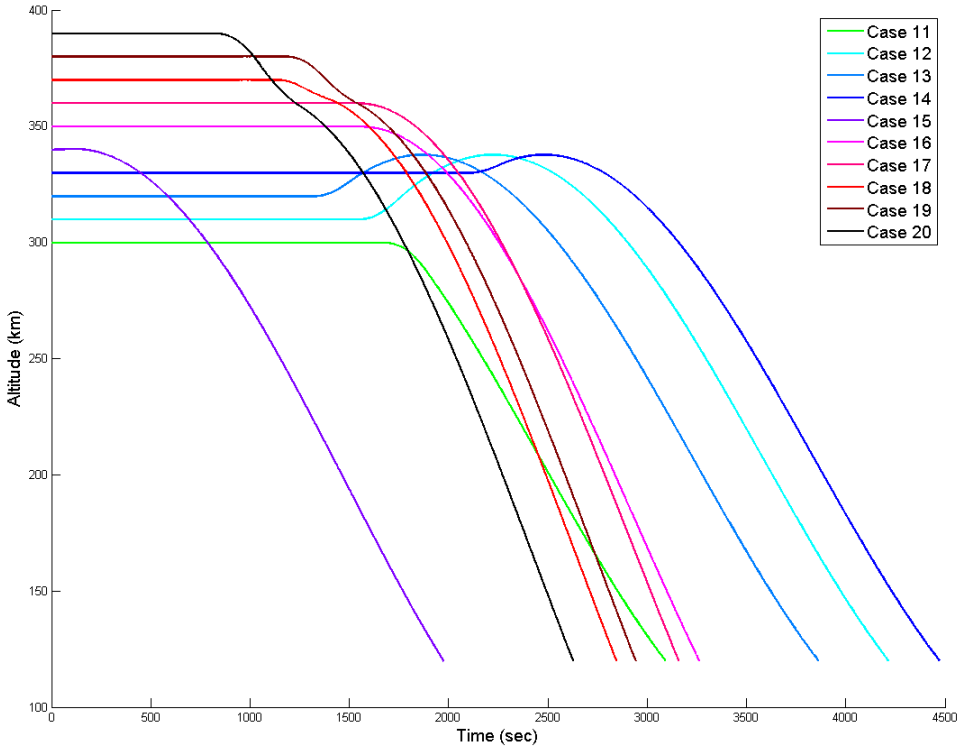

Figure 4.5 Vehicle altitude during flight for coast-burn-coast solution of circular cases 11 through 20

The inplane trajectory for Case 6 and 16 is shown in Figures 4.8 and 4.9. Coast 1 in Figures 4.8 and 4.9 denotes the optimal coast found in the CBC solution and not the manual coast needed to meet the timing requirement to ensure a maneuver within the specified crossrange distance tolerance. After the manual coast is over and guidance begins, the vehicle continues to coast a specified time determined by the guidance solution. The vehicle then burns to place itself on a transfer orbit necessary to meet the required EI conditions. After the burn is completed the vehicle coasts to EI.

Figure 4.10 shows the change in ΔV as initial orbit altitude increases for cases 1 - 20. The ΔV decreases as altitude increases from 200 km to 340 km. This corresponds to

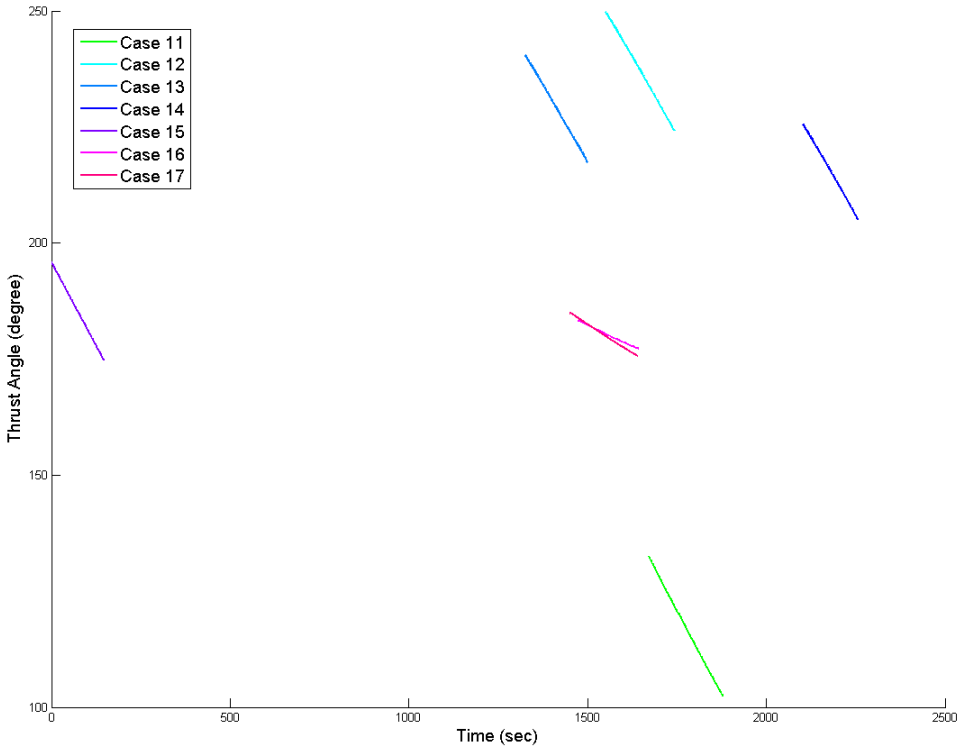

Figure 4.6 Thrust angle during burn for coast-burn-coast solution of circular cases 11 through 17

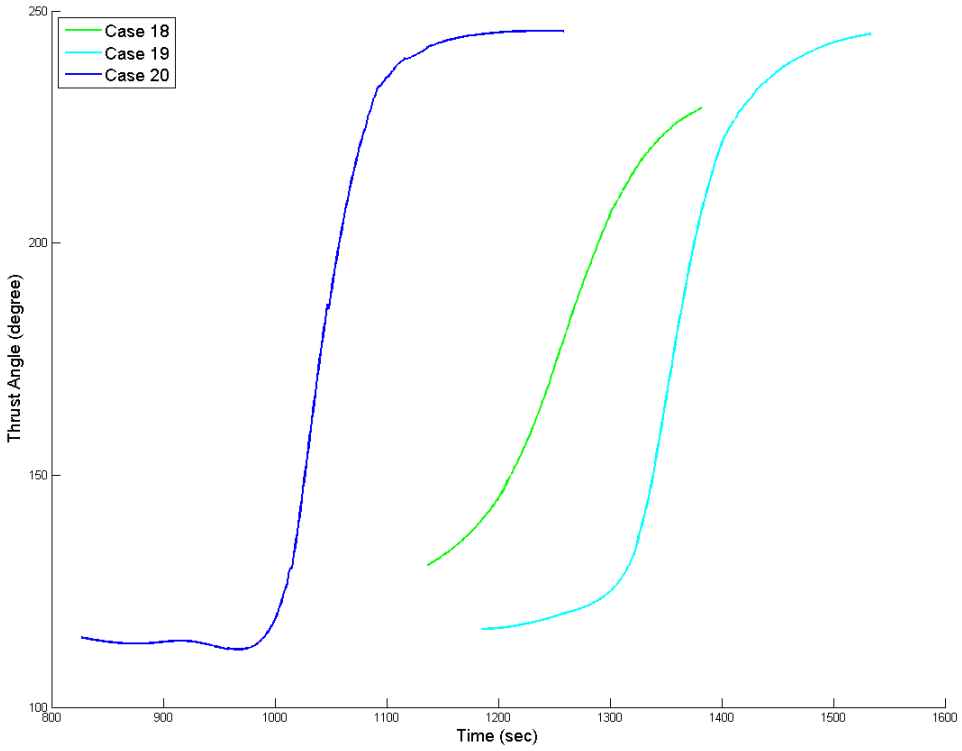

Figure 4.7 Thrust angle during burn for coast-burn-coast solution of circular cases 18 through 20

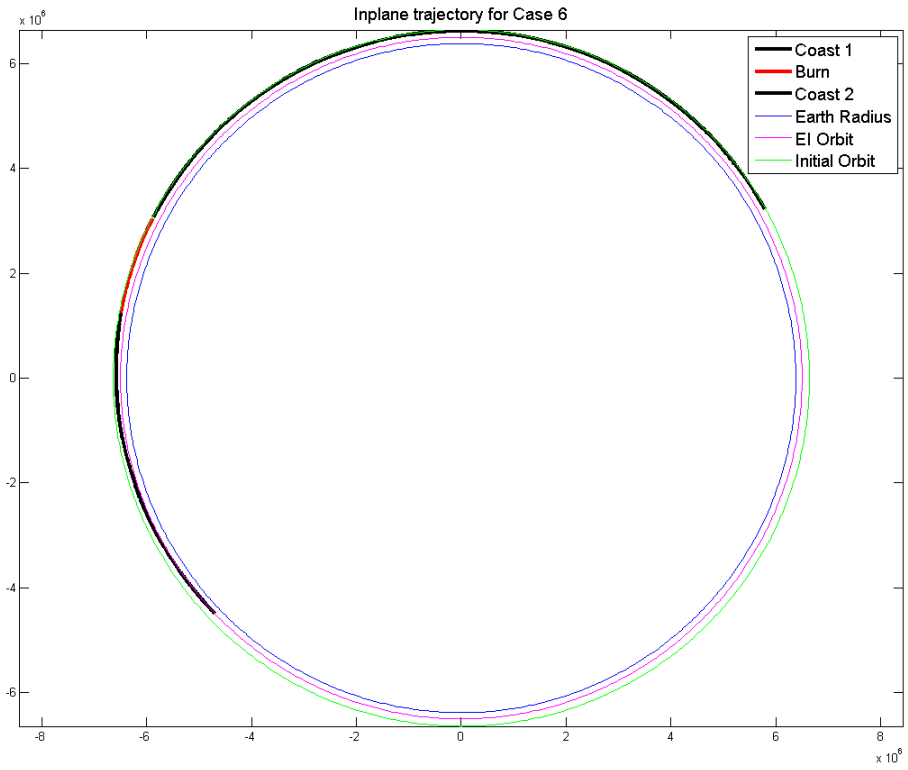

Figure 4.8 Inplane trajectory of Case 6

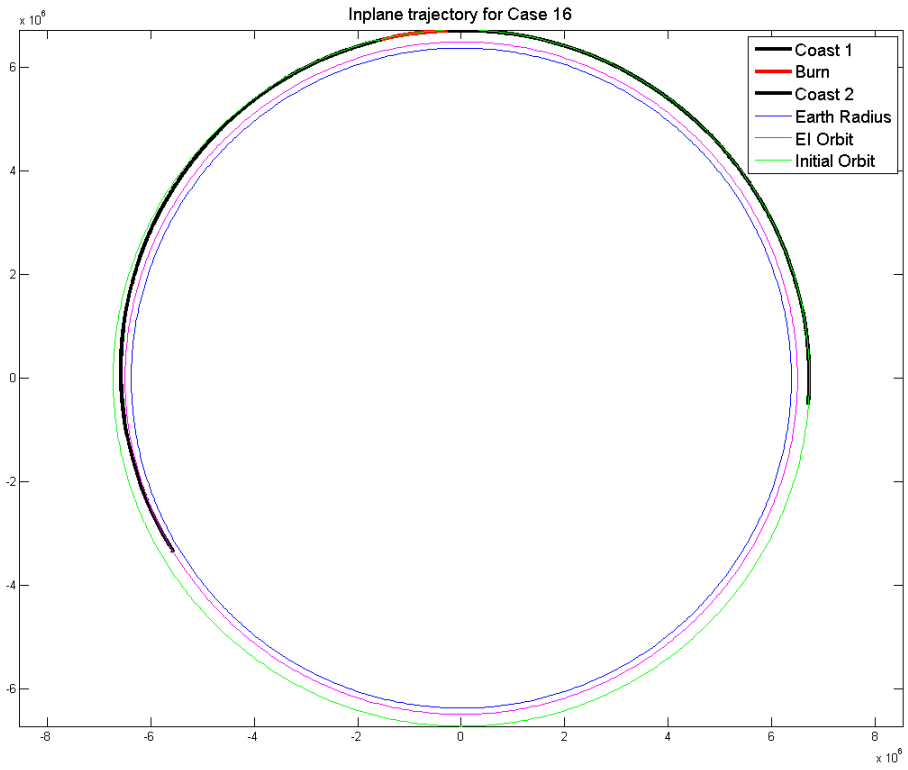

Figure 4.9 Inplane trajectory of Case 16

the impulsive results. After 340 km the ΔV increases dramatically. The orbit altitude of the International Space Station is approximately 340 km. For most Shuttle missions the Orbiter returns from the International Space Station orbit with a burn time of approximately 2.5 minutes, which corresponds to a ΔV of less than 100 m/s. This coincides with the numerical results in Table 4.4 that show the shortest burn time for deorbit from an altitude of 340 km.

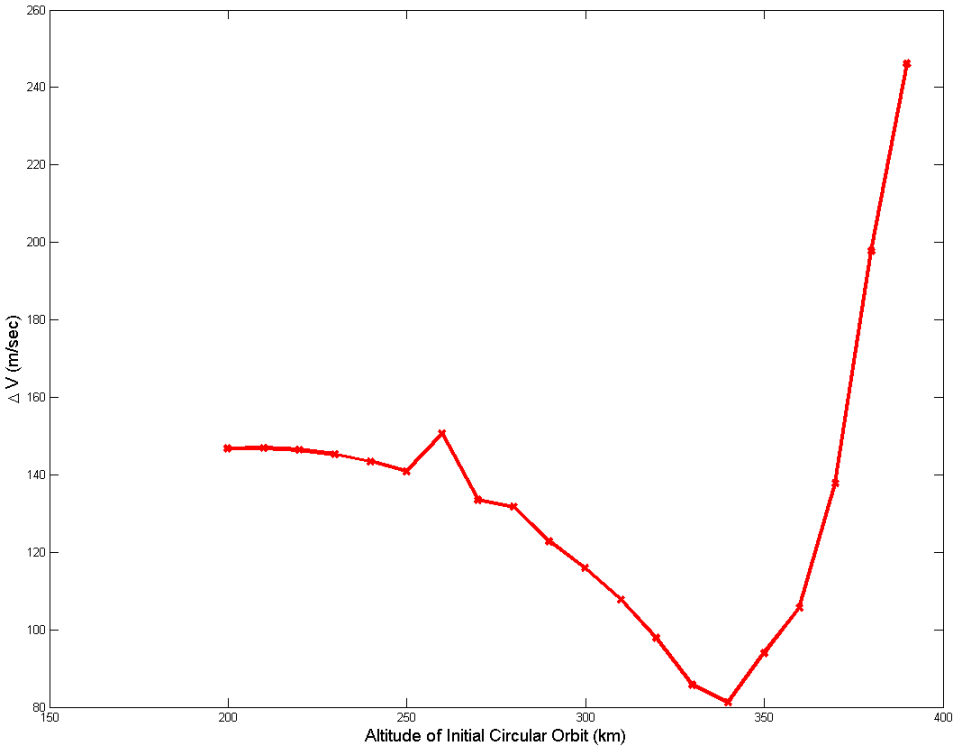

Figure 4.10 ΔV of coast-burn-coast solutions with terminal conditions set 3 (Eqs. (3.66)–(3.68), (3.76), (3.77), (3.80), and (3.54)) for cases 1 - 20

As shown in Table 4.4, case 7 has an increase in burn time when it should be decreasing. This is attributed to the variable EI conditions of flight path angle and velocity. Since a range of values can be targeted at EI, this variation in burn time is allowable. Both case 6 and case 8 have a final EI flight path angle of $-.805$ deg while case 7 has

a final EI flight path angle of -1.0367 deg. Also, the crossrange distance at EI for case 7 is much smaller than the other cases. The longer burn time was necessary to achieve the required EI values that were targeted and be within the required crossrange distance tolerance. The targeted EI conditions of case 7 are different from the previous and subsequent cases because of the manual coast. The algorithm did not find a solution that met the crossrange and burn time constraints such that the targeted EI conditions of cases 6 and 8 were met. The algorithm found a solution that met the constraints and appropriate EI conditions with an increased burn time.

EI conditions of flight path angle and velocity are fixed for the results in Table 4.5, which is setup the same way as Table 4.4. The targeted conditions are a flight path angle of -1 degrees and a corresponding velocity of 7879.5 m/s from the Shuttle functional relationships. The results show the decrease in burn time as the altitude of the orbit increases until an altitude of 340 km and then the burn time increases sharply. This coincides with the Space Shuttle deorbiting from the International Space Station at 340 km.

Comparing the variable EI conditions of terminal conditions set 3 (Eqs. (3.66)–(3.68), (3.76), (3.77), (3.80), and (3.54)) and the specified EI conditions of set 5 (Eqs. (3.90)–(3.97) and (3.54)) , there is a significant difference in burn time, especially for Case 1 with a difference of 17 seconds. This is a significant difference given that fuel conservation is a major goal in space flight. Allowing for variable flight path angle and velocity relations at EI results in smaller burn times for the majority of the low altitude cases. As the initial orbit altitude increases, the difference in burn time is less. The other noticeable difference is in the initial coast time found as part of the CBC solution. As shown in Table 4.5, the optimal initial coast time was found to be zero as part of the guidance solution for all cases except 4, 5, 10, and 16 - 20. The values of crossrange distance at EI are within standard tolerances with the largest EI crossrange distance being 1205 km (Case 10) and the smallest is 47 km (Case 19).

Table 4.5 Results for circular cases 1 - 20 with coast-burn-coast formulation, set 5 (Eqs. (3.90)–(3.97) and (3.54)) terminal constraints and constrained crossrange

Case	M CT (s)	CT 1(s)	BT (s)	CT 2 (s)	ΔV (m/s)	CR at EI	FPA at EI (deg)
1	24137.89	0.00	278.00	3069.52	156.9948	0.1155	-0.9711
2	24196.34	0.00	276.00	3010.76	156.4405	0.1157	-0.9703
3	23514.82	0.00	276.00	2949.05	155.7593	0.1632	-0.9730
4	21583.34	255.14	273.00	5871.10	154.0398	0.0837	-0.9745
5	21431.90	399.00	269.68	5936.78	151.8254	0.0802	-0.9725
6	23650.50	0.00	269.99	2767.40	152.3673	0.1665	-0.9680
7	23724.13	0.00	258.00	2704.50	145.4507	0.1666	-0.9681
8	23487.80	0.00	250.00	2639.80	140.8751	0.1863	-0.9667
9	23851.50	0.00	241.00	2571.77	135.6583	0.1680	-0.9670
10	22260.24	1346.28	229.00	2500.49	128.8536	0.1890	-0.9637
11	23934.02	0.00	218.00	2423.53	122.4978	0.1680	-0.9641
12	23947.83	0.00	203.00	2339.17	114.0078	0.1792	-0.9599
13	23911.68	0.00	185.00	2238.88	103.7247	0.1890	-0.9585
14	24080.57	0.00	164.00	2110.19	91.7796	0.1878	-0.9564
15	29259.50	0.00	136.00	1758.26	76.6165	0.1192	-0.9478
16	81709.59	1255.96	274.00	1714.84	154.2706	0.0307	-1.0000
17	81506.08	948.55	381.00	1613.64	217.0116	0.0630	-1.0000
18	81657.70	1138.90	454.00	1632.28	260.1319	0.0353	-1.0000
19	82519.44	782.03	528.00	1492.60	304.3873	0.0074	-1.0000
20	82116.31	1142.65	623.00	1271.82	362.7329	0.0180	-1.0000

Figure 4.11 shows the change in ΔV as initial orbit altitude increases for cases 1 - 20 for the fixed EI flight path angle and velocity. ΔV decreases as altitude increases from 200 km to 340 km. After 340 km, ΔV increases dramatically. Figure 4.11 shows the same trend as Figure 4.10. This coincides with the impulsive results in Section 4.1. After 370 km altitude, the impulse increases dramatically because more thrust is required to place the vehicle on a Keplerian orbit that will intersect EI with the correct conditions. The targeted flight path angle changes when the altitude increased from 340 km altitude to the higher altitudes. The new targeted flight path angle corresponds to a transfer orbit with higher apogee altitude (see Table 4.3). To illustrate the rapid rise in ΔV more clearly, Figure 4.12 shows the plot for select cases from 1 to 22. As shown for case 22, the required ΔV to deorbit is very large, over 2600 m/s.

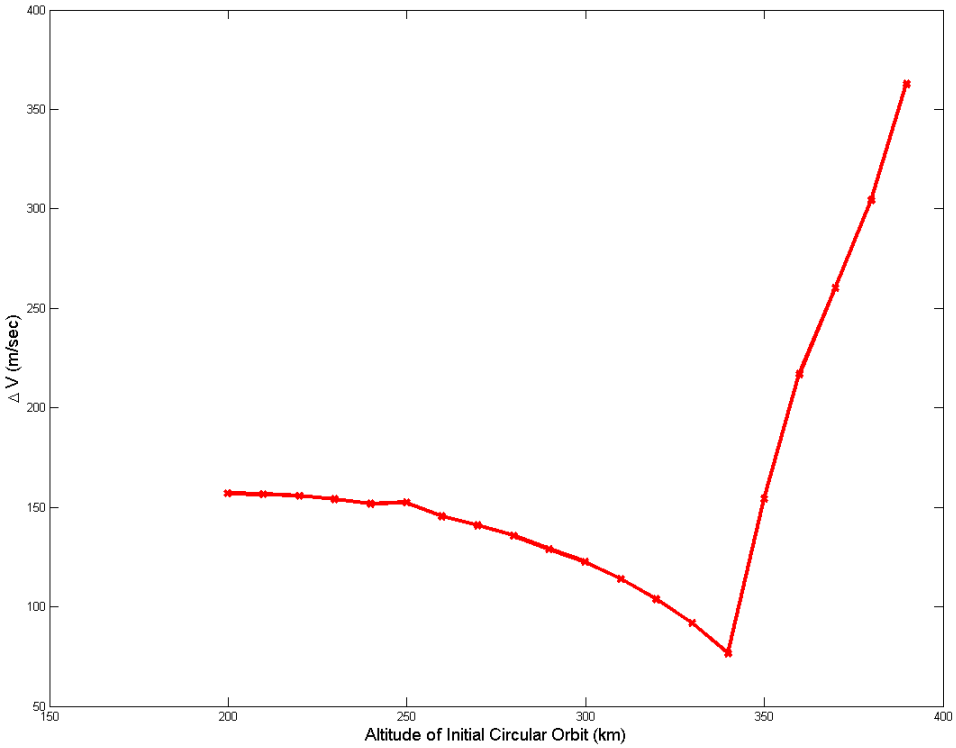

Figure 4.11 ΔV of coast-burn-coast solutions with terminal conditions set 5 (Eqs. (3.90)–(3.97) and (3.54)) for cases 1 - 20

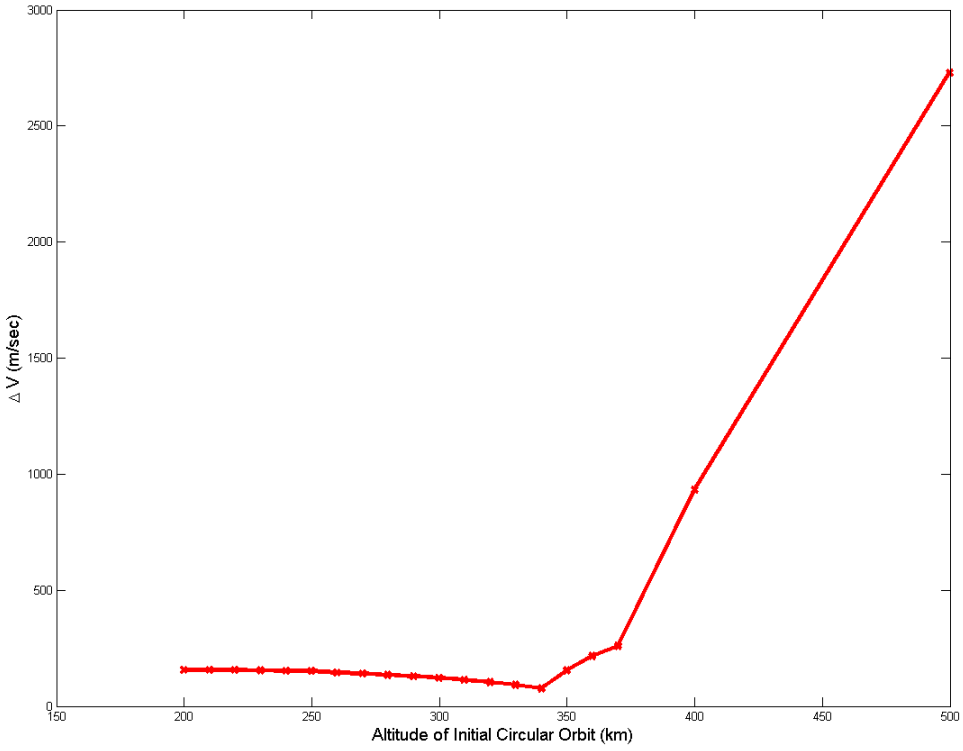

Figure 4.12 ΔV of coast-burn-coast solutions with terminal conditions set 5 (Eqs. (3.90)–(3.97) and (3.54)) for cases 1 - 22

Table 4.6 Results for circular cases 1 - 20 with coast-burn-coast formulation, set 3 (Eqs. (3.66)–(3.68), (3.76), (3.77), (3.80), and (3.54)) terminal constraints and unconstrained crossrange

Case	M CT (s)	CT 1(s)	BT (s)	CT 2 (s)	ΔV (m/s)	CR at EI	FPA at EI (deg)
1	21352.89	1170.68	261.00	3270.50	146.7741	0.2070	-0.8050
2	21331.34	948.36	261.00	3204.35	146.8950	0.2268	-0.8050
3	21359.82	1049.13	260.00	3138.55	146.3713	0.2228	-0.8050
4	21533.34	769.08	258.00	3072.61	145.1976	0.2339	-0.8050
5	21611.90	784.03	255.00	3006.18	143.3575	0.2324	-0.8050
6	21490.50	713.00	250.95	2939.68	140.8234	0.2492	-0.8050
7	21629.13	854.03	245.00	2870.55	137.5856	0.2361	-0.8050
8	75807.28	503.15	238.00	6267.70	133.5259	0.1674	-0.8050
9	75702.75	615.01	229.00	2726.89	128.6819	0.3934	-0.8050
10	75928.34	789.40	219.00	2649.01	122.8632	0.3735	-0.8050
11	76124.07	940.05	207.00	2565.03	115.9443	0.3576	-0.8050
12	21842.83	1422.99	192.00	2472.23	107.7224	0.2149	-0.8050
13	21866.68	1465.79	175.00	2361.84	97.8341	0.2188	-0.8050
14	22435.57	2103.42	153.00	2214.77	85.7313	0.1525	-0.8050
15	78768.23	0.00	144.00	1769.59	80.3256	0.3037	-0.9849
16	26478.46	1473.99	168.00	1619.76	93.9454	0.0287	-1.2912
17	26577.45	1449.71	189.00	1519.83	105.6377	0.0284	-1.5131
18	80072.70	10.66	245.00	1459.95	137.5913	0.2331	-1.6000
19	80329.44	0.00	349.00	1427.66	197.8641	0.2128	-1.6000
20	79861.31	0.00	451.00	1493.36	258.3111	0.2320	-1.6000

4.3 Unconstrained vs. Constrained Crossrange

The effect of the crossrange distance constraint on the solution is examined. Cases 1 - 20 are run without the crossrange distance constraint in the outer loop and results are shown in Table 4.6. Table 4.6 is constructed the same as Table 4.5. The largest crossrange value at EI is in case 9 at a value of 2509 km. This crossrange distance is unacceptably high and the vehicle will not be able to cover such a long crossrange distance during the entry phase of flight.

Table 4.7 shows the differences in burn time and the final crossrange distance at EI for both the constrained and unconstrained cases. Column 1 is the case number, column 2 is the difference in burn time between the two methods, column 3 is the crossrange distance at EI with the outerloop constraint, and column 4 is the crossrange distance without the outerloop constraint. The burn time does not vary for most cases between the constrained and unconstrained crossrange distance cases. Case 7 has the largest

difference in burn time. The final EI flight path angle for the unconstrained case is $-.805$ degrees while for the constrained case is -1.0367 degrees. The variable flight path angle and velocity at EI are the cause of this difference in burn time and not the crossrange distance constraint. The final coast time from the end of the burn to EI does not differ greatly from the final coast for the constrained cases. The area of significant difference is in the initial coast time of the combined manual coast and initial coast of the CBC solution. Different $\mathbf{1}_{HAC}$ vectors are targeted in the solutions so a direct comparison cannot be made between the constrained and unconstrained solutions. However, since the burn time and final coast times do not vary dramatically, the only other variation comes from initial coast time. Case 16 and 17 met the crossrange tolerance by chance. The manual coast times for these cases are long enough so that the optimal CBC solution meets the tolerance naturally. There is a significant difference in final crossrange distance at EI between the constrained and unconstrained cases. The unconstrained cases differ by upwards of 1000 km from the constrained cases. The final crossrange at EI for cases 14, 16, and 17 are the same. This is because the optimal solution of the constrained problem is also an optimal solution for the unconstrained problem.

4.4 Single vs. Multiple Burn Solutions for High Altitude Orbit

For higher altitude circular orbits, multiple burns are a more effective method for the deorbit maneuver. For example, when the Space Shuttle completes a mission to the Hubble Telescope, a two burn maneuver is used to reach the high altitude of Hubble. For altitudes higher than 370 km, the burn time increases rapidly in the single burn case. BC results for higher altitude orbits are shown in Table 4.8. Column 1 is the case number, column 2 is the manual coast time, and columns 3 and 4 list the burn time, and final coast time all in seconds. Column 5 is the equivalent impulse of the burn

Table 4.7 Difference in burn time and crossrange at EI between the constrained and unconstrained crossrange coast-burn-coast solutions for cases 1 - 20

Case	BT Diff(s)	CR at EI with constraint (km)	CR at EI without constraint (km)
1	0	1173	1320
2	0	1185	1446
3	.45	1211	1421
4	0	1202	1491
5	0	1155	1482
6	.95	0	1590
7	23	20	1505
8	0	942	1067
9	6.13	804	2509
10	0	663	2382
11	0	768	2280
12	0	1078	1370
13	0	968	1395
14	0	972	972
15	2	299	1936
16	0	183	183
17	0	181	181
18	0	65	1486
19	0	122	1357
20	0	77	1479

time, column 6 is the crossrange at EI and column 7 is the flight path angle at EI. The burn time can be almost 2500 seconds for an altitude of 1100 km. This is unacceptable for a shuttle type vehicle with weight constraints. There would not be enough fuel to complete a 2500 second burn. The final mass at the end of the burn is not negative but for a burn time of 2500 seconds, the mass decreases around 40000 kg. The Shuttle does not have 40000 kg of fuel readily accessible to burn for such a maneuver.

For cases 21 - 28, the altitude of the orbit is so large that no impulsive solution exists that targets the appropriate EI conditions. The large burn times of the BC solution are necessary to place the vehicle on a Keplerian orbit that intersects EI with the required EI conditions met. The vehicle has to burn to compensate for the difference in altitude between the initial orbit and the desired transfer orbit. To see if the requirement on large amounts of propellant can be replaced, multiple burns are used. More specifically, a two burn solution with an intermediate coast for the BCB solution and two burns with

Table 4.8 Results for circular cases 21 - 28 with burn-coast formulation, set 3 (Eqs. (3.66)–(3.68), (3.76), (3.77), (3.80), and (3.54)) terminal constraints and constrained crossrange

Case	M CT (s)	BT (s)	CT (s)	ΔV (m/s)	CR at EI	FPA at EI (deg)
21	22298.80	1199.00	3050.93	740.4153	0.1754	-0.8050
22	22892.21	1328.00	2716.51	832.1036	0.1506	-0.8050
23	26019.22	1307.00	855.49	817.0973	0.0710	-0.8050
24	25168.60	1496.00	943.09	955.3187	0.1077	-0.8050
25	22451.70	1827.00	674.96	1213.6192	0.2773	-1.6001
26	23307.45	1840.00	447.91	1224.3499	0.2363	-1.6000
27	23180.81	2132.00	577.89	1472.8062	0.2175	-1.6001
28	24981.79	2491.00	3881.10	1805.5433	0.1320	-1.3452

Table 4.9 Results for circular cases 21 - 28 with burn-coast-burn-coast formulation, terminal constraints set 3 (Eqs. (3.66)–(3.68), (3.76), (3.77), (3.80), and (3.54)) and constrained crossrange

Case	M CT (s)	BT 1(s)	CT 1 (s)	BT 2 (s)	CT 2	ΔV 1 (m/s)	ΔV 2 (m/s)	CR at EI	FPA at EI (deg)
21	78248.31	240.00	2769.72	134.00	4046.53	134.6148	78.0426	0.0019	-0.8050
22	23162.21	283.00	1998.62	236.00	2283.62	159.8659	139.7210	0.0849	-0.8050
23	23359.22	210.00	2985.19	315.00	2022.00	117.9562	185.1712	0.0255	-1.0295
24	21213.60	269.00	2941.11	324.00	1896.05	151.4162	192.7081	0.1693	-0.8050
25	19566.70	328.00	1757.58	281.00	6069.51	185.7052	168.5805	0.0824	-0.8050
26	21992.45	276.00	2444.15	383.00	1920.93	155.4823	229.5779	0.1455	-0.8050
27	78123.25	329.00	2325.53	426.00	1937.13	186.4047	259.2863	0.1466	-0.8050
28	23176.79	366.00	2435.17	459.00	1962.66	208.0804	282.2811	0.0570	-0.8050

an intermediate and final coast for the BCBC solution. An initial coast outside of the manual coast is avoided because the algorithm has a hard time handling more than four arcs numerically. Table 4.9 shows the results of the BCBC solution for cases 21 through 28. Column 1 is the case number, column 2 is the manual coast time, and columns 3, 4, 5 and 6 list the first burn time, intermediate coast time, final burn time, and final coast time all in seconds. Columns 7 and 8 are the equivalent impulses of the corresponding burn times, column 9 is the crossrange at EI and column 10 is the flight path angle at EI.

The altitude for cases 21 - 28 with the BCBC solution is shown in Figure 4.13. The corresponding thrust angles for the first and second burns are shown in Figures 4.14 and

4.15. The trend of the thrust angle for the first burn is the same for cases 21 - 28. The thrust angles greater than 180 degrees are for cases 23 and 24 and this corresponds to an increase in altitude during the first burn. For cases 21 and 25 the altitude of the vehicle goes below EI altitude. The second burn thrust angle for these cases differs from the trend of the other cases. Case 25 has an increasing thrust angle greater than 180 degrees. The thrust angle for case 21 is less than 180 degrees and has a different pattern than the other angles. The different thrust angle pattern correspond to the vehicle altitude going below EI altitude.

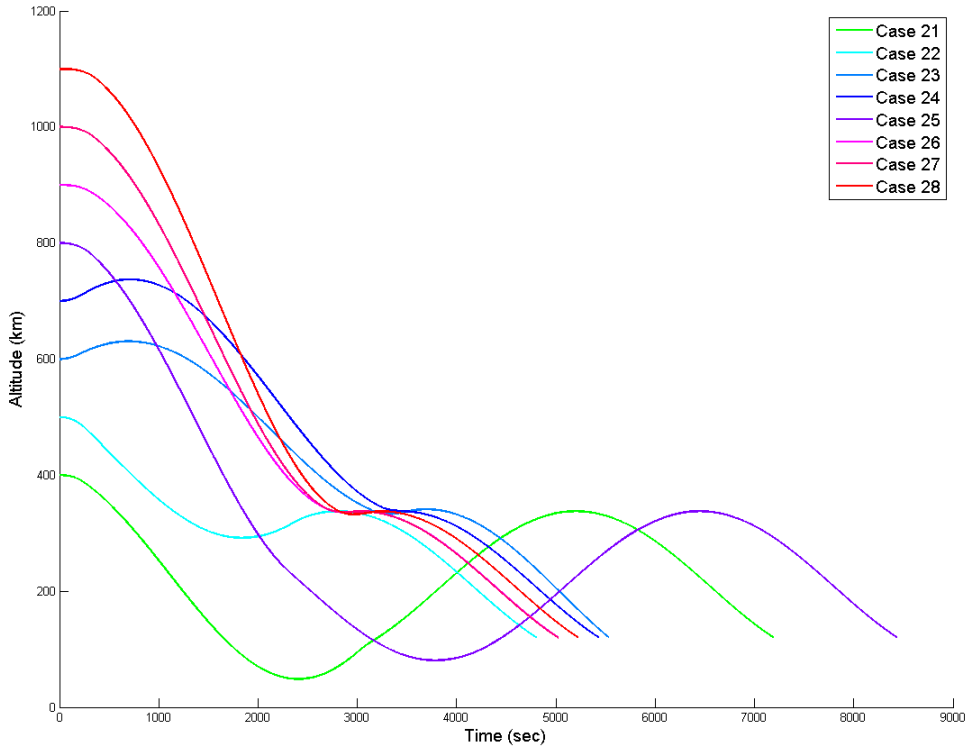

Figure 4.13 Altitude for cases 21 - 28 with burn-coast-burn-coast solution and terminal constraints set 3 (Eqs. (3.66)–(3.68), (3.76), (3.77), (3.80), and (3.54)).

In previous work a multiple burn maneuver was constructed by first burning to an intermediate orbit and then after completing one period of the intermediate transfer

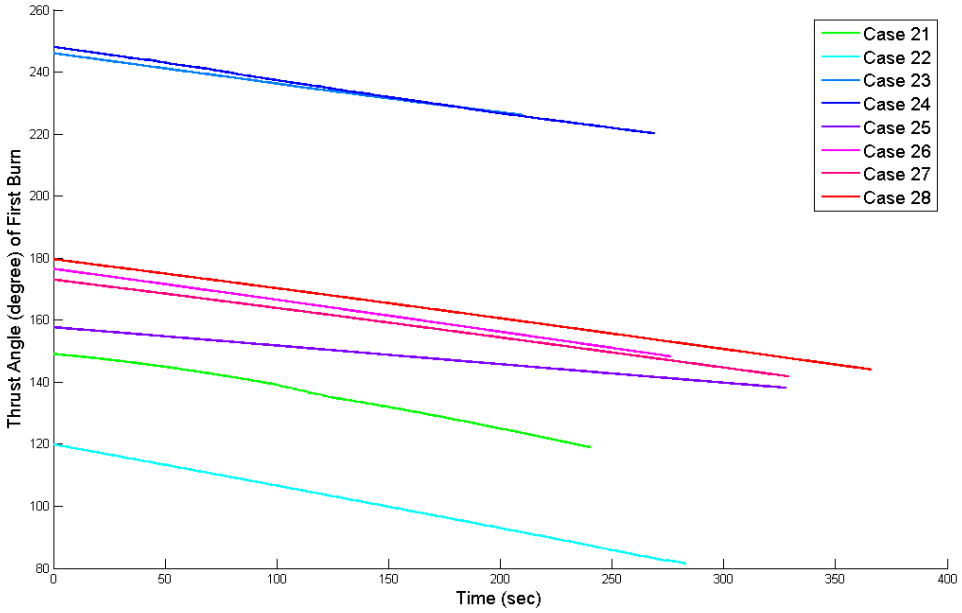

Figure 4.14 Thrust angle during first burn for burn-coast-burn-coast solution of circular cases 21 through 28

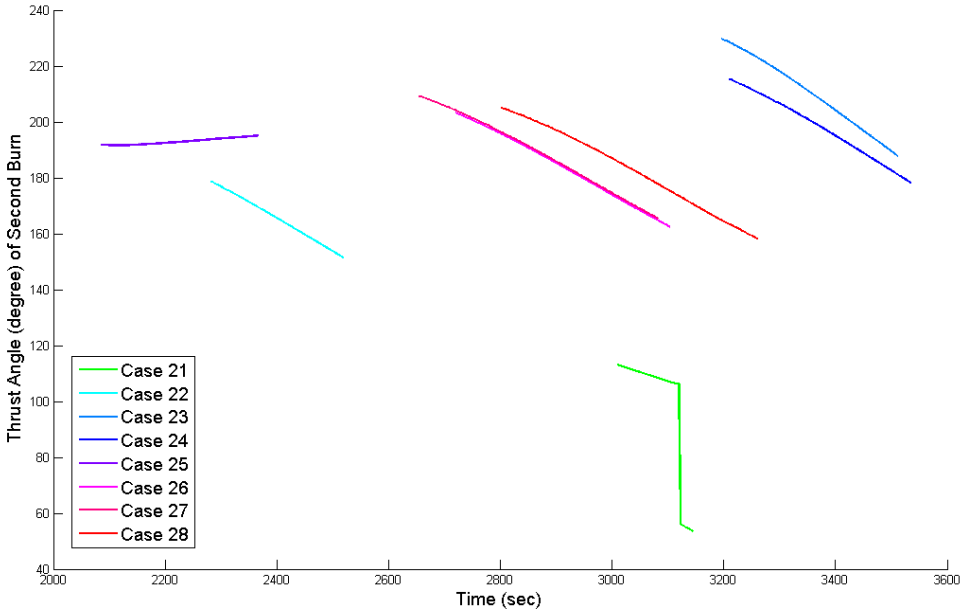

Figure 4.15 Thrust angle during second burn for burn-coast-burn-coast solution of circular cases 21 through 28

orbit, burning to a transfer orbit to get to EI. Column 4 in Table 4.9 shows the intermediate coast times of the flights. The coast times in column 4 of Table 4.9 are too small to represent one full orbital period on the intermediate transfer orbit. The final coast times for cases 21 and 25 is significantly longer than the final coast in the other cases. The vehicle coasts on the final transfer orbit for more than half the period of the orbit. The final transfer orbit must intersect with the EI orbit of 120 km altitude at some point or points along the trajectory and therefore must have an orbit altitude less than 120 km for some part of the orbit. The longer the vehicle stays on the final transfer orbit, the more likely the vehicle will travel below the EI altitude of 120 km. For example, the final coast for case 25 is greater than 6000 seconds. During the final coast the vehicle travels below an altitude of 120 km. There is no constraint in the solution process that keeps this type of trajectory from occurring. Figures 4.16 and 4.17 show sample BCBC coast trajectories for cases 25 and 26. Figure 4.16 shows the final trajectory traveling below the 120 km altitude of EI and then increasing in altitude till reaching EI with the required conditions met.

The final coast is removed and Cases 21 through 28 are run using a BCB solution. The results are shown in Table 4.10 where column 1 is the case number, 2 is the manual coast time, columns 3,4, and 5 are the first burn time, intermediate coast time, and final burn time, columns 6 and 7 are the equivalent impulses of the corresponding burns times, column 8 is the crossrange at EI, and column 9 is the flight path angle at EI. Inplane trajectories for cases 25 and 26 are shown in Figures 4.18 and 4.19. By not allowing the final coast, the vehicle never goes below an altitude of 120 km.

Table 4.11 shows the total burn times and ΔV of each type of solution from cases 21 through 28. Column 1 is the case number, columns 2 and 3 are the BC burn time and its corresponding ΔV, columns 4 and 5 are the BCBC burn time and its corresponding ΔV, and columns 6 and 7 are the BCB burn time and its corresponding ΔV. For cases 22 through 28, multiple burns yielded much smaller total burn times with the BCB solution

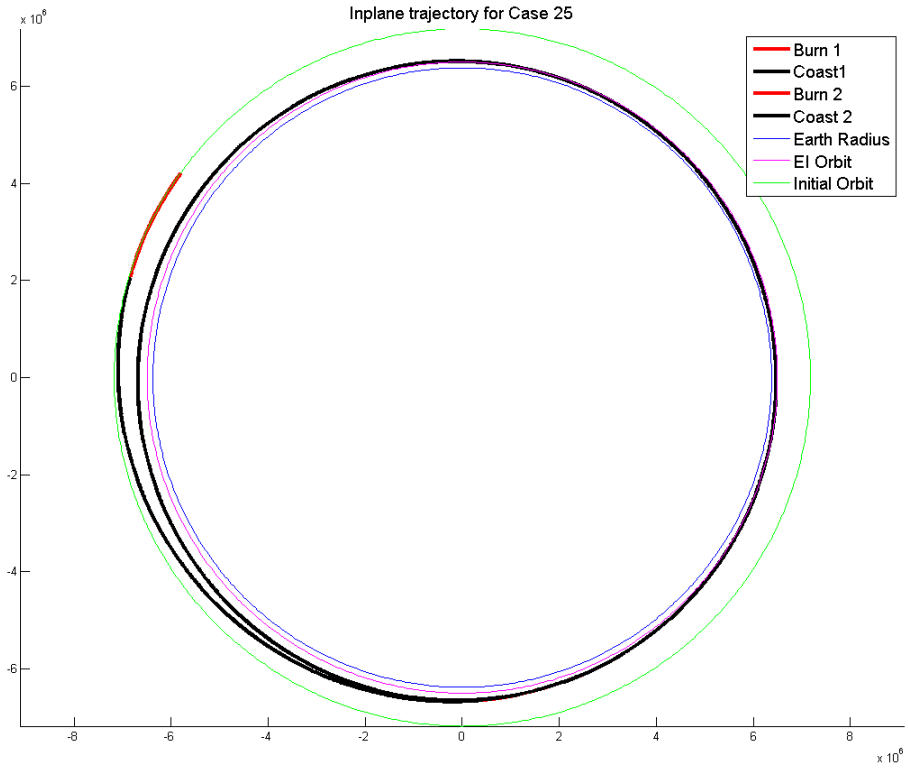

Figure 4.16 Inplane trajectory of Case 25 with burn-coast-burn-coast trajectory

Table 4.10 Results for circular cases 21 - 28 with burn-coast-burn formulation, terminal constraints set 3 (Eqs. (3.66)–(3.68), (3.76), (3.77), (3.80), and (3.54)) and constrained crossrange

Case	M CT (s)	BT 1(s)	CT (s)	BT 2 (s)	ΔV 1 (m/s)	ΔV 2 (m/s)	CR at EI	FPA at EI (deg)
21	25683.80	241.00	2210.00	134.00	135.2798	77.3834	0.0655	-1.6004
22	23337.21	234.00	2504.00	148.00	131.6584	85.8360	0.1962	-0.8053
23	23279.22	272.00	2527.00	192.00	153.0651	112.7210	0.1933	-0.8049
24	23383.60	326.00	2575.00	257.00	184.5747	152.9777	0.1760	-0.8046
25	23841.70	361.00	1806.00	241.00	204.8530	144.6582	0.1945	-1.7884
26	24342.45	375.00	2087.00	288.00	213.0808	173.9578	0.1407	-1.4174
27	80063.25	403.00	2339.00	316.00	229.6619	192.3832	0.1479	-0.8096
28	81702.15	444.00	2263.00	347.00	253.8444	213.6566	0.0434	-0.8445

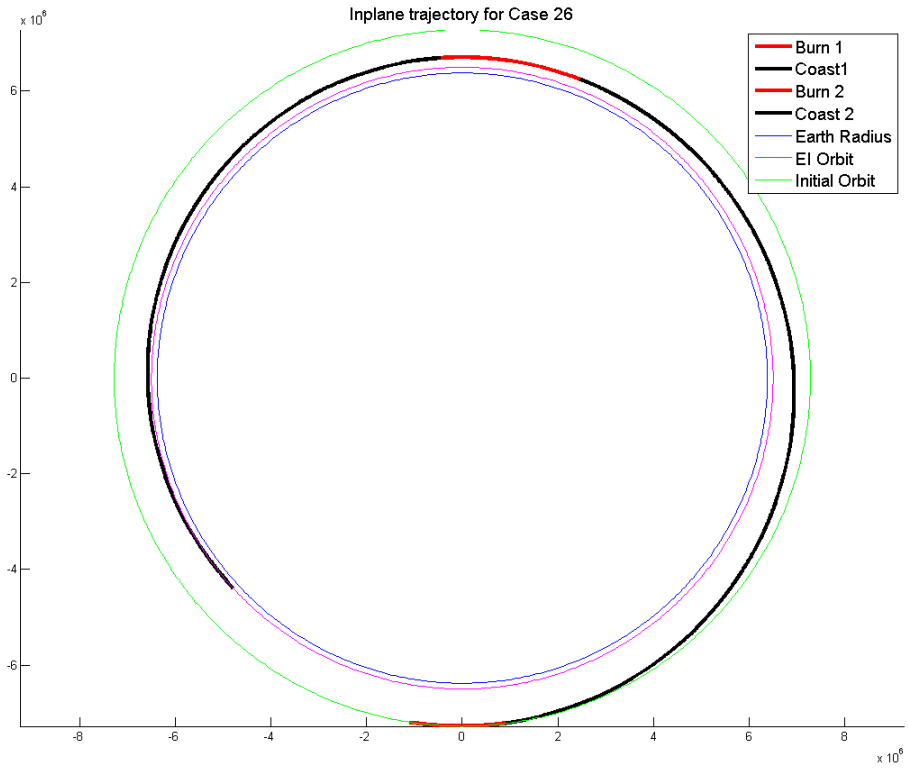

Figure 4.17 Inplane trajectory of Case 26 with burn-coast-burn-coast trajectory

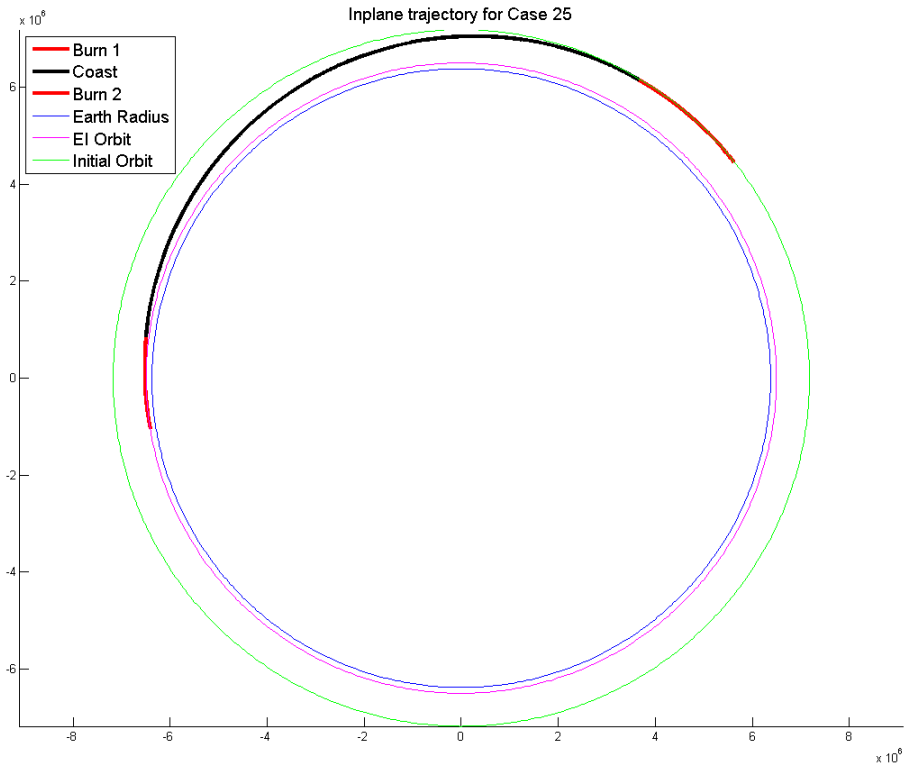

Figure 4.18 Inplane trajectory of Case 25 with burn-coast-burn trajectory

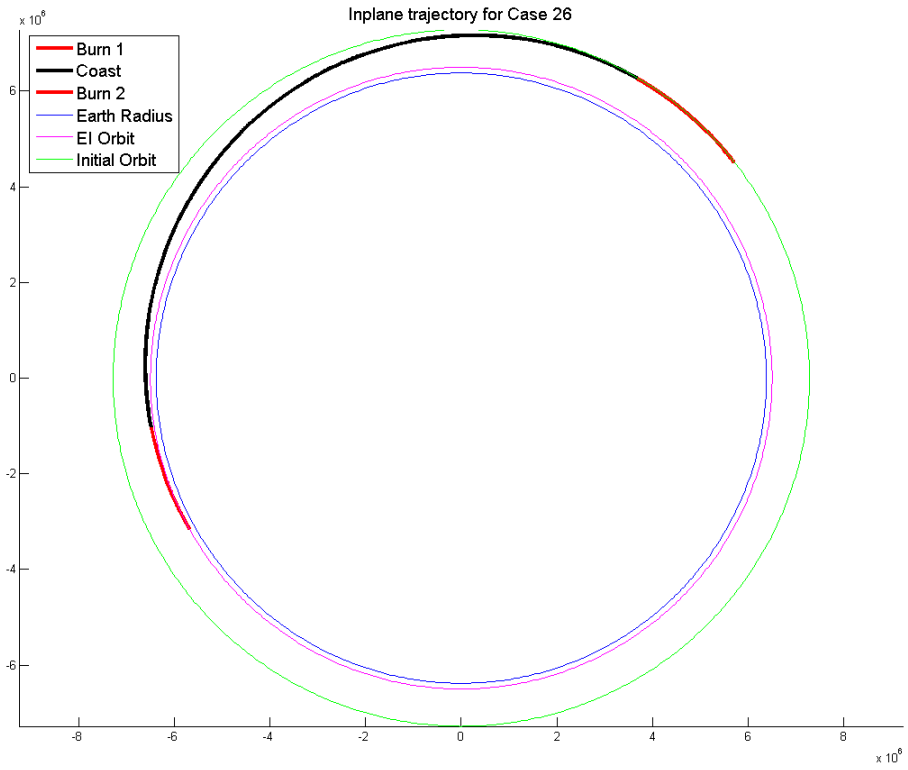

Figure 4.19 Inplane trajectory of Case 26 with burn-coast-burn trajectory

Table 4.11 ΔV and Burn Time for burn-coast, burn-coast-burn-coast, and burn-coast-burn solutions for cases 21 - 28 with constrained crossrange and terminal conditions set 3 (Eqs. (3.66)–(3.68), (3.76), (3.77), (3.80), and (3.54))

Case	BC BT (s)	BC ΔV (m/s)	BCBC BT (s)	BCBC ΔV (m/s)	BCB BT (s)	BCB ΔV (m/s)
21	1199.00	740.4153	374.00	212.66	374.27	212.66
22	1328.00	832.1036	519.00	299.59	381.81	217.49
23	1307.00	817.0973	525.00	303.13	463.91	265.79
24	1496.00	955.3187	593.00	344.12	582.13	337.55
25	1827.00	1213.6192	609.00	354.29	601.93	349.51
26	1840.00	1224.3499	659.00	385.06	662.58	387.04
27	2132.00	1472.8062	755.00	445.69	718.40	422.05
28	2491.00	1805.5433	825.00	490.36	790.34	467.50

yielding the smallest of all total burn times. For vehicles like NASA's Space Shuttle, BCB is a completely impractical solution. Because the vehicle has to rotate in order to rotate its engines during a burn, the vehicle will not be in a suitable alignment once it reaches entry. Depending on the thrust vector direction, during a BCB flight the vehicle could reach entry and go into the atmosphere engines first, which is undesirable. Figure 4.20 shows the variation of ΔV over initial orbit altitude for the BC, BCBC, and BCB formulations. The BC solution has high ΔV in comparison to the two burn maneuvers. For altitudes of 400, 700, 800, and 900 km the difference in burn time of the two burn maneuvers is less than 11 seconds. For the other altitudes, the burn times differ by more than 30 seconds. The manual coast times differ between the different solution formulations for each case. This means that the optimal control problem is solved with different initial conditions, as well as a different number of arcs. It is difficult to directly compare the two burn maneuvers with each other because two different problems are being solved.

4.5 Summary

The major findings in this chapter are as follows:

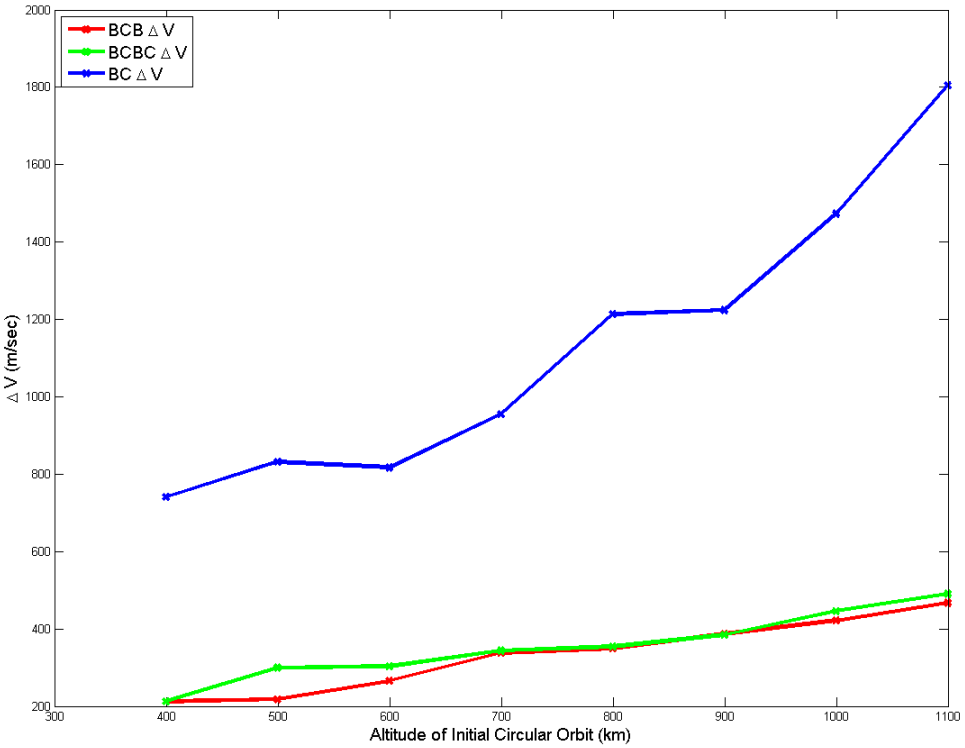

Figure 4.20 ΔV for cases 21 - 28 for burn-coast, burn-coast-burn-coast, and burn-coast-burn solutions with terminal conditions set 3 (Eqs. (3.66)–(3.68), (3.76), (3.77), (3.80), and (3.54))

- The EI conditions determine the transfer orbit of the deorbit maneuver. There is a specified altitude, such that for any higher altitude, there does not exist an impulsive solution that places the vehicle on a Keplerian transfer orbit to meet the required EI conditions.

- For low altitude circular orbits, the burn time decreases as altitude increases till an orbit altitude of 340 km. After 340 km, as altitude increases, the burn time increases. The burn times agree with Shuttle mission data for missions that deorbited from the International Space Station orbit.

- A crossrange constraint at EI has little effect on required burn time for the vehicle to deorbit safely. If the crossrange is not constrained, the vehicle would be required to travel a large crossrange distance during entry, which is undesirable.

- Allowing for variable velocity and flight path angle at EI allows for a range of values to be targeted, with the final values at EI being determined by the guidance solution. Unexpected increases or decreases in burn time are accounted for by the variable EI conditions.

- Single burns for high altitude orbits are not optimal. Burn time increases rapidly with increasing altitude after 340 km. The two burn maneuver with or without final coast has shorter total burn time than the single burn maneuver.

CHAPTER 5. Single Burn Deorbit Guidance for Initial Elliptic Orbit

The Shuttle generally deorbits from circular orbits about the Earth. Consequently, there is not much previous Shuttle work to use as a guide in studying the elliptic deorbit problem. Refs. [5], [8], and [9] state that the optimal deorbit point is at apogee on an elliptic orbit of eccentricity greater than .01 for EI conditions constrained by flight path angle and altitude. For orbits with lower eccentricity, the optimal deorbit point is nonapogee. This chapter explores the single finite time burn for elliptic orbits. More specifically, Section 1 explores the optimal coast-burn-coast solution for the elliptic orbit. The deorbit problem is solved using impulsive maneuvers in Section 2. Section 3 compares the impulsive results with nominal burn and ten time nominal burn results. The altitude is unconstrained in the algorithm and Section 4 explores the ramifications of this. The results of the chapter are summarized in the final section. The cases tested are listed in Table 5.1 where e is the eccentricity of the initial orbit, i is the inclination of the initial orbit, Ω is the longitude of the ascending node, X, Y, and Z are the components of the position in the ECI frame, and $\dot{X}$, $\dot{Y}$, and $\dot{Z}$ are the components of the velocity in the ECI frame. All results assume Keplerian motion for the coast arcs.

5.1 Solution for Low Altitude Orbits

The CBC formulation is used to solve the deorbit guidance problem for elliptic orbits. Table 5.2 shows the results for cases 1 through 20 with terminal constraints set 3 (Eqs.

Table 5.1 Test Cases for Elliptical Orbits

Case	Perigee Altitude (km)	e	i (deg)	Ω (deg)	X (km)	Y (km)	Z (km)	$\dot{X}$ (km/s)	$\dot{Y}$ (km/s)	$\dot{Z}$(km/s)
1	200	0.02	50	240	1541.808	-4725.575	4407.144	5.568	4.492	3.070
2	200	0.04	50	240	1556.627	-4770.996	4449.504	5.599	4.400	3.157
3	200	0.06	50	240	1571.159	-4815.535	4491.041	5.630	4.309	3.243
4	200	0.08	50	240	1585.411	-4859.217	4531.780	5.661	4.221	3.328
5	200	0.10	50	240	1599.392	-4902.067	4571.743	5.692	4.135	3.411
6	250	0.02	50	240	1553.527	-4761.495	4440.643	5.547	4.475	3.058
7	250	0.04	50	240	1568.459	-4807.261	4483.325	5.578	4.383	3.145
8	250	0.06	50	240	1583.101	-4852.138	4525.178	5.609	4.293	3.231
9	250	0.08	50	240	1597.462	-4896.152	4566.227	5.640	4.205	3.315
10	250	0.10	50	240	1611.549	-4939.328	4606.493	5.671	4.119	3.398
11	300	0.02	50	240	1565.247	-4797.414	4474.142	5.526	4.458	3.047
12	300	0.04	50	240	1580.291	-4843.526	4517.146	5.557	4.367	3.133
13	300	0.06	50	240	1595.044	-4888.741	4559.315	5.588	4.277	3.219
14	300	0.08	50	240	1609.513	-4933.088	4600.673	5.619	4.189	3.303
15	300	0.10	50	240	1623.706	-4976.589	4641.243	5.650	4.104	3.385
16	350	0.02	50	240	1576.966	-4833.334	4507.641	5.506	4.442	3.035
17	350	0.04	50	240	1592.124	-4879.790	4550.967	5.537	4.350	3.122
18	350	0.06	50	240	1606.987	-4925.345	4593.452	5.567	4.261	3.207
19	350	0.08	50	240	1621.564	-4970.023	4635.120	5.598	4.174	3.290
20	350	0.10	50	240	1635.863	-5013.850	4675.994	5.629	4.088	3.373
21	400	0.02	50	240	1588.686	-4869.253	4541.140	5.485	4.425	3.024
22	400	0.04	50	240	1603.956	-4916.055	4584.788	5.516	4.334	3.110
23	400	0.06	50	240	1618.929	-4961.948	4627.589	5.547	4.245	3.195
24	400	0.08	50	240	1633.615	-5006.959	4669.566	5.577	4.158	3.278
25	400	0.10	50	240	1648.020	-5051.112	4710.744	5.608	4.073	3.360
26	500	0.02	50	240	1612.125	-4941.093	4608.139	5.446	4.394	3.003
27	500	0.04	50	240	1627.620	-4988.585	4652.431	5.476	4.303	3.088
28	500	0.06	50	240	1642.815	-5035.155	4695.863	5.507	4.215	3.172
29	500	0.08	50	240	1657.717	-5080.830	4738.460	5.537	4.128	3.255
30	500	0.1	50	240	1672.335	-5125.634	4780.245	5.567	4.044	3.336

Table 5.2 Results for coast-burn-coast solution with terminal constraints set 3 (Eqs. (3.66)–(3.68), (3.76), (3.77), (3.80), and (3.54))

Case	M CT (s)	CT 1(s)	BT (s)	CT 2 (s)	Δ V (m/s)	ν at burn	CR at EI	FPA at EI (deg)
1	24846.3347	650.8512	128.0000	998.9871	71.4851	292.8292	0.1706	-0.8050
2	82066.4640	864.3285	309.0000	599.4942	174.6104	301.1641	0.1020	-1.6000
3	26498.4153	1099.0577	416.0000	692.9387	237.6660	314.7949	0.0374	-0.8050
4	81659.1289	818.6259	691.0000	272.5663	405.0271	299.3458	0.1275	-1.6000
5	28470.5842	807.7071	954.0000	25.9430	574.4288	295.4000	0.0619	-0.8050
6	25836.4056	1816.8086	215.0000	2029.1652	120.5628	58.8670	0.0388	-1.5063
7	25991.9158	1052.2498	316.0000	1005.2247	178.5387	318.3508	0.0592	-0.8050
8	81081.2544	772.8025	541.0000	2187.4833	312.5342	17.1648	0.0545	-0.8050
9	28676.7649	1063.0000	947.3422	1394.1813	569.2668	13.6654	0.1785	-1.6000
10	23263.6922	1079.3861	1092.0000	1446.8922	666.7196	4.7439	0.1541	-1.6000
11	81313.4752	876.9429	278.0000	1013.8847	156.5502	301.2840	0.1248	-1.6000
12	27150.8167	1122.5797	427.0000	1714.9962	243.7125	20.6198	0.0719	-1.6000
13	80889.6786	891.9058	566.0000	859.4004	327.6903	309.5097	0.1424	-1.6000
14	28903.7408	961.8619	712.0000	1555.2952	418.2014	359.1771	0.1818	-1.6000
15	84730.4221	2728.0714	885.0000	2113.6579	528.8143	312.2272	0.3211	-0.8280
16	82335.3259	1129.6057	317.0000	1218.4916	179.2075	324.2491	0.0278	-1.6000
17	27150.6886	1047.0813	488.0000	1211.6046	280.5744	354.2714	0.0388	-1.6000
18	29203.7754	0.0000	604.0000	1731.4250	351.1901	358.6241	0.1438	-1.6001
19	23986.4931	0.0000	823.0000	1462.1724	488.5277	359.6925	0.1931	-1.6001
20	80059.2847	1866.8114	1083.0000	2365.4611	660.5565	306.7991	0.0042	-0.8050

(3.66)–(3.68), (3.76), (3.77), (3.80), and (3.54)) used. The 1-st column is the case number corresponding to Table 4.1. The 2-nd column is the manual coast needed to target the desired $\mathbf{1}_{HAC}$ positions. A manual coast in the range of 20000 to 30000 seconds means the closest $\mathbf{1}_{HAC}$ was targeted while a manual coast time greater than 80000 seconds means the second desired $\mathbf{1}_{HAC}$ was targeted. The 3-rd, 4-th, and 5-th columns are the times of the three arcs for the optimal coast-burn-coast solution. Using the rocket equation with an engine I_{sp} of 313 seconds, the ΔV is calculated given the initial mass and final mass after the burn time. This is shown in column 6. The true anomaly at the beginning of the burn time is presented in column 7. The final crossrange at EI is given in column 8 and the flight path angle at EI is given in column 9. The crossrange distance tolerance at EI is set to 1000 km or .1568 radians.

The final crossrange at EI for cases 1, 9, 14, 15, and 19 is higher than the desired .1568 radians. Case 15 is greater than .1568 radians by over .1568 radians or 1000 km. The crossrange distance tolerance was met in the outerloop but when the closed loop

simulation was called, the solution was updated each second and changed to reach the desired EI conditions. Cases 1, 9, 14, and 19 are greater than the desired crossrange distance by less than 250 km.

The optimal deorbit point is at a nonapogee position for highly eccentric orbits. The optimal burn begins at a point that is near perigee instead of apogee. The transfer orbit results from Section 4.1 hold for elliptic orbits as well. The same entry conditions are used. Therefore, the transfer orbit altitudes for the targeted entry conditions vary from 338 km to 364 km (see Table 4.3). For cases 16 - 20 with perigee altitude equal to 350 km, the optimal place to deorbit is close to perigee so the vehicle will travel on the transfer orbit that meets the EI conditions.

As shown in Table 5.2, the burn time increases as eccentricity increases for a perigee altitude orbit. This trend is shown in Figure 5.1. Figure 5.1 also shows the variation of ΔV over initial orbit eccentricity given the initial orbits perigee altitude.

The burn time for case 10 is higher than the burn time of case 15 by approximately 200 seconds. The longer burn time is caused by several different factors. A different flight path angle at EI is targeted for each of the two cases. Also, case 10 targets the first $\mathbf{1}_{HAC}$ while the case 15 targets the second $\mathbf{1}_{HAC}$. This is evident by the significantly longer manual coast time for case 15. Targeting different $\mathbf{1}_{HAC}$ vectors means that the CBC problem is solved given a different initial position between the cases. By the problem setup, there exists a unique optimal solution given each initial position of the vehicle on the initial orbit.

The same type of burn time discrepancy also occurs between case 9 and 19. The largest difference in the solutions is the lack of an optimal initial coast in the CBC solution for case 19. The manual coast in case 9 is greater than the manual coast in case 19 by 4500 seconds. The initial position used for the optimal CBC simulation for case 19 is farther along the orbit than the initial position of case 9. These factors all contribute to the difference in burn time.

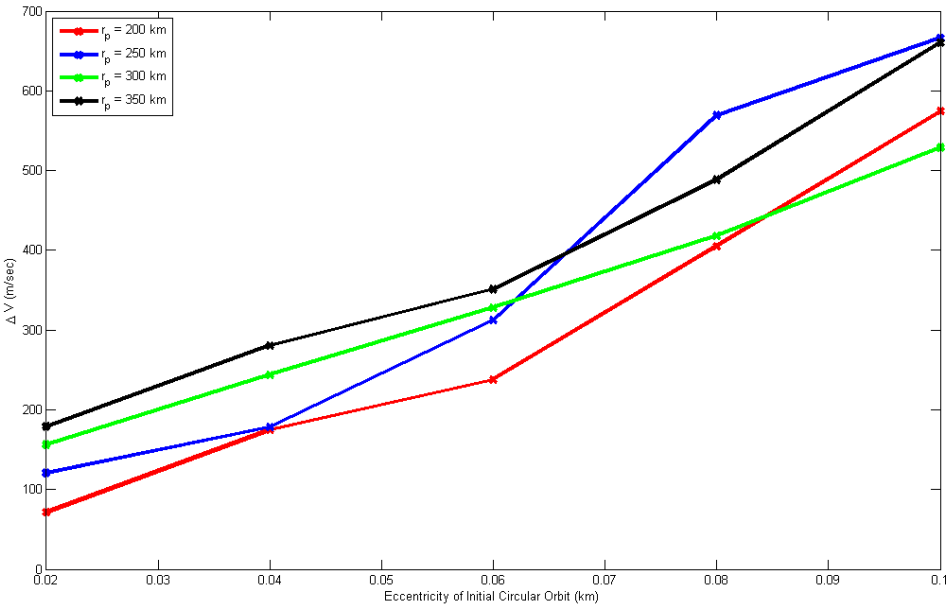

Figure 5.1 ΔV of coast-burn-coast solutions with terminal conditions set 3 (Eqs. (3.66)–(3.68), (3.76), (3.77), (3.80), and (3.54)) for cases 1 - 20

5.2 Impulsive Deorbit Maneuver

In Refs. [5], [8] and [9], it is shown that the optimal deorbit point for minimum ΔV is at apogee. In section 2.5 it was shown, using the method presented in Ref. [8], that for elliptic orbits with eccentricity greater than 0.01 the optimal deorbit point will be apogee. For initial orbits with an eccentricity less than 0.01, the optimal deorbit point will be off apogee. In these previous works, the EI flight path and EI altitude are specified but the velocity is kept unconstrained. These leads to unacceptably large EI velocity values. Figure 5.2 shows the EI velocity for each deorbit position from the method presented in Ref. [8] for a flight path angle of -1 degrees, eccentricity of 0.06, and a perigee altitude of 200 km. Deorbiting from apogee yields the highest EI velocity of 8.0827 km/s, which exceeds the highest acceptable values of 7.884 km/s for EI velocity for shuttle-type vehicles. In Ref. [9] a relationship between flight path angle and velocity was allowed in the formulation of the solution. The solution in the paper was not reproduced because the equations are ill-conditioned. Inspecting the figures in Ref. [9], the values of semi-major axis for the initial orbits placed the vehicles on an orbit that naturally intersected the EI orbit without traveling on a transfer orbit.

Using the method from Ref. [8] with the EI velocity restricted yielded different results. The approach from Ref. [8] is as follows:

The velocity impulse required to deorbit is

$$\Delta \mathbf{V} = \dot{\mathbf{r}}_{E1} - \dot{\mathbf{r}}_1 \tag{5.1}$$

where $\dot{\mathbf{r}}_1$ and $\dot{\mathbf{r}}_{E1}$ are the velocity vectors before and after the deorbit impulse. The velocity vectors may be rewritten as

$$\dot{\mathbf{r}}_{E1} = V_{E1} \sin \gamma_{E1} \mathbf{U}_0 + V_{E1} \cos \gamma_{E1} \mathbf{V}_0 \tag{5.2}$$

$$\dot{\mathbf{r}}_1 = V_1 \sin \gamma_1 \mathbf{U}_0 + V_1 \cos \gamma_1 \mathbf{V}_0. \tag{5.3}$$

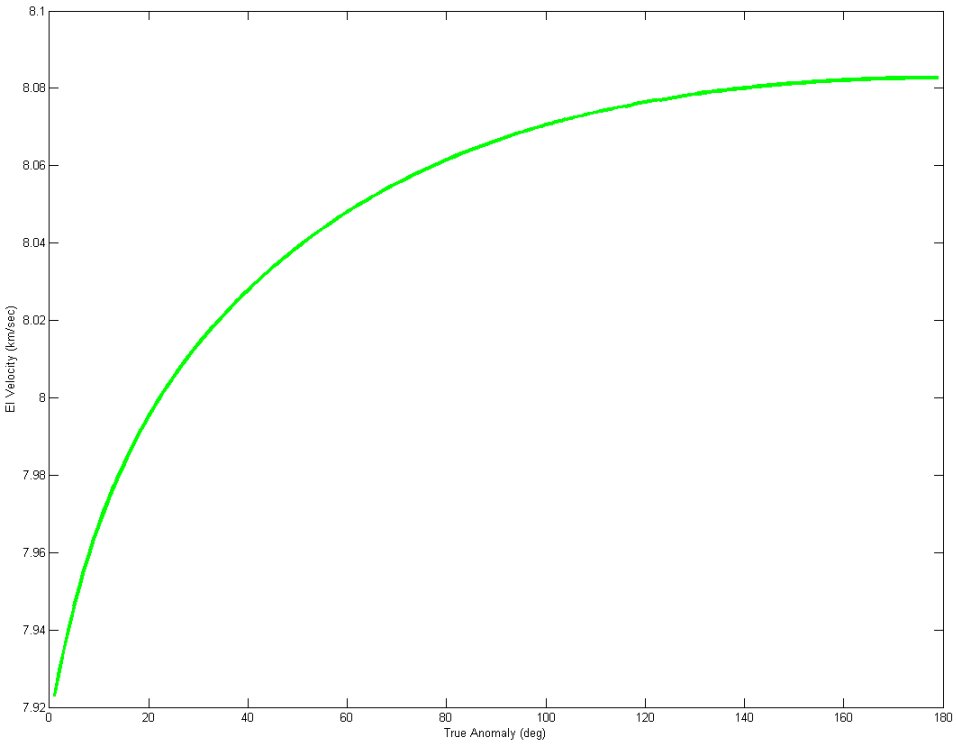

Figure 5.2 EI velocity versus true anomaly deorbit position for Orbit with eccentricity of .06, perigee altitude of 200 km, and EI flight path angle of -1 deg

The speeds before and after deorbit are V_1 and V_{E1}, with respective flight path angles γ_1 and γ_{E1}. $\mathbf{U}_0$ is a unit vector in the direction of position vector $\mathbf{r}_1$ and $\mathbf{V}_0$ is a unit vector advanced in plane 90 degrees from $\mathbf{U}_0$ in the direction of motion. Because the ΔV is impulsive, position vectors $\mathbf{r}_1$ and $\mathbf{r}_{E1}$ are identical. Define $\xi = V_1 \cos\gamma_1$ and $\eta = V_1 \sin\gamma_1$. The square of the velocity impulse may then be written as

$$\Delta V^2 = V_{E1}^2 + V_1^2 - 2\xi V_{E1} \cos\gamma_{E1} - 2\eta V_{E1} \sin\gamma_{E1}. \tag{5.4}$$

Utilizing the laws of conservation of angular momentum and energy, γ_{E1} and V_{E1} are related to reentry conditions, denoted by subscript $E1$, by

$$V_{E1}^2 = \alpha + V_{E2}^2 \tag{5.5}$$

$$V_{E1} \cos\gamma_{E1} = \lambda V_{E2} \tag{5.6}$$

where V_{E2} is the reentry velocity, $\alpha = 2\mu(1/r_{E1} - 1/r_{E2})$ and $\lambda = r_{E2}/r_{E1} \cos\gamma_{E2}$. Defining a new independent variable $\zeta = V_{E1} \sin\gamma_{E1}$, V_{E1} and V_{E2} may be rewritten as

$$V_{E1}^2 = \frac{\zeta^2 - \lambda^2\alpha}{1 - \lambda^2} \tag{5.7}$$

$$V_{E2}^2 = \frac{\zeta^2 - \alpha}{1 - \lambda^2} \tag{5.8}$$

and

$$V_{E1} \cos\gamma_{E1} = \lambda\sqrt{\frac{\zeta^2 - \alpha}{1 - \lambda^2}}. \tag{5.9}$$

Impulse velocity may then be written as

$$\Delta V^2 = \frac{\zeta^2 - \lambda^2\alpha}{1 - \lambda^2} - 2\xi\lambda\sqrt{\frac{\zeta^2 - \alpha}{1 - \lambda^2}} - 2\eta\zeta + V_1^2. \tag{5.10}$$

Modern methods allow the finding of the minimum of Eq. (5.10) without taking the partial derivatives with respect to ζ and setting Eq. (5.10) equal to zero. One such method is Matlab's fminunc to solve Eq. (5.10) for the minimum impulse and corresponding position with the constraint of EI flight path angle and altitude. The altitude

was constrained at 120 km and the flight path angle to -1 degrees. The results were the same for cases 1 through 20 with the optimal deorbit point being at apogee for minimum ΔV.

Constraining the EI velocity changes the problem. The velocity at EI is constrained using the following equation:

$$V_{E2}^{*} - \sqrt{\frac{\zeta^2 - \alpha}{1 - \lambda^2}} = 0 \tag{5.11}$$

where V_{E2}^{*} is the desired EI velocity. Matlab's fmincon with interior-point algorithm and function tolerance of 1e-6 is used to solve Eq. (5.10) with the constraint Eq. (5.11). This yields the impulsive thrust and optimal deorbit point for the given initial orbit with restricted flight path angle, altitude, and velocity. The EI velocity and flight path angle resulting from the CBC deorbit guidance solution for cases 1 through 20 was used in Matlab's fmincon as V_{E2}^{*} and EI flight path angle. Table 5.3 shows the solution of the minimization problem for cases 1 - 20. Column 1 is the case number, column 2 and 3 in the minimum impulse and location, column 4 is specified EI velocity and column 5 is the specified EI flight path angle.

In Ref. [8] it was noted that the true anomaly results are symmetric about apogee/perigee. This holds true for the results in Table 5.3. The method presented in Ref. [8] does not take into account the movement of the vehicle on the orbit, either prograde or retrograde. Thus, the symmetry is based off of geometry but is not applicable to real space flight. As shown in Table 5.3, the optimal deorbit point is not at apogee for the cases with constrained velocity. The optimal deorbit point is closer to perigee. In Ref. [22] it is shown that to achieve the greatest change in semi-major axis with respect to minimizing ΔV, the impulse should be applied at perigee, assuming a collinear burn. However, in Ref. [8] there is no such assumption made. The results shown in Table 5.3 show the minimum ΔV impulse and its location for the specified flight path angle and velocity at EI. The impulse and its location place the vehicle on a transfer orbit that intersects

Table 5.3 Impulsive maneuver results for case 1 - 20.

Case	$\Delta V_{IMPULSE}$	$\nu_{IMPULSE}$ at burn	EI Velocity (m/s)	EI FPA (deg)
1	72.8240	299.1480	7884.8759	-0.8050
2	149.5324	330.5239	7884.8717	-0.8050
3	225.5003	19.7267	7884.8714	-0.8050
4	300.7492	14.8850	7884.8706	-0.8050
5	397.7853	17.3032	7863.8424	-1.6000
6	121.0849	298.3927	7866.4491	-1.5063
7	178.3630	334.5276	7884.8737	-0.8050
8	275.7187	24.3088	7863.8674	-1.6001
9	351.4796	18.7068	7863.8502	-1.6000
10	406.4772	10.6489	7881.4832	-0.8280
11	153.2076	314.8305	7863.8448	-1.6000
12	229.3335	334.0101	7863.8507	-1.6000
13	304.7304	18.5582	7863.8468	-1.6000
14	379.4192	14.5516	7863.8567	-1.6001
15	453.4195	12.0354	7863.8593	-1.6000
16	181.6814	19.7148	7863.8474	-1.6000
17	257.5231	348.1829	7863.8458	-1.6000
18	332.6390	8.5886	7863.8405	-1.6000
19	407.0495	6.7983	7863.8455	-1.6000
20	480.7742	5.6631	7863.8517	-1.6001

with the EI orbit of 120 km altitude with the specified flight path angle and velocity values.

5.3 Impulsive vs. Nominal Thrust Deorbit

As shown in the previous section, when EI velocity is constrained, the optimal deorbit point is not at apogee but closer to perigee. Table 5.4 shows the results of CBC deorbit guidance solution with nominal thrust, ten times nominal thrust, and the impulse results from Matlab's fmincon. The guidance solution was run without the crossrange constraint.

The ten times nominal thrust cases have burn times about ten times less than the nominal thrust burn time. This gives a more representative optimal deorbit ΔV and location to the impulsive answer than the nominal case. Restricting the EI velocity moves the optimal deorbit point from apogee to near perigee. For a given perigee altitude orbit the lower the eccentricity, the farthest from perigee the optimal deorbit point is and,

Table 5.4 Elliptic orbit burn and location results for nominal thrust, ten times thrust, and impulsive thrust

Case	ΔV_{NOM}	ν_{NOM} at burn	$\Delta V_{\times 10NOM}$	$\nu_{\times 10NOM}$ at burn	$\Delta V_{IMPULSE}$	$\nu_{IMPULSE}$ at burn
1	119.5929	81.5364	80.3200	314.1446	72.8240	299.1480
2	150.1657	314.7394	168.0086	317.9382	149.5324	330.5239
3	237.6660	314.8116	220.7293	18.5056	225.5003	19.7267
4	387.1319	308.8135	312.1576	2.6586	300.7492	14.8850
5	515.2163	291.6685	368.4867	7.7607	397.7853	17.3032
6	120.5628	58.4451	121.4245	295.8076	121.0849	298.3927
7	178.5387	318.4214	196.1852	324.2110	178.3630	334.5276
8	379.5361	21.9778	272.9914	2.0441	275.7187	24.3088
9	476.4646	8.7110	333.1219	3.5339	351.4796	18.7068
10	666.6787	290.9976	395.5766	9.2879	406.4772	10.6489
11	156.5502	301.5907	149.5781	313.6239	153.2076	314.8305
12	243.7125	20.4773	224.1504	332.3498	229.3335	334.0101
13	342.0568	8.9193	279.2341	14.6674	304.7304	18.5582
14	472.7698	359.3177	371.1478	12.4188	379.4192	14.5516
15	752.0423	307.1321	467.9419	18.0909	453.4195	12.0354
16	181.2846	12.4683	206.2609	12.0814	181.6814	19.7148
17	280.5744	354.1920	243.4512	356.7278	257.5231	348.1829
18	328.2031	350.9790	346.9118	3.7416	332.6390	8.5886
19	412.0338	338.4590	398.3862	4.4621	407.0495	6.7983
20	632.0678	304.9165	471.2662	3.7704	480.7742	5.6631

as eccentricity increases the closer the deorbit point is to perigee. This is clear in the impulsive and ten times thrust case shown in Figures 5.3 and 5.4.

As eccentricity increases for the ten times nominal thrust cases, the optimal deorbit position moves farther from perigee. This is because the ten times thrust cases are solved using the guidance solution, which has the manual coast as part of the solution process. The manual coast alters the solution process. For the nominal thrust case, shown in Figure 5.5, the distance from perigee for the optimal deorbit position does not follow the same pattern as the ten times nominal thrust and impulsive thrust cases. The burn time of the nominal case is several hundred seconds. Due to long burn times, the true anomaly at the beginning of the burn will differ greatly from the impulsive maneuver. As the eccentricity increases, the length of the burn increases. Because the burn time is so much longer, the farther from perigee the vehicle is when the burn begins.

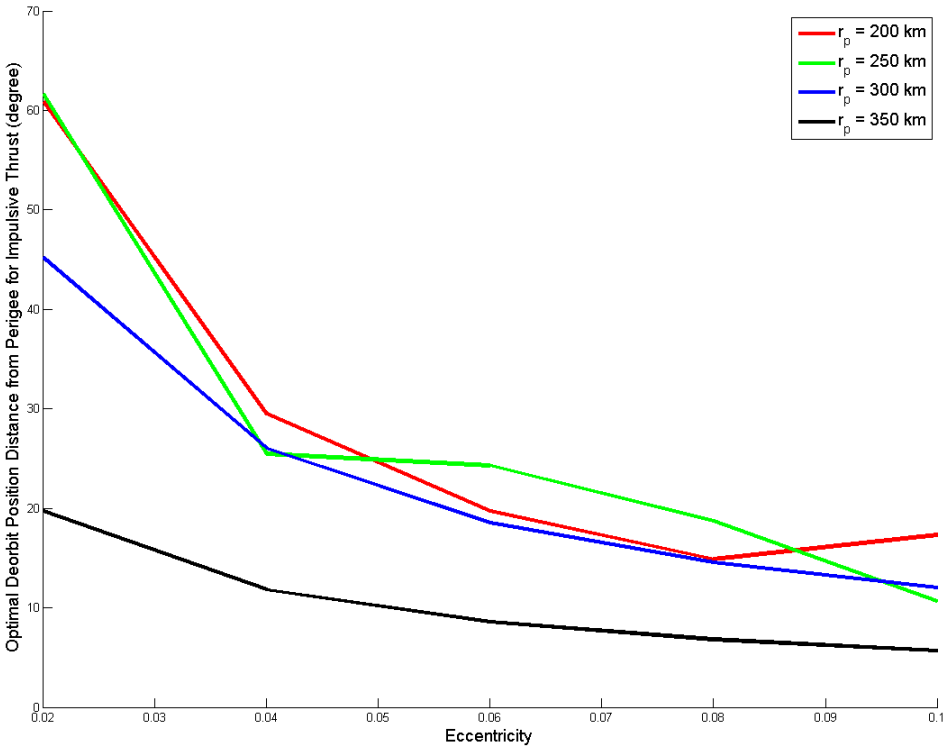

Figure 5.3 Optimal deorbit position distance from perigee of impulsive ΔV versus eccentricity for given orbit perigee altitude values of 200 km, 250 km, 300 km, and 350 km

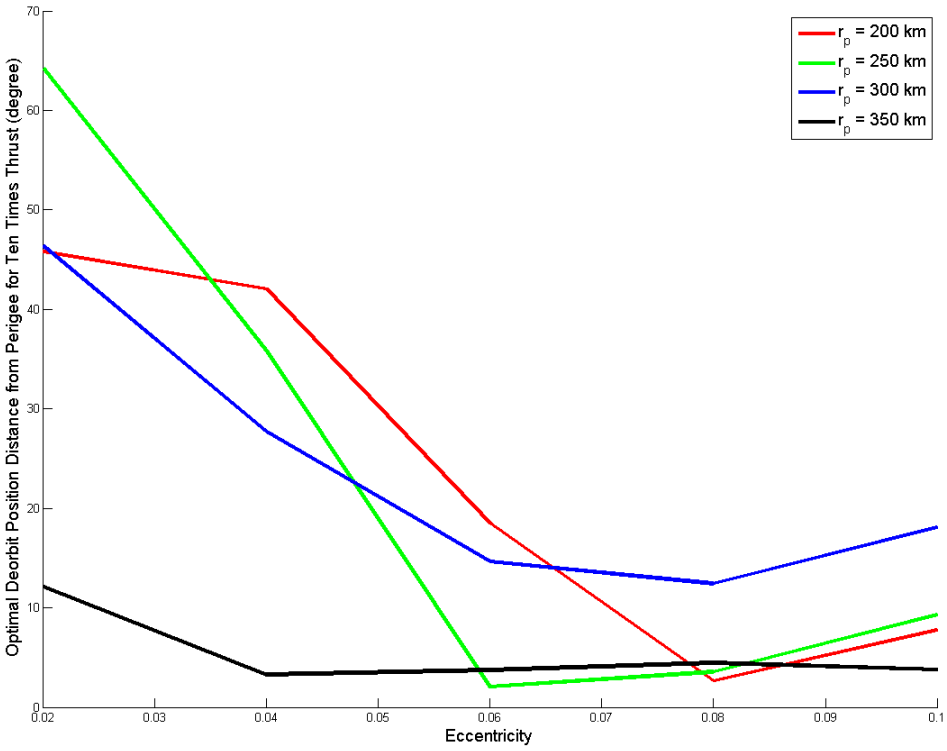

Figure 5.4 Optimal deorbit position distance from perigee of x10 nominal thrust ΔV versus eccentricity for given orbit perigee altitude values of 200 km, 250 km, 300 km, and 350 km

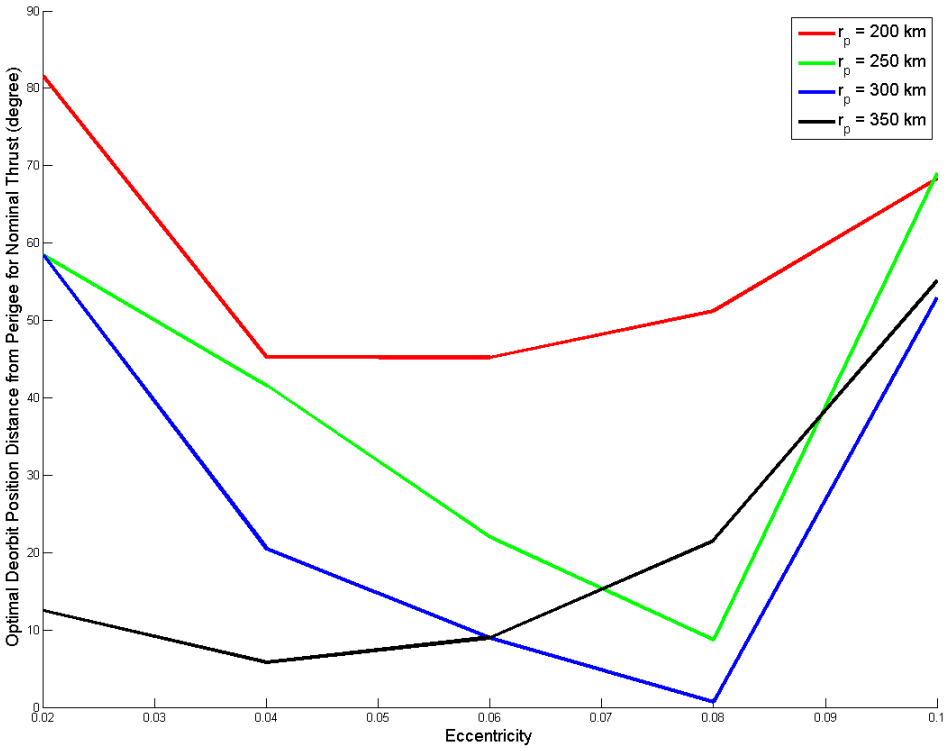

Figure 5.5 Optimal deorbit position distance from perigee of nominal thrust ΔV versus eccentricity for given orbit perigee altitude values of 200 km, 250 km, 300 km, and 350 km

5.4 Unconstrained Altitude

As mentioned in the previous chapter, there is no altitude constraint in the problem formulation. Therefore, the optimal solution may place the vehicle on an elliptic orbit with perigee altitude less than zero. Figures 5.6 and 5.8 show the altitude for the BC solution for cases 1 - 20. The thrust angle during the burn time of each test case BC solution is shown in Figures 5.7 and 5.9. There is no discernable pattern of flight path angle and altitude for the BC solution of elliptical cases 1 - 20.

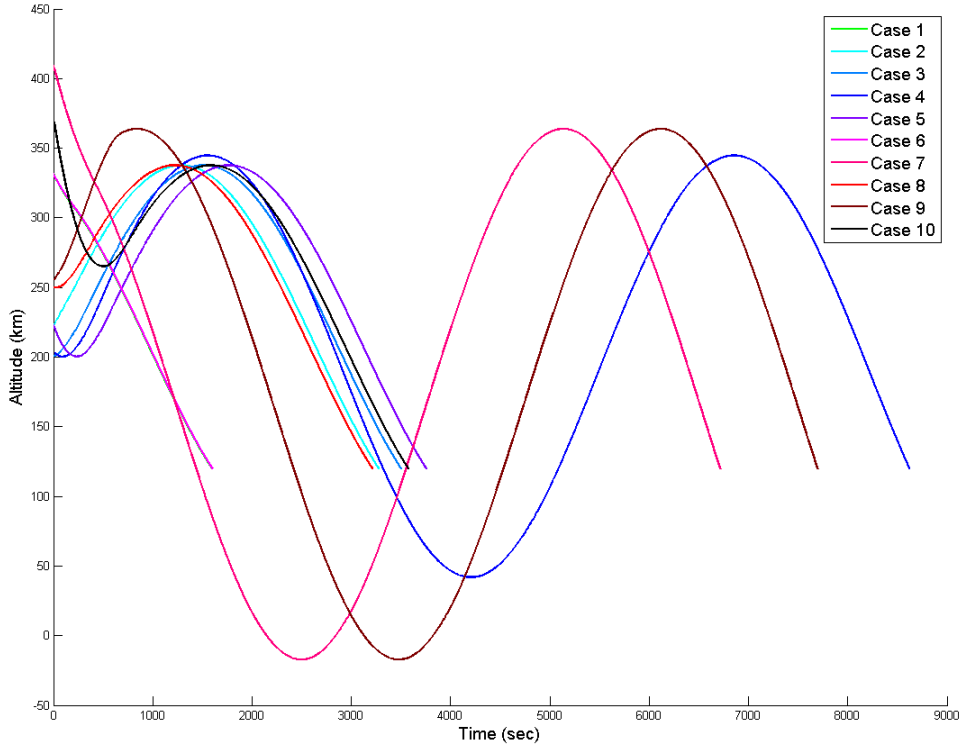

Figure 5.6 Altitude for burn-coast solution for cases 1 - 10 with terminal constraints set 3 (Eqs. (3.66)–(3.68), (3.76), (3.77), (3.80), and (3.54)) and constrained crossrange

In Figure 5.6 case 4, 7, and 9 have transfer orbits that travel below the EI altitude of 120 km with case 7 and 9 traveling below an altitude of zero or within the Earth. The

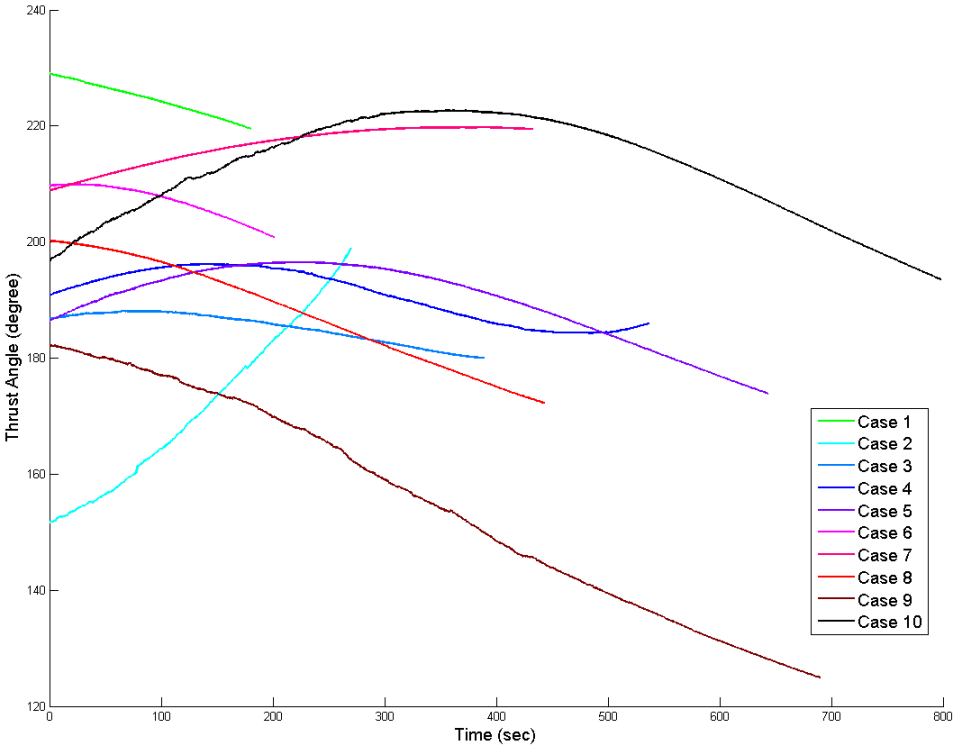

Figure 5.7 Thrust angle for burn-coast solution for cases 1 - 10 with terminal constraints set 3 (Eqs. (3.66)–(3.68), (3.76), (3.77), (3.80), and (3.54)) and constrained crossrange

transfer orbit has an apogee altitude the same as the initial orbit deorbit point altitude. The vehicle then travels along the transfer orbit through perigee and apogee and back towards perigee, where it reaches EI having satisfied the required conditions. Because the perigee altitude of the transfer orbit is less than zero, the vehicle travels within the Earth. This same type of solution is shown in cases 12, 13, 14, 18, and 19 in Figure 5.8. The inplane trajectory for case 4 in Figure 5.10 shows the vehicle traveling within the Earth. For cases 1, 2, 3, 5, 6, 8, and 10 the vehicle does not travel below EI altitude because it meets the EI conditions of velocity, flight path angle, and altitude earlier on the transfer orbit and does not have to keep coasting along the transfer orbit.

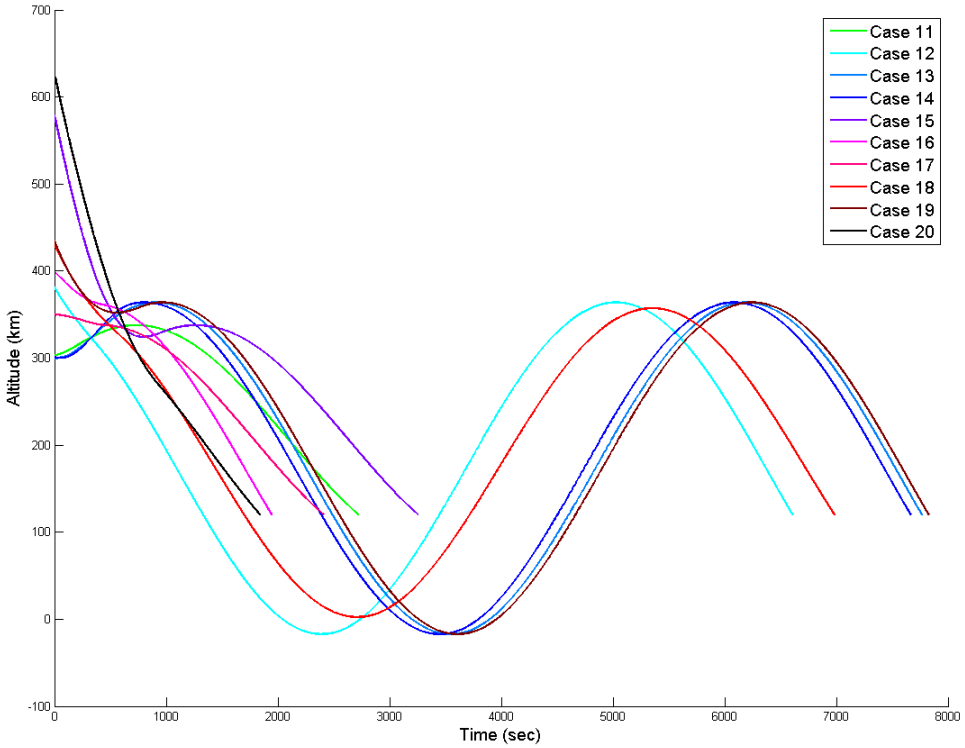

Figure 5.8 Altitude for burn-coast solution for cases 11 - 20 with terminal constraints set 3 (Eqs. (3.66)–(3.68), (3.76), (3.77), (3.80), and (3.54)) and constrained crossrange

Cases 6, 7, 10, 15, and 10 in Figures 5.6 and 5.8 all begin the deorbit maneuver at a

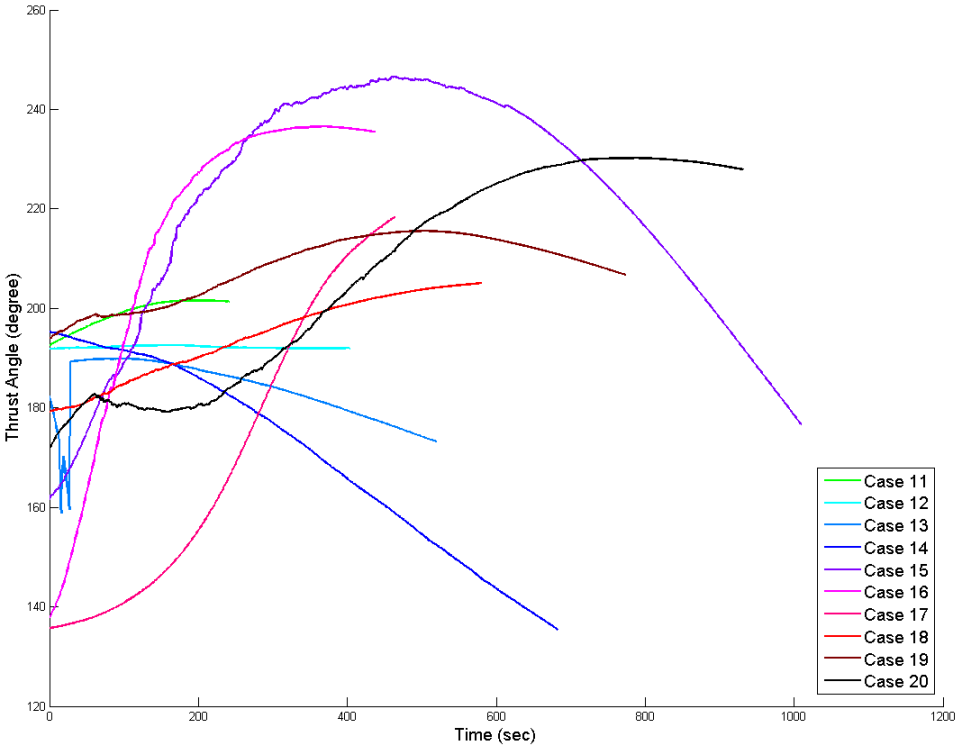

Figure 5.9 Thrust angle for burn-coast solution for cases 11 - 20 with terminal constraints set 3 (Eqs. (3.66)–(3.68), (3.76), (3.77), (3.80), and (3.54)) and constrained crossrange

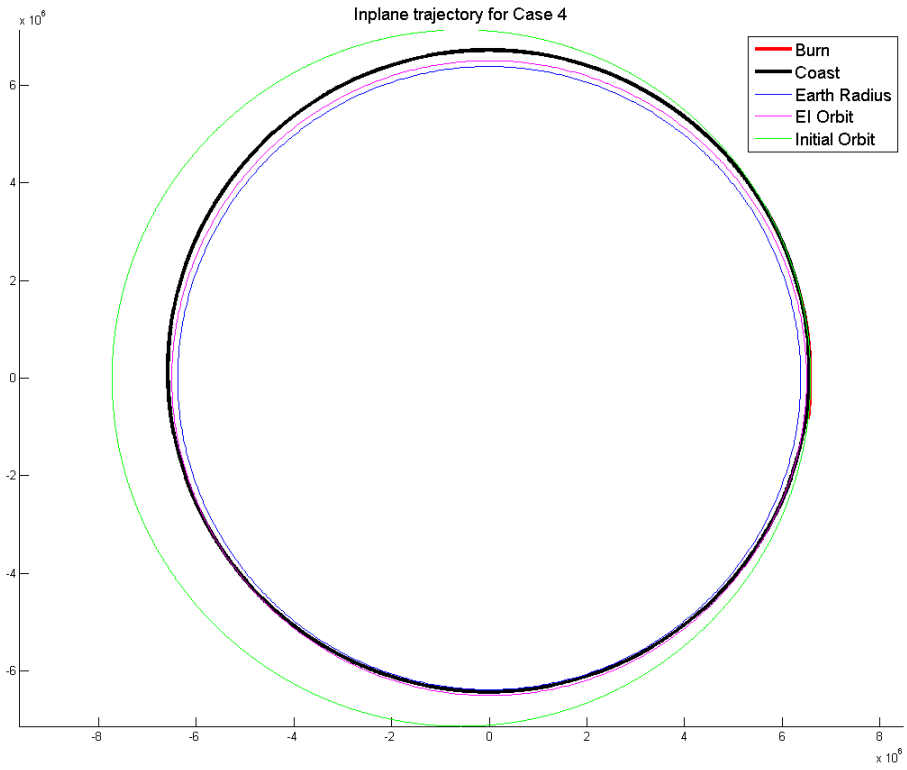

Figure 5.10 Inplane trajectory for case 4 burn-coast solution

higher altitude than the other cases. The vehicle is farther away from perigee when the burn begins than the other cases. This coincides with the results in Table 5.4 where the burn begins at a distance of between 40 and 50 degrees from perigee.

In Figure 5.11, the BCBC solution vehicle altitude for cases 11 - 20 is shown. The final transfer orbit has a perigee altitude less than zero altitude for those cases with altitude less than zero. For the BCB solution, shown in Figure 5.12, the altitude of the vehicle does not descend below EI until it has reached EI with the required constraints met. The final coast and coast time is the determining factor in whether or not the vehicle travels through Earth's atmosphere on it's final orbit. The final coast is crucial for Shuttle type vehicles that need to rotate up to 180 degrees to direct the thrust vector in the correct direction. If the Shuttle is not nose first with correct flight path angle going into entry, the vehicle could burn upon entry. However, with the final coast being part of the solution, the vehicle faces the chance of being placed in a final transfer orbit with perigee less than zero altitude.

5.5 Summary

The major findings in this chapter are as follows:

- For a given initial orbit perigee altitude, the burn time increases as eccentricity increases. As initial orbit perigee altitude increases, the burn time increases.

- If EI velocity is constrained, the optimal deorbit point for an initial elliptic orbit is not apogee. In fact the burn begins closer to perigee than apogee. For higher eccentricity orbits, the burn time increases and the optimal deorbit point moves father away from perigee.

- The EI conditions determine the transfer orbit parameters. Impulse solutions exist for those cases whose perigee altitude is equal to or less than the apogee altitude

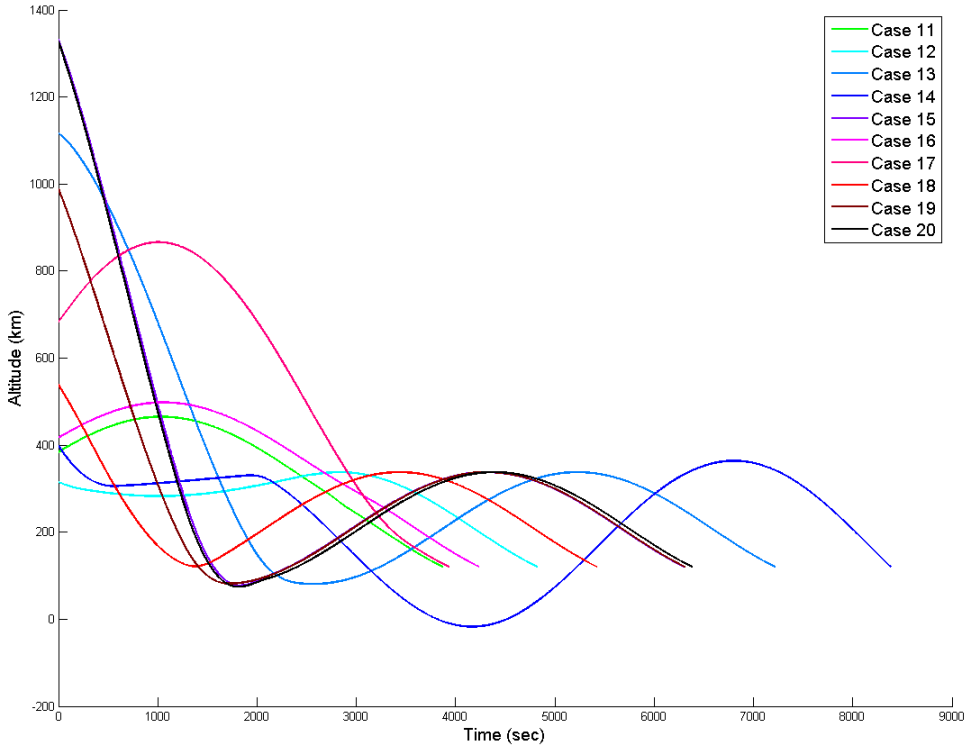

Figure 5.11 Altitude for burn-coast-burn-coast solution for cases 11 - 20 with terminal constraints set 3 (Eqs. (3.66)–(3.68), (3.76), (3.77), (3.80), and (3.54)) and constrained crossrange

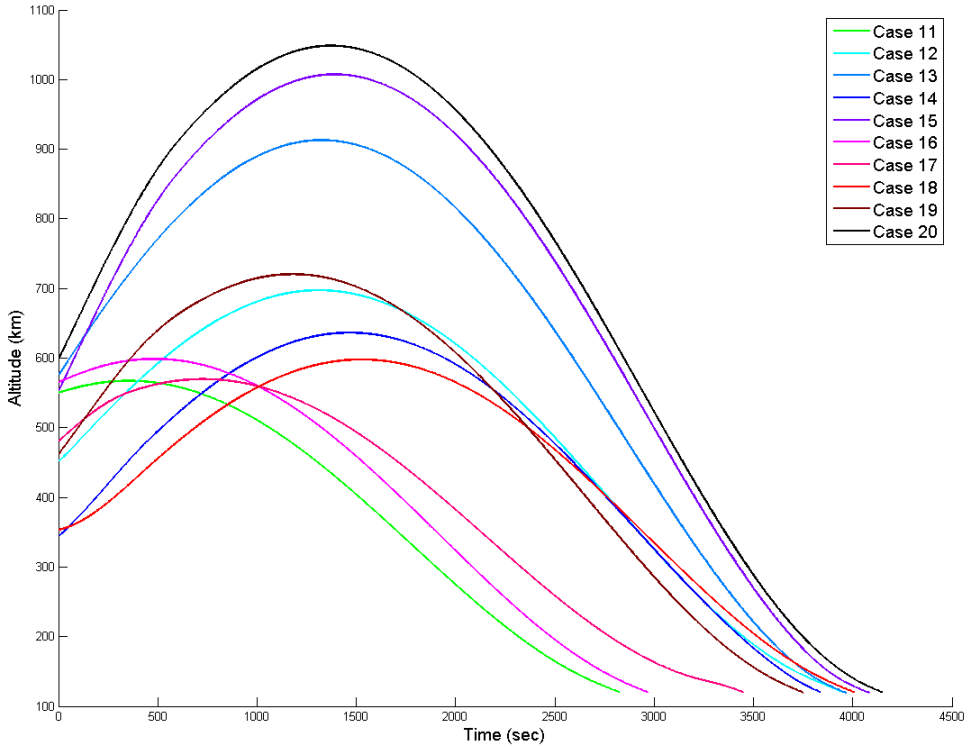

Figure 5.12 Altitude for burn-coast-burn solution for cases 11 - 20 with terminal constraints set 3 (Eqs. (3.66)–(3.68), (3.76), (3.77), (3.80), and (3.54)) and constrained crossrange

of the transfer orbit.

- There is no altitude constraint in the problem formulation. The vehicle may be placed on a transfer orbit with a perigee altitude less than zero.

- If the final coast time is long enough, the vehicle may travel into and out of Earth's atmosphere before reaching EI with the correct terminal conditions met. These solutions are not possible and are avoided.

CHAPTER 6. Multiple Burn Deorbit Guidance for Initial Elliptic Orbit

The previous chapter explored the single deorbit burn for initial elliptic orbits. The unconstrained altitude for both single and double burns was also explored. In Ref. [2], the benefits of two burns are discussed. For certain cases, a two burn maneuver has a smaller total ΔV than a single burn. The BC, BCB, and BCBC results for cases 1 -30 are presented in tables in this section. Section 1 presents the BC results and Section 2 presents the two burn maneuver results. A summary of results is presented in the final section.

6.1 Single Burn Solution for Elliptic Orbit

The BC solution for cases 1 - 30 are shown in Table 6.1. Column 1 is the case number, column 2 is the manual coast time, and columns 3 and 4 list the burn time, and final coast time all in seconds. Column 5 is the equivalent impulse of the burns time, column 6 is the crossrange distance at EI and column 7 is the flight path angle at EI. Cases 26 - 30 have high burn times. The high burn times are undesirable but necessary to place the vehicle on an orbit that would achieve desired EI conditions. The impulsive results shown in Section 4.1 hold for elliptic orbits as well. Therefore, for a given set of EI conditions, there exists an altitude for an initial elliptic orbit, such that for any higher altitude orbit no impulsive deorbit solution exists. Therefore, the vehicle must burn longer to place the vehicle on the correct transfer orbit. As stated earlier,

the Space Shuttle does not have the capacity to carry enough fuel to complete such long burns.

Cases 28 and 30 fail, which is why the EI flight path angles are not within the range of acceptable flight path angles allowed by the piecewise formulations. Figure 6.1 shows the thrust angle during the burn for cases 26 - 30. Cases 26, 27, 28 and 29 all have a sharp increase or decrease in thrust angle during the burn. For cases 28 and 29, this sharp increase resembles a discontinuity. The thrust vector is not a continuous function so it might be such that a discontinuity is part of the optimal solution of the problem. Cases 26 and 27 have a sharp decline but is not of the discontinuous nature. The thrust angle of case 30 spans over 700 degrees over 700 seconds of flight during the final segment of flight. This means the vehicle does a full rotation more than once around its center of mass during flight. There is no obvious reason for this so further study must occur. Cases 21 - 25 are shown in Figure 6.2. The altitude for the burn-coast solution is shown in Figure 6.3. The solution for cases 21 - 24, 27, and 28 all reach altitudes below 100 km and with the exception of 27, all go below the Earth's atmosphere.

The solutions follow the expected trend of burn time increasing as eccentricity increases for a given initial orbit perigee altitude. The long burn times are undesirable. The cases with long final coast time are also undesirable because the vehicle may coast along the transfer orbit within the Earth's atmosphere. To address these problems, two burn solutions with and without final coast are explored.

6.2 Two Burn Solutions for Elliptic Orbit

The BCBC solution for cases 1 - 30 are shown in Table 6.2. Column 1 is the case number, column 2 is the manual coast time, and columns three, four, five, and six list the first burn time, intermediate coast time, final burn time, and final coast time all in seconds. Columns 7 and 8 are the equivalent impulses of the corresponding burns times,

Table 6.1 Results of burn-coast solution with terminal constraints set 3 (Eqs. (3.66)–(3.68), (3.76), (3.77), (3.80), and (3.54)) and constrained crossrange

Case	M CT (s)	BT (s)	CT (s)	ΔV (m/s)	CR at EI	FPA at EI (deg)
1	25146.3347	180.0000	1415.0457	100.6844	0.1631	-0.8050
2	27698.9897	270.0000	3005.1861	152.3097	0.1077	-0.8050
3	80736.0997	389.0000	3110.6389	221.6373	0.0766	-0.8050
4	23090.5682	537.0000	8084.6529	309.8202	0.1549	-1.1553
5	79742.3369	643.0000	3110.7809	374.7656	0.1239	-0.8050
6	25776.4056	201.0000	1399.2120	112.3513	0.1225	-0.8050
7	78039.9765	433.0000	6281.7065	247.3438	0.0435	-1.6000
8	81581.2544	443.0000	2767.8107	253.5345	0.0411	-0.8050
9	23576.7649	690.0000	7005.5142	404.5451	0.1268	-1.6000
10	80354.7688	798.0000	2774.9952	472.8914	0.0963	-0.8050
11	83253.4752	241.0000	2479.9063	135.2225	0.0347	-0.8050
12	79241.4042	403.0000	6204.8221	229.7801	0.0267	-1.6000
13	22937.6181	520.0000	7246.2512	299.9801	0.0904	-1.6000
14	23663.7408	682.0000	6983.7298	399.3046	0.1304	-1.6000
15	80970.4221	1009.0000	2247.8618	610.8415	0.0772	-0.8050
16	26619.3788	437.0000	1508.1091	250.0447	0.0465	-1.5604
17	80785.9879	464.0000	1946.8945	265.9536	0.1431	-0.8050
18	22633.7754	580.0000	6402.6443	335.9912	0.0208	-1.4595
19	23491.4931	773.0000	7053.7352	456.4748	0.1297	-1.6000
20	23997.3212	931.0000	908.6664	559.0871	0.2209	-1.0792
21	78696.1411	553.0000	6524.7574	319.8928	0.0219	-1.6000
22	22232.3959	677.0000	6872.1479	396.4816	0.0314	-1.6000
23	22900.6815	688.0000	6404.5749	402.8619	0.0449	-1.6000
24	23820.0187	849.0000	7016.4790	505.8027	0.1532	-1.6001
25	24472.8361	877.0000	1095.2604	523.6698	0.1820	-1.6001
26	80349.0611	1350.0000	2793.5441	848.1597	0.0602	-0.8050
27	23000.8210	1782.0000	4439.5242	1177.4774	0.0042	-0.8049
28	23566.7292	1502.0000	4620.3165	959.6202	0.0254	-3.7738
29	24199.3788	1336.0000	1408.2171	837.5472	0.1502	-1.6001
30	82096.2584	2456.0000	4637.7829	1774.6432	0.2402	-12.7632

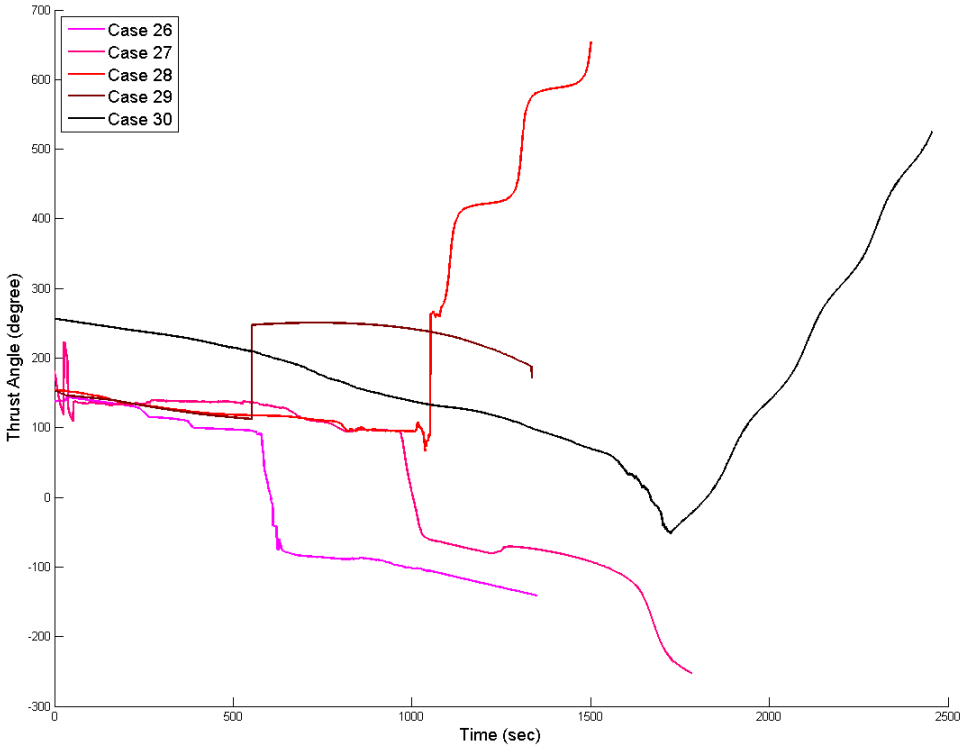

Figure 6.1 Thrust angle for cases 26 - 30 with a burn-coast solution and terminal conditions set 3 (Eqs. (3.66)–(3.68), (3.76), (3.77), (3.80), and (3.54)) and constrained crossrange.

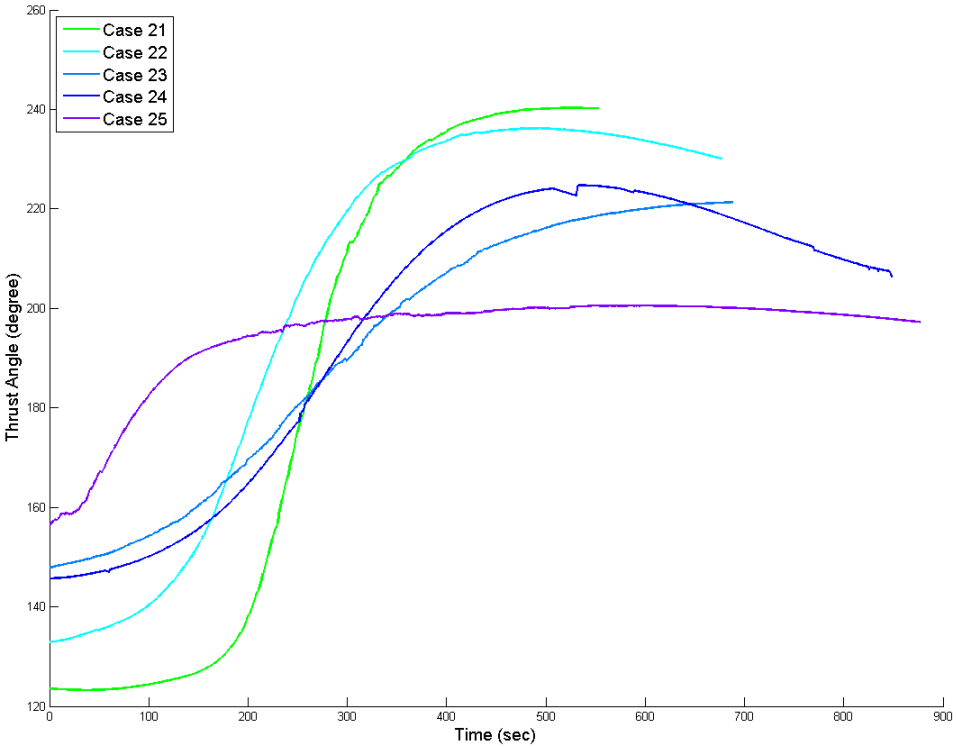

Figure 6.2 Thrust angle for cases 21 - 25 with a burn-coast solution and terminal conditions set 3 (Eqs. (3.66)–(3.68), (3.76), (3.77), (3.80), and (3.54)) and constrained crossrange.

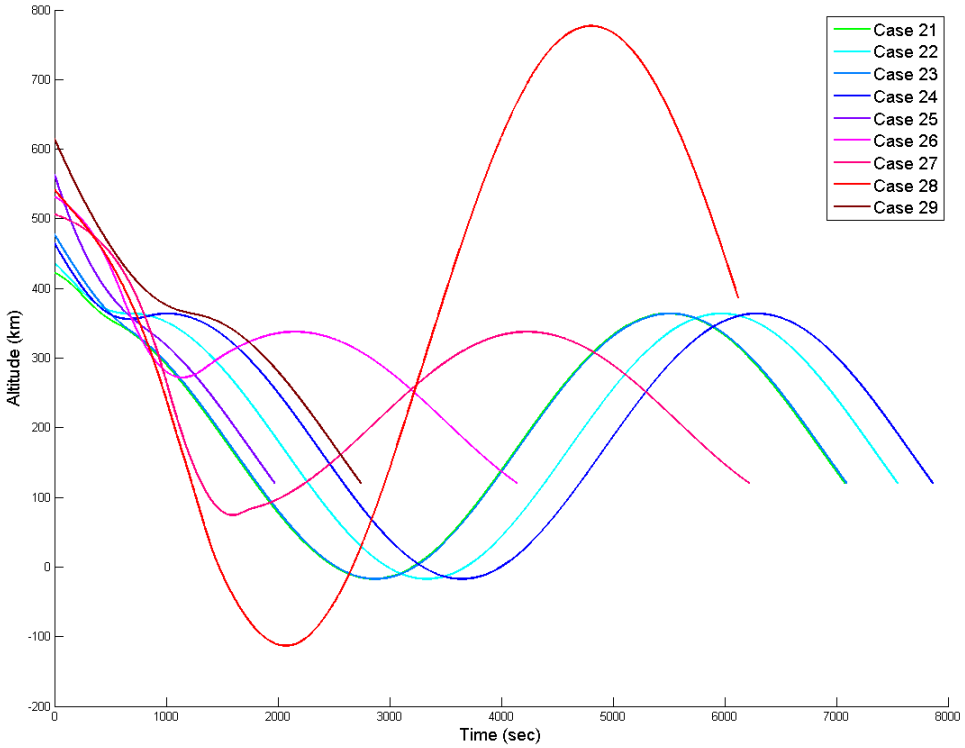

Figure 6.3 Altitude for burn-coast solution for cases 21 - 29 with terminal constraints set 3 (Eqs. (3.66)–(3.68), (3.76), (3.77), (3.80), and (3.54)) and constrained crossrange

Table 6.2 Results for burn-coast-burn-coast solution with terminal constraints set 3 (Eqs. (3.66)–(3.68), (3.76), (3.77), (3.80), and (3.54)) and constrained crossrange

Case	M CT (s)	BT 1(s)	CT1 (s)	BT 2 (s)	CT2 (s)	ΔV 1 (m/s)	ΔV 2 (m/s)	CR at EI	FPA at EI (deg)
1	22896.33	51.00	2480.46	77.00	5743.10	28.5242	43.1013	0.1252	-0.8050
2	22943.99	146.00	3271.60	165.00	16.50	81.2606	94.7438	0.1758	-0.8050
3	27838.42	293.00	1490.32	98.00	2996.33	165.4367	57.2858	0.2191	-0.8050
4	22470.57	461.00	1093.46	170.00	2864.35	264.1772	103.6291	0.1427	-0.8050
5	26915.58	140.00	2401.15	720.00	4505.09	78.2369	434.6249	0.3445	-0.8280
6	22516.41	97.00	2767.54	189.00	1304.86	53.8243	107.4232	0.1545	-0.8050
7	22956.92	207.00	3092.77	149.00	429.39	116.1210	86.1174	0.1571	-0.8050
8	20457.21	70.00	2049.52	435.00	3467.78	38.9415	251.8149	0.1798	-0.8049
9	22761.76	575.00	1465.89	205.00	1710.38	333.4032	128.0728	0.1645	-1.0427
10	23793.69	419.00	871.05	368.00	7152.14	239.3203	226.6542	0.2119	-1.6000
11	22522.42	112.00	2599.14	206.00	950.61	62.4124	117.9818	0.1855	-0.8050
12	79641.40	245.00	2236.69	138.00	2200.87	137.7520	80.7202	0.0621	-0.8050
13	20377.62	158.00	1795.45	451.00	4811.80	88.0058	266.2738	0.1086	-0.8049
14	23188.74	586.00	1309.26	253.00	6233.73	339.6230	159.6272	0.1458	-1.6000
15	22647.61	222.00	1032.95	881.00	4163.19	124.3312	550.0466	0.0220	-0.8049
16	22649.38	118.00	2806.56	164.00	1147.21	65.5832	93.5662	0.1539	-0.8050
17	24045.69	138.00	3130.16	291.00	372.09	77.1059	168.5911	0.0840	-0.8050
18	22308.78	307.00	988.43	333.00	3794.25	173.7916	199.7221	0.0997	-0.8049
19	22421.49	243.00	1024.36	550.00	4489.48	136.7078	333.4073	0.0359	-0.8049
20	22997.32	263.00	964.58	870.00	4282.88	148.3514	547.4708	0.0054	-0.8050
21	22892.27	138.00	2891.94	193.00	1161.94	76.9371	110.6104	0.1288	-0.8050
22	22747.40	278.00	3137.59	172.00	1676.84	156.6483	101.0481	0.0818	-0.8050
23	23495.68	402.00	3353.65	183.00	1756.63	229.4313	110.1978	0.0062	-0.8050
24	24575.02	557.00	3163.68	241.00	1361.71	322.1709	150.4837	0.0389	-0.8051
25	25167.84	622.00	3199.58	187.00	541.97	362.2082	118.1995	0.0274	-0.8050
26	23400.86	170.00	3120.28	266.00	1302.68	95.1618	154.4127	0.0659	-0.8050
27	23680.82	294.00	3110.90	251.00	1196.69	165.9116	149.1019	0.0484	-0.8050
28	23801.73	487.00	3003.04	210.00	1393.50	279.5887	129.0651	0.0253	-0.8050
29	25474.38	443.00	3332.70	424.00	551.23	253.6179	263.7664	0.0598	-0.8050
30	26001.25	606.00	3308.39	324.00	600.49	352.3282	206.3903	0.0992	-0.8050

column 9 is the crossrange at EI and column 10 is the flight path angle at EI.

Figures 6.4 - 6.5 show the thrust angle for the first and second burn for cases 21 - 30 with a BCBC solution. Figure 6.6 shows the altitude for cases 21 - 30 with a BCBC solution. Using a BCBC solution, the altitude of the solution never goes below 120 km. For the single burn cases, the thrust angles and altitude have a trend. For example, when the vehicle travels on a transfer orbit with apogee altitude greater than the initial orbit altitude, the thrust angle is greater than 180 degrees. With two burn maneuvers, this type of trend is not as evident. There are no large discontinuities in the two burn solution as there are in the one burn solution.

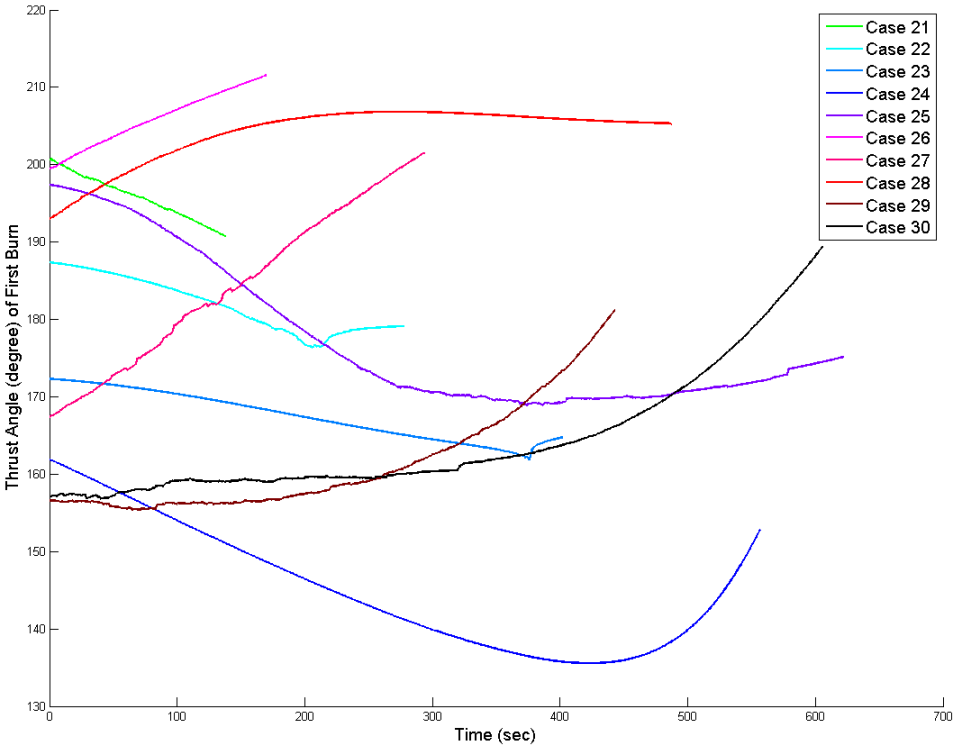

Figure 6.4 Thrust angle during first burn for burn-coast-burn-coast solution of elliptical cases 21 through 30 with terminal constraints set 3 (Eqs. (3.66)–(3.68), (3.76), (3.77), (3.80), and (3.54)) and constrained crossrange

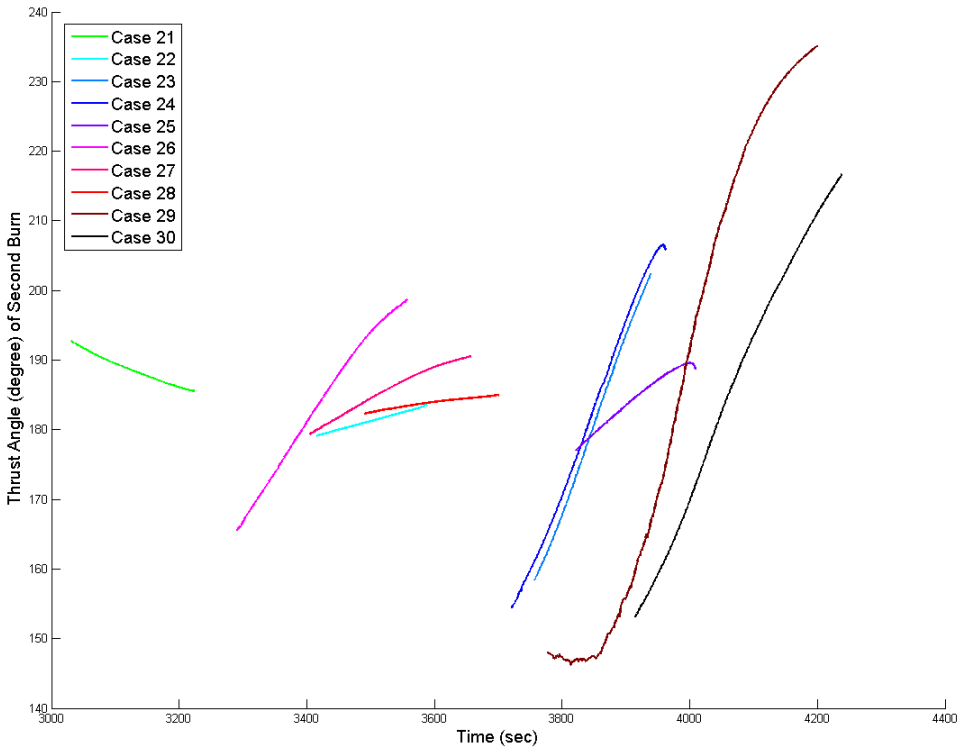

Figure 6.5 Thrust angle during second burn for burn-coast-burn-coast solution of elliptical cases 21 through 30 with terminal constraints set 3 (Eqs. (3.66)–(3.68), (3.76), (3.77), (3.80), and (3.54)) and constrained crossrange

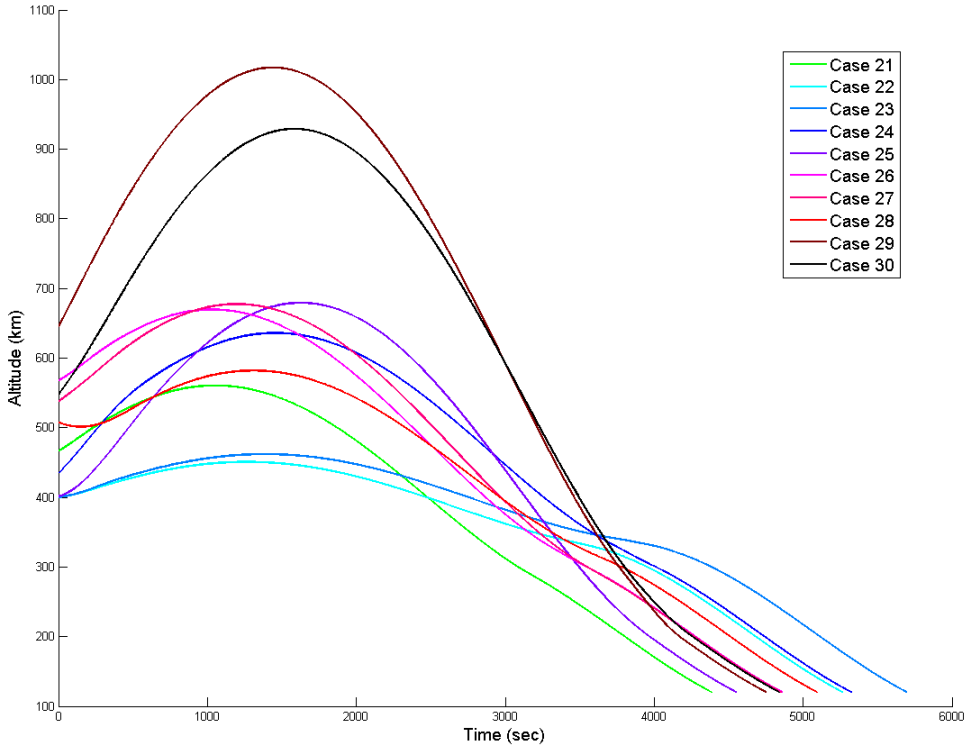

Figure 6.6 Altitude for burn-coast-burn-coast solution for cases 21 - 30 with terminal constraints set 3 (Eqs. (3.66)–(3.68), (3.76), (3.77), (3.80), and (3.54)) and constrained crossrange

Table 6.3 Results for burn-coast-burn solution with terminal constraints set 3 (Eqs. (3.66)–(3.68), (3.76), (3.77), (3.80), and (3.54)) and constrained crossrange

Case	M CT (s)	BT 1(s)	CT (s)	BT 2 (s)	ΔV 1 (m/s)	ΔV 2 (m/s)	CR at EI	FPA at EI (deg)
1	27586.33	130.00	2723.99	11.98	72.6253	6.7374	0.0744	-0.8053
2	22853.99	153.00	3154.00	143.00	85.2349	81.2616	0.1911	-0.8376
3	23518.42	390.00	3121.00	188.00	222.1091	112.7683	0.1327	-0.8051
4	24025.57	533.00	3123.00	199.00	307.4967	122.4838	0.0904	-0.8055
5	24510.58	727.00	2985.00	161.00	427.3120	103.0930	0.0582	-0.8168
6	23176.41	100.00	2825.00	191.00	55.7456	108.0645	0.1919	-0.8050
7	80719.98	98.00	3091.00	224.00	54.5837	127.3935	0.0833	-1.0790
8	23872.21	368.00	3231.00	267.00	209.0434	160.3713	0.0994	-0.8050
9	23871.76	700.00	2879.00	281.00	410.5597	181.2231	0.0999	-0.8060
10	24743.69	720.00	3211.00	211.00	423.2980	135.3416	0.0259	-0.8051
11	23767.42	101.00	2592.85	130.78	56.3993	73.9708	0.1726	-0.8051
12	23170.82	173.00	3581.00	199.00	96.5147	114.6731	0.1387	-0.8051
13	24032.62	207.00	3461.00	298.00	115.7449	174.4145	0.0827	-0.8569
14	24078.74	485.00	3202.00	150.00	278.6694	90.8443	0.0882	-0.8500
15	25337.61	593.00	3170.00	321.00	344.2286	203.1318	0.0081	-0.8207
16	23679.38	135.00	2690.00	143.00	75.2949	81.1341	0.1692	-0.8049
17	23350.69	365.00	2890.00	195.00	207.1529	116.1150	0.1594	-0.8050
18	23313.78	438.00	3436.00	135.00	250.4019	80.8555	0.1260	-0.8054
19	24566.49	592.00	2975.00	182.00	343.7622	113.6103	0.0625	-0.8053
20	25612.32	598.00	3229.00	322.00	347.0347	204.4070	0.0300	-0.8119
21	23612.27	179.00	2901.86	257.69	99.8455	149.6458	0.1497	-0.8051
22	24027.40	275.00	3007.00	241.00	155.2226	142.3145	0.1113	-0.8050
23	24135.68	313.00	3858.00	333.00	177.0156	199.4675	0.0418	-0.8052
24	24515.02	500.00	3423.00	208.00	287.8989	127.3364	0.0414	-0.8167
25	25607.84	653.00	3042.00	254.00	381.2935	161.9781	0.0170	-0.9230
26	23600.86	254.00	2715.00	163.00	143.0586	94.7081	0.1637	-0.8049
27	23820.82	369.00	2886.00	172.00	209.5250	102.5050	0.1307	-0.8088
28	24541.73	432.00	3160.00	231.00	246.8502	140.2942	0.0594	-0.8051
29	25274.38	536.00	3127.00	270.00	309.1284	167.9514	0.0052	-0.8826
30	26281.25	669.00	3109.00	337.00	391.4105	217.4034	0.0707	-0.8819

The results for the BCB solution for cases 1 - 30 are shown in Table 6.3 where column 1 is the case number, column 2 is the manual coast time, coumns 3,4, and 5 are the first burn time, intermediate coast time, and final burn time, columns 6 and 7 are the equivalent impulses of the corresponding burns times, column 8 is the crossrange distance at EI, and column 9 is the flight path angle at EI.

Table 6.4 gives a summary of the burn time and corresponding ΔV for the solution given the different formulations for cases 1 - 30. For each case, the very initial position before the manual coast begins is the same for the different solution formulations. However, the manual coast between the different formulations is different. For example,

case 1 for BCB has a manual coast time of 27586.33 seconds, BCBC has a manual coast time of 22896.33, and BC has a manual coast time of 25146.3347 seconds. This means that the initial position used in solving the optimal control problem is different for each case. There is almost a 5000 second difference in manual coast between the BCBC and BCB solution. 5000 seconds on a 250 km perigee altitude orbit with eccentricity of .04 would place the initial positions of the vehicle for the different formulations in different positions. The problem is being solved from two different initial states, which for some of the cases is as far as half an orbit away.

Intuition would dictate that the BCBC formulation would yield a better result in terms of fuel expenditure because of the final coast. The results in Table 6.4 give a different result for some cases. Column 1 is the case number, columns 2 and 3 are the BC burn time and its corresponding ΔV, columns 4 and 5 are the BCBC burn time and its corresponding ΔV, and columns 6 and 7 are the BCB burn time and its corresponding ΔV. For example in case 7, the BCBC has a 34 second higher burn time. In case 7, the BCBC solution targets the second $\mathbf{1}_{HAC}$ while the BCB solution targets the first. This is because the guidance solution could not find a BCBC solution that was within the burn bounds and the crossrange constraint for the closest $\mathbf{1}_{HAC}$. Therefore, the second $\mathbf{1}_{HAC}$ was targeted. In case 6, the total burn times differ by 5 seconds. The manual coast times differ by less than a thousand seconds for the BCB and BCBC solution formulations for case 6. The initial position of the vehicle is not as different as for case 7 and hence the solution is not as drastically different. One way to help with this discrepancy would be to add an initial optimal coast to the problem but this is hard to handle numerically in the algorithm.

Figures 6.7 - 6.12 show the trend of the BC, BCB, and BCBC solutions for a given eccentricity and initial orbit perigee altitude for cases 1 - 30. For low perigee altitude, low eccentricity, single BC gives the best solution. As seen in Figure 6.7 the BC formulation gives the lowest ΔV solution of the three solution formulations. For all three cases, as

Table 6.4 ΔV and Burn Time for burn-coast, burn-coast-burn-coast, and burn-coast-burn solutions for cases 1-30 with constrained cross-range and terminal conditions set 3 (Eqs. (3.66)–(3.68), (3.76), (3.77), (3.80), and (3.54))

Case	BC BT (sec)	BC ΔV	BCBC BT (sec)	BCBC ΔV	BCB BT (sec)	BCB ΔV
1	180.0000	100.6844	128.0000	71.6255	141.9766	79.3627
2	270.0000	152.3097	311.0000	176.0045	296.0000	166.4965
3	389.0000	221.6373	391.0000	222.7225	578.0000	334.8774
4	537.0000	309.8202	631.0000	367.8063	732.0000	429.9805
5	643.0000	374.7656	860.0000	512.8618	888.0000	530.4050
6	201.0000	112.3513	286.0000	161.2475	291.0000	163.8101
7	433.0000	247.3438	356.0000	202.2383	322.0000	181.9772
8	443.0000	253.5345	505.0000	290.7565	635.0000	369.4147
9	690.0000	404.5451	780.0000	461.4760	981.0000	591.7828
10	798.0000	472.8914	787.0000	465.9745	931.0000	558.6396
11	241.0000	135.2225	318.0000	180.3942	231.7845	130.3701
12	403.0000	229.7801	383.0000	218.4722	372.0000	211.1878
13	520.0000	299.9801	609.0000	354.2795	505.0000	290.1594
14	682.0000	399.3046	839.0000	499.2502	635.0000	369.5137
15	1009.0000	610.8415	1103.0000	674.3777	914.0000	547.3605
16	437.0000	250.0447	282.0000	159.1493	278.0000	156.4290
17	464.0000	265.9536	429.0000	245.6970	560.0000	323.2679
18	580.0000	335.9912	640.0000	373.5138	573.0000	331.2573
19	773.0000	456.4748	793.0000	470.1151	774.0000	457.3725
20	931.0000	559.0871	1133.0000	695.8222	920.0000	551.4417
21	553.0000	319.8928	331.0000	187.5475	436.6920	249.4912
22	677.0000	396.4816	450.0000	257.6965	516.0000	297.5371
23	688.0000	402.8619	585.0000	339.6291	646.0000	376.4831
24	849.0000	505.8027	798.0000	473.6546	708.0000	415.2354
25	877.0000	523.6698	809.0000	480.4077	907.0000	543.2716
26	1350.0000	848.1597	436.0000	249.5746	417.0000	237.7668
27	1782.0000	1177.4774	545.0000	315.0135	541.0000	312.0301
28	1502.0000	959.6202	697.0000	408.6538	663.0000	387.1444
29	1336.0000	837.5472	867.0000	517.3843	806.0000	477.0798
30	2456.0000	1774.6432	930.0000	558.7185	1006.0000	608.8139

the eccentricity increased, the ΔV increased. This is the case for all the initial perigee altitude cases.

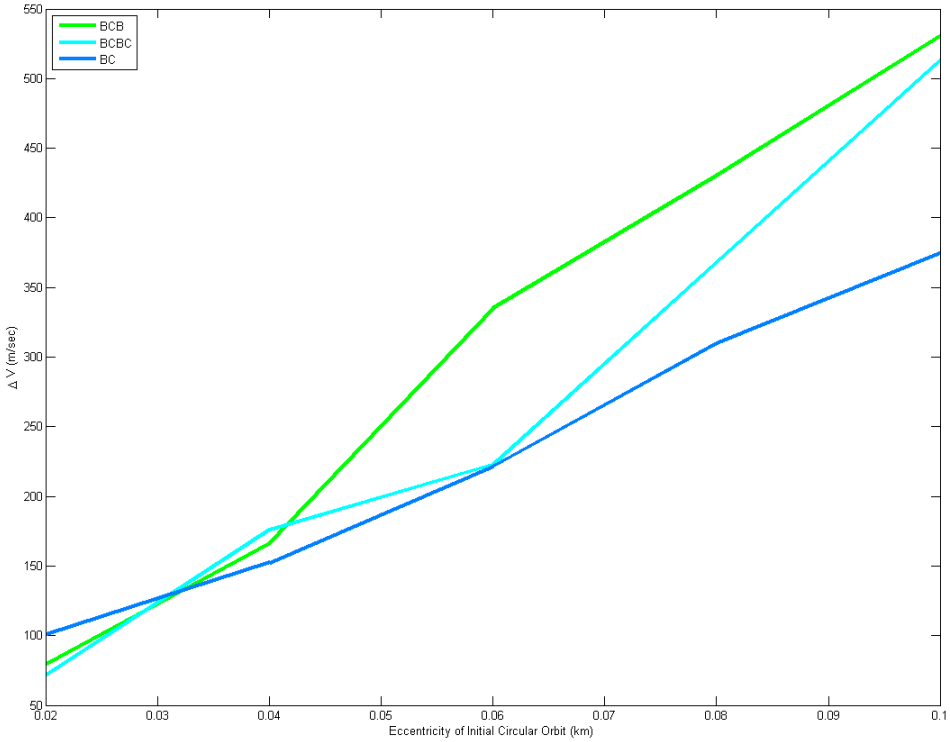

Figure 6.7 ΔV for burn-coast, burn-coast-burn, and burn-coast-burn-coast solution for given initial perigee altitude orbit of 200 km

For the cases in Figure 6.8 where the perigee altitude is 250 km, the burn-coast-burn-coast formulation yielded a smaller ΔV than the burn-coast-burn formulation. As eccentricity increases the burn-coast solution offers the better solution with smaller ΔV. The single burn solution is the most appropriate way to solve the problem. For eccentricity of .04 the two burn methods offer a better solution. This is caused by the different coast times of the solution. The final coast of the burn-coast solution is almost twice the coast time of the two burn solutions. Also, the burn-coast method targets a different EI flight path angle.

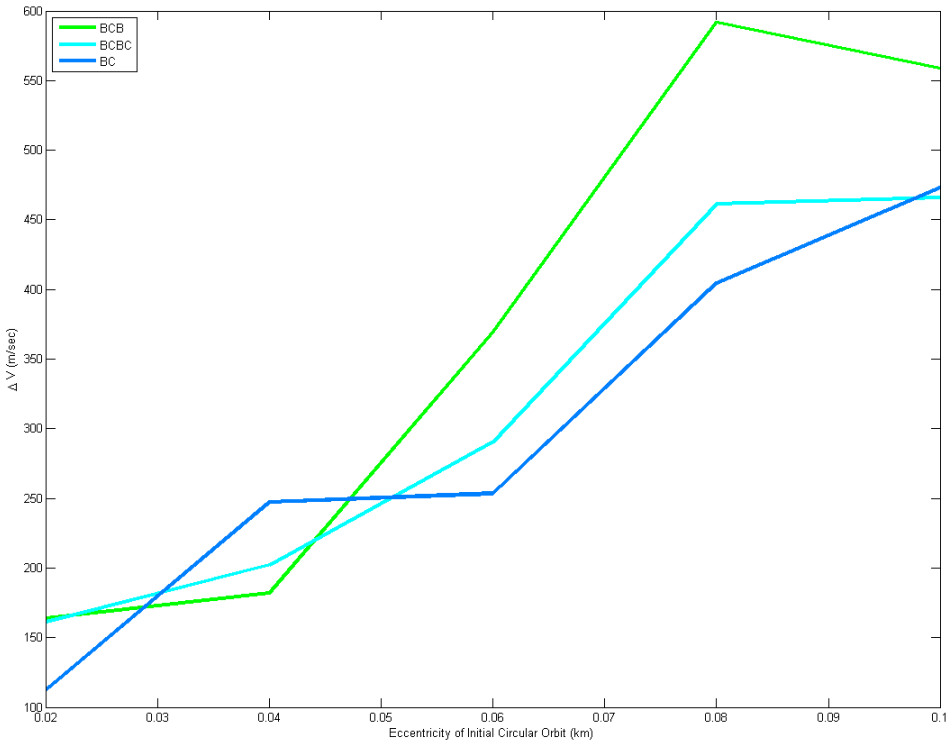

Figure 6.8 ΔV for burn-coast, burn-coast-burn, and burn-coast-burn-coast solution for given initial perigee altitude orbit of 250 km

For perigee altitude of 300 km, burn-coast-burn and burn-coast solution formulations offer the best results in terms of ΔV. Figure 6.9 shows an almost linear trend of increasing ΔV for the three solution formulations. This trend shows that for increasing eccentricity of a given initial perigee altitude, the burn time and ΔV increase. For low eccentricities, two burn maneuver has the smaller ΔV for initial orbit perigee altitude 350 km shown in Figure 6.10. As eccentricity increases, the BC and BCB solutions appear to converge around the same total ΔV. The BCBC solution gives the worst result in terms of ΔV as eccentricity increases.

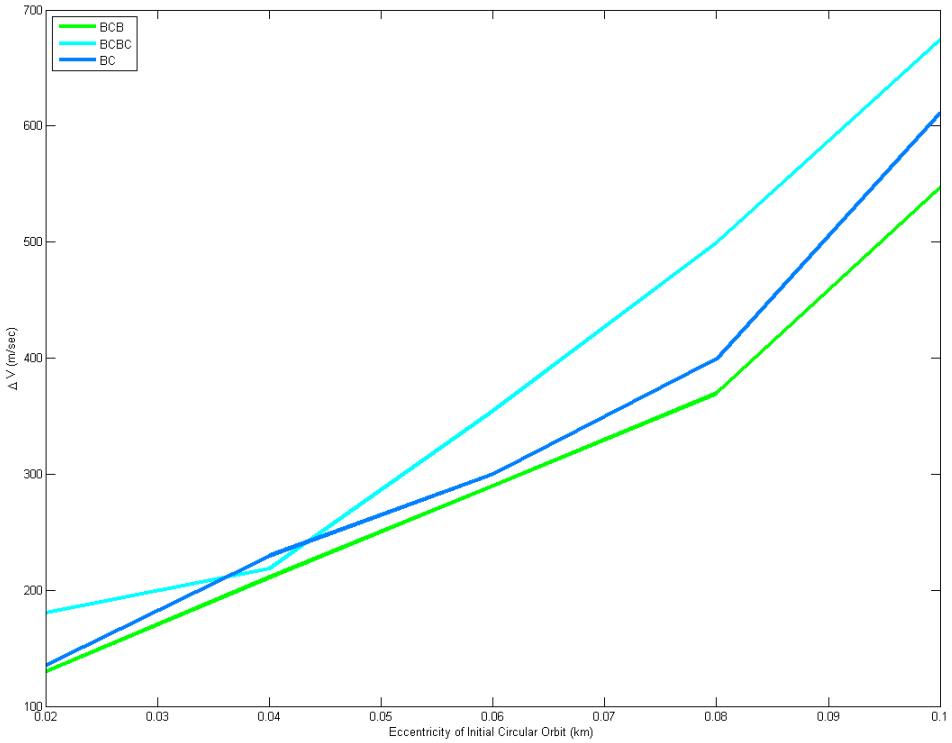

Figure 6.9 ΔV for burn-coast, burn-coast-burn, and burn-coast-burn-coast solution for given initial perigee altitude orbit of 300 km

For the cases with initial orbit perigee altitude of 400 and 500 km, the two burn maneuvers give the best solution in terms of minimizing burn time and total burn time.

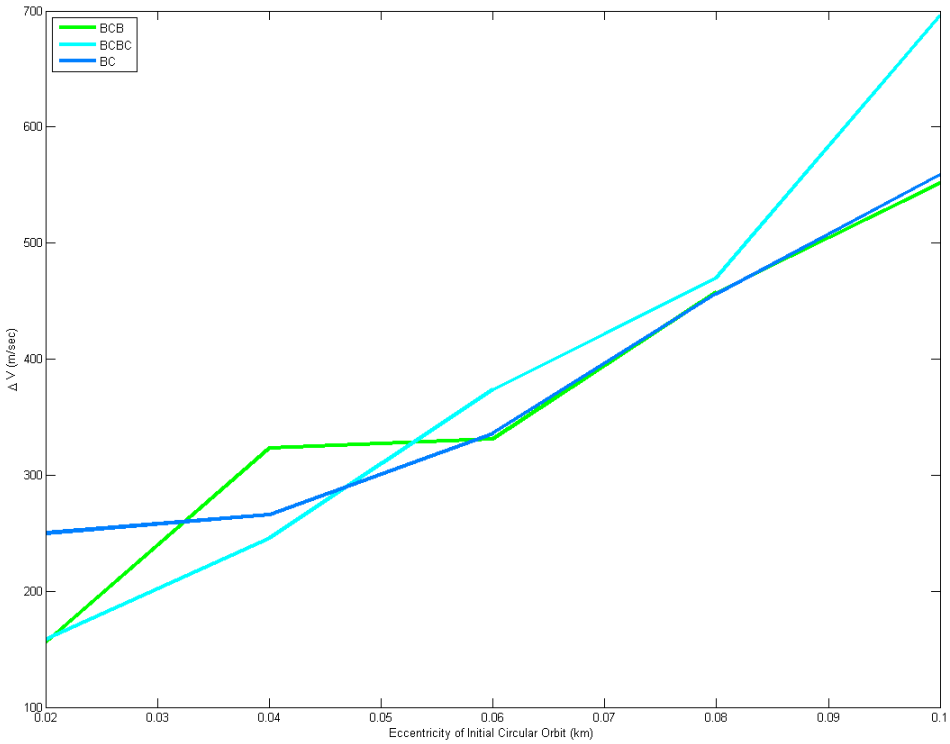

Figure 6.10 ΔV for burn-coast, burn-coast-burn, and burn-coast-burn–coast solution for given initial perigee altitude orbit of 350 km

There is no impulsive solution for initial perigee altitude orbits of 400 km and higher that meet the required EI conditions. Specifically, no Keplerian orbit exists that the vehicle could travel on to meet the required EI conditions. Hence, a two burn maneuver is required for the vehicle to achieve EI conditions. The results are shown in Figures 6.11 and 6.12. For 400 km perigee altitude initial orbit BCBC gave the best result. As the eccentricity increased, all the solution formulations converged with BC giving the best solution for an eccentricity of .10. For a 500 km perigee altitude initial orbit the two burn maneuvers were the more optimal. The BC maneuver has very long burn times for the elliptic orbits with such a high perigee altitude, which is undesirable. The two burn maneuvers have much smaller burn times that are more desirable.

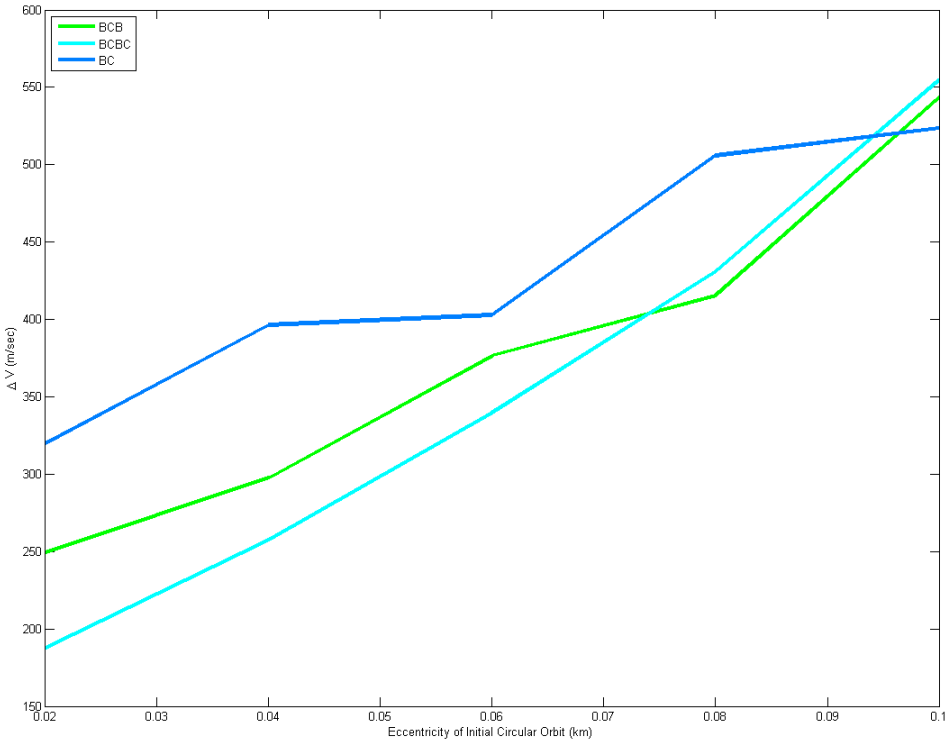

Figure 6.11 ΔV for burn-coast, burn-coast-burn, and burn-coast-burn–coast solution for given initial perigee altitude orbit of 400 km

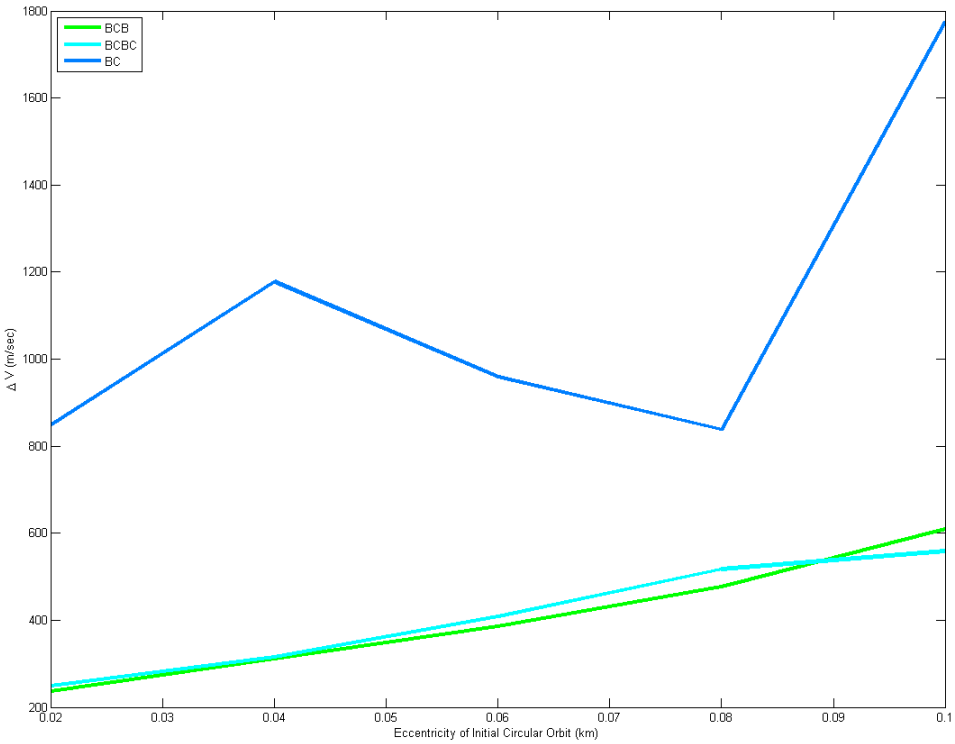

Figure 6.12 ΔV for burn-coast, burn-coast-burn, and burn-coast-burn–coast solution for given initial perigee altitude orbit of 500 km

6.3 Summary

The major findings in this chapter are as follows:

- For low altitude elliptic orbits, the single burn coast solution formulation provided the best results in terms of minimizing ΔV.
- As eccentricity increases for a given initial orbit perigee altitude, the burn time increases for both the single and two burn maneuvers.
- There does not exist an impulsive solution for initial orbits with perigee altitude greater than 360 km. The impulsive solution is determined by the EI conditions. Increased burn times are required to place the vehicle on orbit that meets EI conditions.
- For high altitude elliptic orbits (360 km perigee altitude and above) the two burn maneuvers provide the best results in terms of minimizing ΔV. Two burn maneuvers offer most efficient method of placing vehicle on correct transfer orbit that meets EI conditions.
- The burn coast burn solution offered the best results for the two burn maneuvers.

CHAPTER 7. J_2 Gravitational Term

The previous chapters solved the guidance problem assuming Keplerian motion. From Ref. [2] and the completed numerical survey in chapter 2, Earth's oblateness and more specifically the J_2 gravitational term has an effect on the EI conditions. This chapter explores the effect of the J_2 gravitational term on the guidance solution. In Section 1, the J_2 gravitational term is added to the simulation but not added to the guidance solution process. The guidance solution is solved assuming Keplerian motion. Section 2 presents results with the J_2 gravitational term added to both the guidance solution and simulation.

7.1 J_2 Gravitational Term in Simulation

To give an overview of the effect, Table 7.1 shows the EI results for the cases listed with the J_2 gravitational term added as part of the simulation. The J_2 gravitational term is not included as part of the vacuum solution to the guidance problem. The guidance problem is solved using Keplerian motion. In Table 7.1 column 1 is the circular orbit case number, column 2 is the final coast time of the BC solution, EI flight path angle is presented in column 3, the percent error of EI flight path angle is column 4, column 5 is the EI altitude, column 6 is the percent error for EI altitude, and columns 7 and 8 are the EI Velocity and the EI velocity percent error.

The J_2 gravitational term has the largest effect on the flight path angle and altitude at EI. At the end of the burn, the vehicle coasts a specified time to EI. This specified

Table 7.1 Final EI conditions with J_2 gravitational term in simulation and terminal constraints set 5 (Eqs. (3.90)–(3.97) and (3.54))

Case	Final CT (sec)	EI fpa (deg)	FPA Error	EI Altitude (m)	Alt Error	EI Velocity (m/s)	Vel Error
1	3064.5342	-1.0140	1.3970	126434.5	5.3621	7871.7575	0.0983
6	5892.3993	-0.9742	2.5760	122165.8	1.8048	7880.8637	0.0173
11	6387.3637	-0.9762	2.3820	124163.0	3.4692	7881.1275	0.0207
16	6942.3112	-0.9974	0.2640	123704.3	3.0869	7878.4122	0.0138
21	5493.5075	-1.0116	1.1590	118842.7	0.9644	7881.6251	0.0270
22	1911.3160	-1.0284	2.8410	109717.7	8.5686	7889.6529	0.1289
23	3623.0013	-1.0205	2.0450	128013.6	6.6780	7875.6487	0.0489
24	1091.3188	-0.9516	4.8440	124699.3	3.9161	7876.8316	0.0339
25	4178.5907	-0.9415	5.8550	113901.7	5.0819	7881.0422	0.0196
26	3921.9833	-0.9737	2.6300	115129.0	4.0592	7880.2885	0.0100
27	1023.3733	-1.0108	1.0800	118421.7	1.3153	7875.9986	0.0444
28	1177.9367	-0.9538	4.6160	125141.6	4.2847	7876.7901	0.0344

time is solved for as part of the guidance solution, which assumes Keplerian motions. The final guidance command is given at the end of the burn. The final coast is then simulated using J_2 equations of motion (Eqs. (3.23)–(3.24)). Since the final coast time was solved for assuming Keplerian motion and the simulation uses J_2 motion and the simulation stops at the end of the specified final coast time, the EI altitude maybe different from the specified 120 km.

The largest percent error in flight path angle is for case 25. This case has both a high initial orbit altitude and a long final coast time. Cases 6, 11, and 16 have long final coast times as well. The change in altitude of cases 6, 11, and 16 is not as large as the change in altitude of case 25 during the final coast. The change in altitude and the long coast time for the final coast lead to the large percent error for the flight path angle at EI.

Allowing for the variable formulation of flight path angle and velocity at EI, Table 7.2 shows the results of the same cases presented in Table 7.1 with terminal constraints case 3. Once again, the J_2 gravitational term is added in the simulation but not in the solution of the guidance problem. Column 1 is the circular orbit case number, column 2 is the final coast time, column 3 is the EI flight path angle, column 4 is the EI altitude,

Table 7.2 Final EI conditions with J_2 gravitational term in simulation and terminal constraints set 3 (Eqs. (3.66)–(3.68), (3.76), (3.77), (3.80), and (3.54)) for initial circular orbit cases.

Case	Final CT (sec)	EI fpa (deg)	EI Altitude (m)	EI Velocity (m/s)
1	3272.8124	-0.8162	126871.2	7878.2795
6	8263.0614	-0.8235	127249.5	7875.8982
11	7888.0277	-0.8306	126648.8	7877.4799
16	3122.1151	-1.0265	148026.7	7881.3677
21	6527.9494	-1.5730	125884.3	7863.5606
22	2824.5906	-0.7712	112857.8	7894.3709
23	3365.6895	-1.6086	118895.4	7863.0860
24	627.7417	-1.6442	117848.2	7862.1676
25	730.0324	-1.5639	122078.7	7864.3665
26	217.0231	-0.8265	119675.3	7885.6104
27	5207.5385	-0.8174	120632.2	7883.9092
28	3961.4512	-1.4844	123167.1	7868.1529

and column 5 is the EI velocity. There is no percent error presented in Table 7.2. Allowing for variable formulations (Eqs. (3.102) and (3.103)) makes the use of percent errors invalid. In Table 7.2 the same difference in altitude at EI as Table 7.1 is shown. The cases with flight path angle not within the alloted range are cases 22, 23, and 24. Case 22 is below the variable flight path angle range by .0338 degrees and cases 23 and 24 are above the variable flight path angle range by .0086 degrees and .0442 degrees respectively.

Table 2.2 gives the final flight path angle at EI for a vehicle coasting from the given altitude to the EI altitude of 120 km. The final fight path angles with J_2 gravitational term in Table 2.2 differ from the flight path angles with Keplerian motion by up to 30 percent. The final path angle can differ by up to 30 percent in Table 2.2 but is still within the bounds of the Shuttle's variable formulation given in Eqs. (3.102) and (3.103). Using a variable formulation allows for flexibility in the flight path angle at EI. This leads to an ease in handling the J2 term and it's effect on flight path angle.

Eliminating the final coast and ending the deorbit flight with a burn counters the effect of the J_2 gravitational term. In Table 7.3 the final EI values are shown for circular cases 21 - 28 with a BCB solution and terminal constraints set 3. Column 1 is the circular

Table 7.3 Final EI conditions for burn-coast-burn solution with J_2 gravitational term in simulation and terminal constraints set 3 (Eqs. (3.66)–(3.68), (3.76), (3.77), (3.80), and (3.54))

Case	EI fpa (deg)	EI Altitude (m)	EI Velocity (m/s)
21	-0.8061	119999.6	7884.8917
22	-0.7986	120191.9	7884.9944
23	-1.6135	121255.3	7865.7466
24	-0.8022	120193.4	7885.6891
25	-0.8184	120191.9	7884.5446
26	-1.6350	119515.2	7864.1597
27	-1.6013	119987.0	7863.8323
28	-1.6046	119990.9	7864.2011

orbit case number, column 2 is the EI flight path angle, column 3 is the EI altitude, and column 4 is the EI velocity. Cases 22, 23, 26, 27, and 28 are outside of the range of flight path angle by less than 3 percent. Because the guidance problem is solved using a closed loop simulation, the guidance command is updated every second of flight. The final burn compensates for the any change in EI conditions the J_2 gravitational term in the simulation causes. Any discrepancy caused by the simulation is compensated for during the next second of flight when the guidance solution is solved again.

7.2 J_2 Gravitational Term in Guidance Solution and Simulation

The results from adding the J_2 gravitational term to the vacuum solution as well as the simulation is shown in Table 7.4. Column 1 is the circular orbit case number, column 2 is the final coast time, column 3 is the EI flight path angle, column 4 is the EI altitude, and column 5 is the EI velocity. The flight path angle at EI for case 1, 21, 22, 27, and 28 are outside the range of flight path angle at EI. Case 1 is out of the range the most by .102 degrees. The other cases are outside the range by less than .005 degrees.

The results in Table 7.4 and 7.2 are not the same. Adding the J_2 gravitational term to the guidance solution changes the problem for the given case and therefore the

Table 7.4 Final EI conditions for burn-coast solution with J_2 gravitational term in simulation and guidance solution and terminal constraints set 3 (Eqs. (3.66)–(3.68), (3.76), (3.77), (3.80), and (3.54))

Case	Final Coast (sec)	EI fpa (deg)	EI Altitude (m)	EI Velocity (m/s)
1	7381.4768	-0.7030	120286.5	7846.6990
6	2109.1078	-0.8101	121604.1	7882.2580
11	2474.8854	-0.8052	120066.2	7884.8125
16	6505.9747	-1.6025	121582.0	7861.9670
21	6524.0645	-0.8016	119691.3	7881.9015
22	6828.8401	-0.8006	119540.0	7885.3638
23	6459.0238	-0.8090	120459.1	7884.3694
24	4399.5295	-0.9036	120507.5	7881.6727
25	6005.2263	-0.8054	120080.0	7884.7924
26	4005.5745	-1.4518	120621.5	7867.1870
27	3221.8767	-1.6042	121345.1	7862.2644
28	111.8199	-0.8033	119844.3	7885.1003

solution will be different. The most striking difference is in the altitude. Adding the J_2 gravitational term to the solution and simulation allowed the vehicle the required altitude. The EI altitude results for the cases with J_2 gravitational term only in the simulation differ greatly from the required altitude.

Besides the solution meeting the altitude requirements, the other main difference in adding the J_2 gravitational term to the guidance solution is the time it takes for the solution to be solved by the computer. Solving for the position and velocity of the vehicle with the J_2 gravitational term requires numerically integrating the equations of motion. Numerical integration is more computational time intensive. Goodyear's method, which is used for modeling Keplerian motion, solves for the position and velocity of the vehicle using an analytical solution. This method is much faster computationally. The partial derivatives of the states are found using an analytical method using Goodyear's method. The partial derivatives with the J_2 gravitational term included must be found using a finite difference method. This adds to the computation time of the solution. The time required to complete the solution is a matter of minutes with the J_2 gravitational term added to the solution. Without the J_2 gravitational term, the computation time is a matter of seconds. Adding the J_2 gravitational term to the simulation does not affect

the computational time.

CHAPTER 8. Conclusion and Future Work

This work solved a optimal deorbit guidance problem given initial orbit and vehicle parameters as inputs. Using the optimal control method, the engine on time, engine off time as well as the direction of the thrust vector is solved for a variety of circular and elliptic initial orbits. For low altitude circular orbits, the single finite time burn was the optimal solution type. The burn time decreased as initial altitude increased till an altitude of 340 km. The transfer orbit for the deorbit maneuver is determined by the EI conditions. There is a specified transfer orbit apogee altitude for a given set of EI conditions. For initial orbits with altitudes higher than the transfer orbit apogee altitude, a longer burn time is required to place the vehicle on the required transfer orbit. For Shuttle type vehicles this initial orbit altitude is shown to be around 370 km. For orbits with higher altitudes, the two burn maneuvers were shown to provide lower total burn time solutions.

For low perigee altitude initial orbits the single finite time burn provides the most optimal solution in terms of minimizing burn time. The optimal deorbit point for initial elliptic orbits is not at apogee and is closer to perigee. If the velocity at EI is unconstrained, then the optimal deorbit point is at apogee. There does not exist an impulsive solution for the higher altitude cases given the desired set of EI conditions. Hence, for higher perigee altitude initial orbits, two burns maneuvers are shown to provide a smaller total burn time than the single burn. As the eccentricity of the initial orbits increases for a given perigee altitude, the burn time increases. The two burn maneuvers are better for higher perigee altitude initial orbits but not for increasing eccentricity for

a given initial perigee altitude. This is because the perigee altitude of the orbit is still low enough to place the vehicle on the required transfer orbit.

Adding the J2 term does have an impact on the EI flight path angle. For fixed EI flight path angle, adding the J2 term to the simulation yields max error of 5 percent. The altitude is affected by the J2 term. Adding the J2 term to the guidance solution and the simulation increases the computation time.

There are a few different areas that need improvement. The first is the initial guess needed to achieve the first initial solution. The current initial guess sets the thrust vector as being at 180 degrees from the velocity vector. As shown in chapters 4, 5, and 6, the thrust angle is almost never a constant 180 degrees but there is a pattern the thrust angles follow given an initial orbit altitude and eccentricity. Setting the initial $\mathbf{p}_V$ to reflect a thrust vector that follows the pattern shown by the results and calculating the corresponding $\mathbf{p}_r$ vector should help in finding an initial solution. Also, the method presented in [27] should be explored to see if that method helps in the finding of the initial solution.

Another area for improvement is in the numerical integration of the solution of the burn arcs. Currently, a quadrature rule is used. This is fine for small burn times of a couple hundred seconds. The burn times significantly increase as altitude and eccentricity increases. A better numerical integration technique should be implemented. Adding the J2 term via numerical integration in the guidance solution more than doubles the computation time. Using a different method, such as an approximate analytical one, would greatly improve the computation time. This should be explored further.

An analytical method for determining the optimal number of finite time burns for a deorbit maneuver would be most useful in solving the autonomous optimal deorbit guidance problem. There currently exists methods for determining the number of required impulsive burns given initial orbit parameters for a fixed time problem. However, to solve for the number of optimal finite time burns for a free final time deorbit problem

would be an epic accomplishment. Whether or not more than two burns would yield better results needs to be studied further.

APPENDIX A. Optimal Control Problem

Optimal Control Theory provides the method by which to solve the deorbit guidance problem such that the minimum fuel amount is optimized [17], [18]. The following section gives a brief overview of the problem setup.

Let the dynamic system be defined by

$$\dot{\mathbf{x}} = \mathbf{f}(\mathbf{x}, \mathbf{u}, t) \tag{A.1}$$

with given initial condition $\mathbf{x}(t_0) = \mathbf{x}_0$ where $\mathbf{x} \in R^n$ is the state vector and $\mathbf{u} \in R^m$ is the control vector. The terminal condition of the system is defined in k equations $(0 \leq k \leq n)$

$$\psi(\mathbf{x}_f) = \begin{pmatrix} \psi_1(\mathbf{x}_f) \\ \vdots \\ \psi_k(\mathbf{x}_f) \end{pmatrix} \tag{A.2}$$

where $\mathbf{x}_f$ is the state at final time t_f. The performance index is defined as

$$J = \phi(\mathbf{x}_f, t_f) + \int_{t_0}^{t_f} L(\mathbf{x}, \mathbf{u}) dt \tag{A.3}$$

where ϕ and L are scalar functions. The optimal control problem is to find the control profile $\mathbf{u}^*(t)$, $t_0 \leq t \leq t_f$ such that $\mathbf{u}^*(t)$ and $\mathbf{x}^*(t)$ satisfy the terminal constraints and state equations while minimizing the performance index.

To help find the optimal solution, a set of necessary conditions that $\mathbf{x}^*(t)$ and $\mathbf{u}^*(t)$ must satisfy are developed. The first condition is a scalar function called the Hamiltonian

$$H = \mathbf{p}^T \mathbf{f}(\mathbf{x}, \mathbf{u}, t) - L(\mathbf{x}, \mathbf{u}) \tag{A.4}$$

$$= \sum_{i=1}^{n} p_i f_i(\mathbf{x}, \mathbf{u}, t) - L(\mathbf{x}, \mathbf{u}) \tag{A.5}$$

where $\mathbf{p}$ is an n-dimensional time dependent vector called the costate vector, which must satisfy the costate equation

$$\dot{\mathbf{p}} = -\frac{\partial H}{\partial \mathbf{x}} = -\frac{\partial \mathbf{f}^T}{\partial \mathbf{x}}\mathbf{p} + \frac{\partial L}{\partial \mathbf{x}}. \tag{A.6}$$

The terminal condition for the costate vector are

$$\mathbf{p}_f = \frac{\partial \phi}{\partial \mathbf{x}_f} + \frac{\partial \psi^T}{\partial \mathbf{x}_f}\nu, \tag{A.7}$$

which is referred to as the transversality condition. ν is a constant multiplier that is determined as part of the solution of the problem. The optimal solution $\{\mathbf{x}^*, \mathbf{u}^*\}$ must satisfy the Pontryagin Maximum Principle:

$$H(\mathbf{p}, \mathbf{x}^*, \mathbf{u}^*, t) = \max_u H(\mathbf{p}, \mathbf{x}^*, \mathbf{u}, t). \tag{A.8}$$

This means that any $t \in [t_0, t_f]$, the Hamiltonian attains it's maximum value with respect to the control with $\mathbf{x}$ fixed at $\mathbf{x}^*(t)$ and $\mathbf{p}$ determined from the necessary conditions.

When $\mathbf{u}$ is unconstrained, the Maximum Principle gives rise to the stationary condition

$$\frac{\partial H(\mathbf{p}, \mathbf{x}^*, \mathbf{u}^*, t)}{\partial \mathbf{u}} = 0. \tag{A.9}$$

For free final time problems, an additional transversality condition is

$$H(t_f) = \frac{\partial \phi}{\partial t_f} \tag{A.10}$$

and if ϕ is not a function of time, then

$$H(t_f) = 0. \tag{A.11}$$

In conclusion, there are $2n$ variables in the state and costate vectors that are governed by the state and costate equations. The initial conditions of the state are given. The

initial conditions of the costate are unknown and must be solved as part of the problem, n unknowns. The constant multipliers ν are unknown and add another k unknowns to the problem. For a free final time problem t_f is unknown and must also be solved for. This gives the total number of unknowns as $n + k + 1$. These unknowns are determined and governed by A.10, A.7, and A.2. The optimal control is determined by the optimality condition A.8. Once the optimal control is determined, the state is found by the solving the state equations.

APPENDIX B. Primer Vector

One of the key parts of space flight is the primer vector. This section gives the definition of the primer vector and proof that the direction of the thrust is in the same direction of the primer vector for optimal space flight based on the work of [20].

Given the 3 DOF point mass equations of vacuum space

$$\dot{\mathbf{r}} = \mathbf{V} \tag{B.1}$$

$$\dot{\mathbf{V}} = \mathbf{g}(\mathbf{r}) + \frac{T\mathbf{1}_T}{m(t)} \tag{B.2}$$

$$\dot{m} = -\frac{T}{g_0 I_{sp}} \tag{B.3}$$

with constraint

$$|\mathbf{1}_T| = 1. \tag{B.4}$$

Construct the Lagrange equation

$$F = -\mathbf{p}_r^T\mathbf{V} - \mathbf{p}_V^T(\mathbf{g}(\mathbf{r}) + \frac{T\mathbf{1}_T}{m(t)}) + p_m\frac{T}{g_0 I_{sp}} + \mu(|\mathbf{1}_T| - 1) \tag{B.5}$$

where $\mathbf{p}_r$, $\mathbf{p}_V$, p_m, and μ are unknown multipliers. The necessary conditions are

$$\dot{\mathbf{p}_V} = -\mathbf{p}_r \tag{B.6}$$

$$\dot{\mathbf{p}_r} = -\mathbf{p}_V^T(\frac{\partial g(\mathbf{r})}{\partial \mathbf{r}}) \tag{B.7}$$

$$\dot{p_m} = \frac{T}{m^2(t)}\mathbf{p}_V^T\mathbf{1}_T \tag{B.8}$$

$$0 = -\frac{T}{m(t)}\mathbf{p}_V + 2\mu\mathbf{1}_T \tag{B.9}$$

and eliminating $\mathbf{p}_r$ gives

$$\ddot{\mathbf{p}_V} = -\mathbf{p}_V^T(\frac{\partial g(\mathbf{r})}{\partial \mathbf{r}}). \tag{B.10}$$

Define the primer vector $\mathbf{p}_V = \mathbf{p}$. Assuming the mass and μ are equal to zero, B.9 implies $\mathbf{p}_V$ and $\mathbf{1}_T$ are in the same direction. If the mass is zero, $\mathbf{1}_T$ is indeterminate and if μ is zero, $\mathbf{p}_v$ vanishes. Using Weierstrass's Condition requires every point on the trajectory to satisfy

$$(\frac{1}{m(t)}\mathbf{p}_V^T\mathbf{1}_T - \frac{p_m}{g_0 I_{sp}})T \geq (\frac{1}{m(t)}\mathbf{p}_V^T\mathbf{1}_T^* - \frac{p_m}{g_0 I_{sp}})T^* \tag{B.11}$$

for all possible values of $\mathbf{1}_T^*$ and m^*. Over a zero thrust arc

$$p_m \geq \frac{T}{m(t)}\mathbf{p}_V^T\mathbf{1}_T^*. \tag{B.12}$$

$\mathbf{p}_V^T\mathbf{1}_T^*$ achieves its maximum value when $\mathbf{1}_T^*$ is aligned with the primer vector and its value is the magnitude of the primer vector. This gives the necessary condition

$$p_m \geq \frac{T}{m(t)}p \tag{B.13}$$

where p is the magnitude of the primer vector. Over a maximum thrust arc $T^* = T$ where T is maximum value of thrust and applying this to the Weierstrass Condition requires

$$\mathbf{p}_V^T\mathbf{1}_T \geq \mathbf{p}_V^T\mathbf{1}_T^* \tag{B.14}$$

Taking $\mathbf{1}_T^* = \mathbf{1}_T$ and $T^* \leq T$ yields

$$p_m \leq \frac{T}{m(t)}\mathbf{p}_V^T\mathbf{1}_T^* \tag{B.15}$$

Equations B.14 and B.15 ensure the Weierstrass Condition. B.14 will be satisfied for all $\mathbf{1}_T^*$ if and only if $\mathbf{p}_V^T\mathbf{1}_T$ takes its maximum value with respect to variations of $\mathbf{1}_T$. This implies the direction of the primer vector and thrust are identical. Thus

$$\mathbf{1}_T = \frac{\mathbf{p}_V}{|\mathbf{p}_V|} \tag{B.16}$$

APPENDIX C. Analytical Multiple Shooting Algorithm

This algorithm description is based off description in Refs. [26] and [28]. Placing nodes at the junction points of the arcs in the trajectory, the multiple shooting method enhances the robustness of the solution method.

Let N be the number of arcs. The number of nodes added to the problem is $N-1$. Figure C.1 shows the setup of these arcs and nodes.

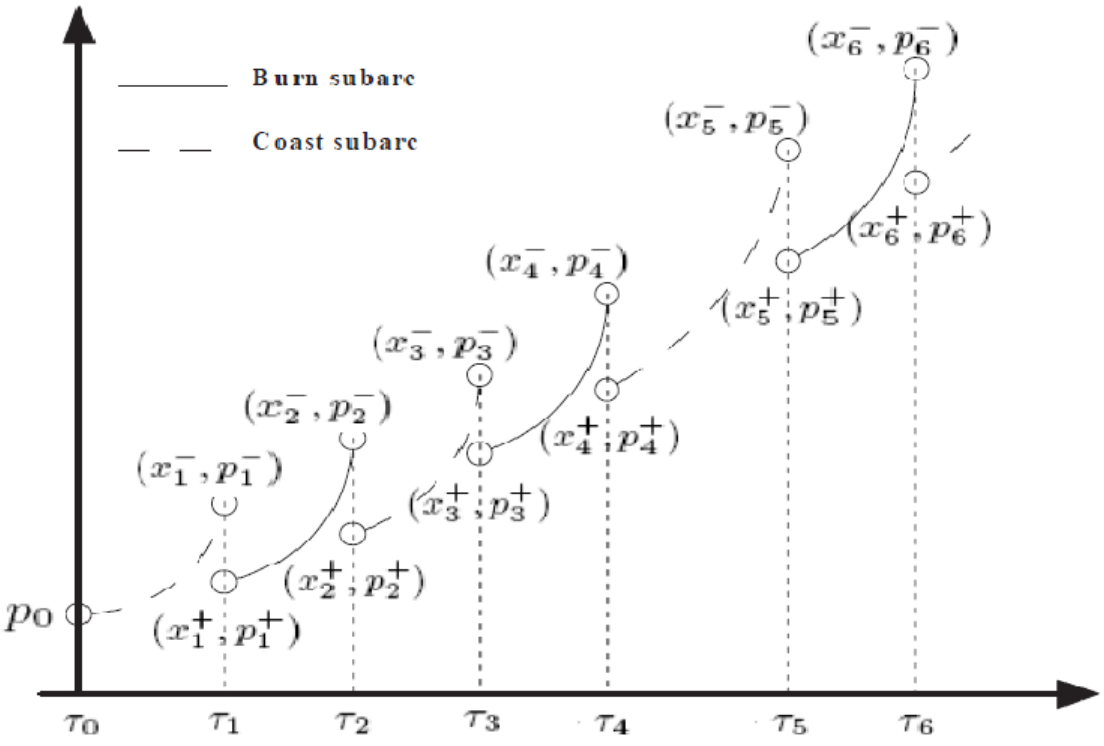

Figure C.1 Multiple Shooting Method for N Arc Problem

The addition of the nodes to the problem increases the number of unknowns by $N-1$.

The number of unknowns to be solved are

$$z = (\mathbf{p}_0, \mathbf{x}_1, \mathbf{p}_1, \tau_1, \ldots, \mathbf{x}_i, \mathbf{p}_i, \tau_i, \ldots, \mathbf{x}_{N-1}, \mathbf{p}_{N-1}, \tau_{N-1}, \tau_f), z \in \mathbf{R}^{13(N-1)+7} \tag{C.1}$$

where $\mathbf{p}_0$ is the initial costate, $\mathbf{p}_i$ is the costate and x_i is the state at nodes $N-1$, τ_i is the time at the $N-1$ nodes, and τ_f is the final time. With the addition of the nodes, new constraints are needed to solve the problem. These constraints are in the form of equality constraints and take the following form:

$$\Phi(\tau_N - \tau_{N-1})\mathbf{p}_{N-1} - \mathbf{p}_N^+ = 0 \tag{C.2}$$

$$\Phi(\tau_N - \tau_{N-1})\mathbf{x}_{N-1} + \Gamma(\tau_N)\mathbf{I}(\tau_N, \tau_{N-1}) - \mathbf{x}_N^+ = 0 \tag{C.3}$$

$$\Psi(\tau_N - \tau_{N-1})\mathbf{x}_{N-1} - \mathbf{x}_N^+ = 0 \tag{C.4}$$

for all N. Eqn. (C.2) ensures that the costate solution at the previous node $N-1$ propagated in time equals the guessed solution at node N. Eqn. (C.3) ensures the same for the state along the burn arcs and eqn. (C.4) ensures the same for the state along the coast arc. The final constraints are the terminal constraints in terms of the final position and velocity

$$s_k(\mathbf{x}_f, \mathbf{p}_f) = 0 \tag{C.5}$$

for $k = 1, \ldots, 6$. The final constraint is the free final time constraint

$$H(\tau_f) = 0. \tag{C.6}$$

The multiple shooting method is now reduced to a rootfinding problem. Powells Hybrid Dogleg method is used to solve for the roots of the problem.

APPENDIX D. Thrust Angle

The thrust angle is the angle between the velocity vector and the thrust vector and is only applicable during burn times. The thrust angle, Θ_{TA}, is found as follows

$$\Theta_{TA} = \arccos(\mathbf{1}_T \cdot \mathbf{V}). \tag{D.1}$$

To determine when the thrust angle is greater than 180 degrees is necessary. It is done as follows. First compute the angular momentum vector for each second of the burn flight

$$\mathbf{h} = \mathbf{r} \times \mathbf{V}. \tag{D.2}$$

Define a vector in the same plane as velocity and position vector as follows

$$\mathbf{n} = \mathbf{V} \times \mathbf{h}. \tag{D.3}$$

Figure D.1 gives a graphical representation of $\mathbf{n}$ in reference to $\mathbf{V}$ and $\mathbf{r}$. If the dot product of $\mathbf{n}$ and $\mathbf{1}_T$ is greater than zero, the thrust angle is less than 180 degrees and if the dot product of $\mathbf{n}$ and $\mathbf{1}_T$ is less than zero, the angle is greater than 180 degrees. For example, Figure D.2 shows a velocity, thrust vector setup with a thrust angle less than 180 and Figure D.3 shows a velocity, thrust vector setup with a thrust angle greater than 180.

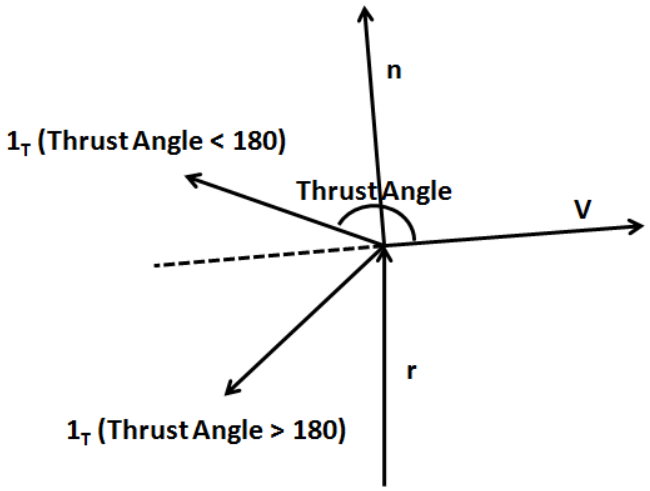

Figure D.1 Thrust angle with reference to velocity and position vectors.

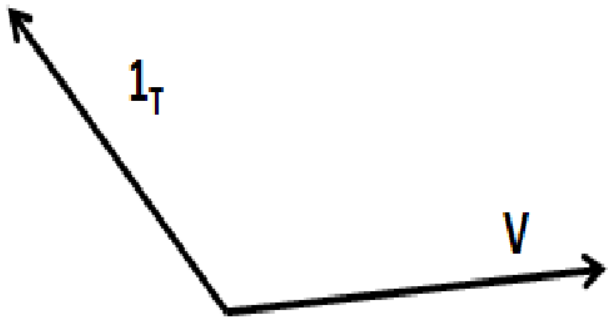

Figure D.2 Sample thrust and velocity vector setup with thrust angle less than 180 degrees.

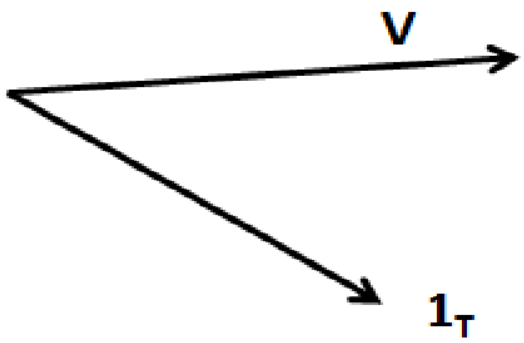

Figure D.3 Sample thrust and velocity vector setup with thrust angle greater than 180 degrees.

BIBLIOGRAPHY

[1] Doggrell, L. "Operationally Responsive Space", URL:http://www.airpower.maxwell.af.mil/airchronicles/apj/apj06/sum06/doggrell.html, June 2006.

[2] Goester, J. F., and Broca, R., "Deorbit Strategies", 42nd International Astronautical Congress, IAF, Montreal, Canada, 1991.

[3] Joosten, B. K., "Descent Guidance and Mission Planning for Space Shuttle", Space Shuttle Tech. Conf., Part 1, 1985, pp. 113-124.

[4] Brand, T. J., Brown, D. W., Higgins, J. P., "Space Shuttle GNC Equation Document No. 24 Unified Powered Flight Guidance", NAS9-10268, June 1973.

[5] Galman, B. A., "Minimum Energy Deorbit", *Journal of Spacecraft*, Vol. 3, No. 7, July 1966.

[6] Robertson, R. L., "Guidance, Flight Mechanics, and Trajectory Optimization", *Mission Constraints and Trajectory Optimization*, Vol. 16, 1968.

[7] Baker, J.M., Baxter, B. E., Arthur, P.D., "Optimum Deboost Altitude for Specified Atmospheric Antry Angle", *AIAA Journal Technical Notes and Comments*, July 1963.

[8] Stern, G. S., "Optimum Deorbit Positioning for Minimum Impulse Reentry", Presented at the AAS Space Flight Mechanics Specialist Conference, July 1966.

[9] Green, A. L., Stern, G. S., "Optimum Deorbit Positioning for Minimum Impulse Reentry with Variable Reentry Conditions", *Journal of the Astronautical Sciences*, Vol. 14, 1968, pp. 302-306.

[10] Lane, P. S., "Minimizing Deorbit Maneuvers by Hodographic Analysis", Proceedings of the 1st AAS/AIAA Annual Spaceflight Mechanics Meeting, Houston, TX, 1991, pp. 25-37.

[11] Vinh, N. X., "Exact Relations of Optimum Switching in the Problem of Impulsive Transfer", *Journal of Astronautical Sciences*, Vol. 17, No. 6, May-June 1970.

[12] Vinh, N. X., Culp, R. D., "Optimal Switching in Coplanar Orbit Transfer", *Journal of Optimization Theory and Applications*, Vol. 7, No. 3, 1971.

[13] Lion, P.M., Handelsman, M., "Primer Vector on Fixed-Time Impulsive Trajectories", *AIAA Journal*, Vol. 6, No. 1. January 1968.

[14] Vinh, N.X., Lu, P., Howe, R.M., Gilbert, E.G. "Optimal Interception with Time Constraint", *Journal of Optimization Theory and Applications*, Vol. 66, No. 3, 1990, pp. 361-390.

[15] Jezewski, D. J., "Autonomous Optimal Deorbit Targeting", Proceedings of the 1st AAS/AIAA Annual Spaceflight Mechanics Meeting, Houston, TX, 1991, pp. 39-56.

[16] Kindler, J. T., Schoettle, U. M., Well, K. H., "Entry Interface Window of Landing Site Coober Pedy for the Experimental Vehicle X-38 V201", AIAA Atmospheric Flight Mechanics Conference, Denver, CO, Aug 14-17 2000, AIAA-2000-4117.

[17] Lewis, F. L., and Syrmos, V. L., *Optimal Control*, 2nd. Edition, John Wiley and Sons, Inc., New York, NY, 1995.

[18] Bryson, A. E., and Ho, Y. C., *Applied Optimal Control*, Hemisphere, Washington, DC, 1975.

[19] Vallado, D., *Fundamentals of Astrodynamics and Applications*, Microcosm, Inc, California, 2001.

[20] Lawden, D.F., *Optimal Trajectories for Space Navigation*, Butterworths and Co LTD, London, 1963.

[21] Walter, U., *Astronautics*, WILEY-VCH Verlag GmbH and Co., Germany, 2008.

[22] Bate, R. R., Mueller, D. D., White, J. E., *Fundamentals of Astrodynamics*, Dover Publications, INC, New York, 1971.

[23] Lu, P., Griffin, B., Dukeman, G., and Chavez, F., "Rapid Optimal Multiburn Ascent Planning and Guidance", *Journal of Guidance, Control, and Dynamics*, Vol. 31, No. 6, 2008, pp. 1656-1664.

[24] Goodyear, W., "Completely General Closed Form Solution for Coordinates and Partial Derivatives of the Two-Body Problem", *The Astronomical Journal*, Vol. 70, No. 3, 1965, pp. 189–192.

[25] Xu, C., Tsoi, R., Sneeuw, N., "Analysis of J2-Perturbed Relative Orbits for Satellite Formation Flying", *International Association of Geodesy Symposia*, Vol. 129, 2005.

[26] Pan, B., Lu, P., Rapid Optimization of Multiburn Rocket Trajectories Revisited, AIAA Paper 2009-6105, Guidance, Navigation, and Control Conference, August 10-13, 2009

[27] Pan, B., Lu, P., Improvements to Optimal Launch Ascent Guidance", AIAA Paper 2010-8174, Guidance, Navigation, and Control Conference, August 2-5, 2010.

[28] Griffin, B., Improvements to an analytical multiple-shooting approach for optimal burn-coast-burn ascent guidance", M. S. Thesis, Iowa State University, 2007.